OUT-OF-PLANE FLEXURAL PERFORMANCE OF GFRP-REINFORCED CONCRETE MASONRY WALLS

Navid Sasanian

A Thesis

in

The Department

of

Building, Civil, and Environmental Engineering

Presented in Partial Fulfillment of the Requirements

for the Degree of Master of Applied Science (Civil Engineering) at

Concordia University

Montréal, Québec, Canada

March 2009

Your file Votre référence
ISBN: 978-0-494-63274-1
Our file Notre référence
ISBN: 978-0-494-63274-1

ABSTRACT

OUT-OF-PLANE FLEXURAL PERFORMANCE OF GFRP-REINFORCED CONCRETE MASONRY WALLS

NAVID SASANIAN

The objective of this thesis is to assess the out-of-plane flexural performance of single-wythe concrete masonry walls that are reinforced with Glass Fibre-Reinforced Polymers (GFRP) rods, as an alternative for steel rebars. Eight 1m×3m full-scale walls were constructed using hollow concrete masonry units and tested in four-point bending with an effective span of 2.4 m between the supports. The walls were tested when subjected to increasing monotonic loads up to failure. The applied loads would represent out-of-plane loads arising from wind, soil pressure, or inertia force during earthquakes.

One wall is unreinforced, another wall is reinforced with customary steel rebars and the other six walls are reinforced with different amounts of GFRP reinforcement. Two of the GFRP-reinforced walls were grouted only in the cells where the rods were placed in order to investigate the effect of the extent of grouting on the performance of the walls. The force-deformation relationship of the walls and the associated strains in the reinforcement were monitored throughout the tests. The relative performance of different walls is assessed in order to quantify the effect of different design variables. The range of GFRP reinforcement ratios covered in the experiments was used to propose a capacity diagram for design of FRP-reinforced masonry walls similar to that of reinforced concrete elements.

A comprehensive analytical study on the behaviour of the tested walls accompanies the experimental program, so that the outcome of the experiments could be

quantified and theoretically predictable. Flexural capacity and out-of-plane lateral deflection of the walls are the major aspects that are tried to be evaluated using available models and methods of analysis. Furthermore, efforts are made to obtain finer predictions closer to results of the tested walls using new methods. Since the analyses carried out in this study showed pleasing agreements with the wall tests, a capacity diagram is developed based on the analyses and proposed to be used in designing concrete masonry walls reinforced with GFRP bars. Lastly, the ductility of the GFRP-reinforced walls has been inspected through different methods, the outcomes of which ensure that the GFRP-reinforced walls have exhibited sufficient deformability prior to failure.

To the moments when I managed
to forget, not think, and remain

ACKNOWLEDGEMENTS

I would like to acknowledge the financial supports of Natural Sciences and Engineering Research council of Canada (NSERC), le Fonds Québécois de la Recherche sur la Nature et les Technologies (FQRNT), and Centre d' Études Interuniversitaire sur les Structures sous Charges Extrêmes (CEISCE).

The experimental phase of this dissertation became possible on account of endless support and sincere collaboration of l'Association des Entrepreneurs en Maçonnerie du Québec (AEMQ), above all Normand Turenne (Président) and Denis Brisebois (Directeur Général). Tomassini et frères Ltée and especially Pierre Tomassini who assisted us extensively in the construction and also through the team research project are also gratefully appreciated. Furthermore, Canada Masonry Design Centre (CMDC) is greatly acknowledged for their contribution in providing us with the aforesaid liaisons.

I would also like to address my heartfelt gratitude to my teacher and advisor Dr. Khaled Galal, who I believe is making history in the BCEE department of Concordia University, for not only did he provide me with all the academic and non-academic helps and supports, but also he motivated me with his unflagging encouragements to carry out a job which seemed to be impossible at the beginning.

This dissertation goes along with the rest of my achievements, abilities and inabilities, for which I am indebted incalculably to my mom and dad, whom I never thanked enough and never will, and my only brother, Vahid, who is the best I have. In heart, I know they deserve more than what I give and express towards them.

Jinoos, Vafa, Niky, and Ariana Nateghi have been my family and a lot more here in Canada and I am and will be always grateful for their love and presence.

I owe an immeasurable debt of appreciation to Riccardo Gioia, without whose help, I would have not been able to carry out the experiments of this dissertation. There were so many moments that with Ricky on my side, I did not have to worry and could go on, since he made even the hardest ones pass safely and successfully.

I wish to express my whole-hearted appreciation to Alp Enginsal, for he did not leave me alone after Ricky and helped me keep going with his smartness and humour. We were strangely able to have fun and laugh in the most disappointing times.

I would also like to thank Sina Fazelpour; he and I may know less than one another what we are doing, but Sina doing what he is doing has always left me with less doubts about what I am doing, and in a way kept me sane.

Last but certainly not least, Mahnaz Sadri who gave me, with her eyes and tiny heart full of beauty, what I did not know I needed so much, deserves my everlasting thanks and much more.

TABLE OF CONTENTS

LIST OF FIGURES

LIST OF TABLES

LIST OF SYMBOLS

A Effective tension area surrounding the reinforcing rods divided by the number of the bars (mm^2)

A_{FRP} Total area of the GFRP reinforcements (mm^2)

A_s Total area of steel reinforcements (mm^2)

b Width of the cross-section (mm)

c Depth of the compression zone in the cross-section of the walls (mm)

d Effective depth of reinforcing rebars (mm)

d_b Diameter of the reinforcing bars (mm)

d_c Concrete cover for the reinforcing bars (mm)

d_{crack} Depth of the crack (mm)

E_m Young's modulus of masonry assemblage (GPa)

E_{FRP} Young's modulus of GFRP bars (GPa)

$E_{elastic}$ Elastic energy absorbed by the masonry wall

$E_{inelastic}$ Inelastic energy absorbed by the masonry wall

E_{steel} Young's modulus of steel rebars (GPa)

E_{total} Total energy absorbed by the masonry wall

f_{FRP} Stress in the GFRP rods (MPa)

f'_m Compressive strength of the masonry assemblage (MPa)

$f_{u,FRP}$ Ultimate tensile strength of the GFRP rods (MPa)

f_y Yield stress of the steel rebars (MPa)

h Thickness of the wall (i.e. depth of the cross-section) (mm)

I_{cr} Moment of inertia of fully cracked section (mm^4)

I_{eff} Effective moment of inertia of the cracked section (mm^4)

I_g Moment of inertia of the gross section (mm^4)

k_{crack} Ratio of the depth of the crack to the maximum depth of the crack

M_a Applied moment of the masonry walls (kN.m)

M_{cr} Cracking moment of the masonry walls (kN.m)

M_n Nominal flexural resistance of the masonry walls (kN.m)

M_s Applied moment at the service stage (kN.m)

P_1, P_2, P_3 Three different points of the loading part of the load-deflection curve

R Modulus of rupture of the masonry assemblage (MPa)

S Predicted slope of the unloading part of the load-deflection curve

S_1, S_2, S_3 Slopes of three different segments of the loading part of the load-deflection curve

u_0 , u_1 Constants used in the stress-strain equation of the masonry

w_{crack} Width of the crack (mm)

x Ratio of strain to strain corresponding to the peak compressive stress in masonry

α_1 Stress block factor

β Constant dependent on the mode of failure

β_1 Stress block factor

$\Delta_{analytical}$ Deflection calculated by cracked section analysis (mm)

Δ_{crack} Calculated extra deflection due to the flexural cracks (mm)

Δ_{total} Total calculated deflection (mm)

Δ_u Deflection at the ultimate failure (mm)

Δ_y	Deflection at the yeilding (mm)
γ	Constant dependent on the type of flexural reinforcement
$\varepsilon_{FRP,u}$	Ultimate tensile strain of the GFRP
ε_m	Compressive strain of masonry
$\varepsilon_{m,u}$	Ultimate compressive strain of masonry
θ	Rotation of the wall at the cracked bed joint
μ	Deformability index
μ_Δ	Displacement ductility
σ_m	Compressive stress in masonry
ρ_{FRP}	GFRP reinforcement ratio
Φ_{FRP}	Reduction factor for GFRP rods
Φ_s	Reduction factor for steel rebars
ψ_s	Curvature of the masonry walls at service stage
ψ_u	Curvature of the masonry walls at ultimate stage

CHAPTER 1

INTRODUCTION AND BACKGROUND

1.1 Background and Statement of the Problem

Unreinforced masonry is known as one of the oldest types of construction materials and has been widely used since ancient times, mostly due to its low construction and maintenance costs, incomparable thermal and sound insulation, reliable fire resistance, and inimitable durability. Ancient masonry structures were built with large structural components in size, to satisfy the conservative empirical methods of design and simple rules of thumb in construction. This type of structures was not excluded from the results of modern engineering in the twentieth century while better understanding of mechanical behaviour of masonry led to developing and improving technical guidelines for designing masonry structures. However, lack of tensile strength has been an obstacle confronting the engineers when it comes to design unreinforced masonry structures for lateral loads. Hence, as a characteristic that can be found in most of the masonry structures, their lateral resistance depends very much on the largeness and own weight of the structural components. Since it is desired to minimize the space occupied by the structural elements, *unreinforced* masonry construction loses its effectiveness compared to other types of structures particularly in high seismicity areas. Walls amongst all masonry components constitute a great portion of a masonry structure as they can be found with massiveness of dimensions and amount of used materials frequently in structural systems. Thus, the need for special attention as per their strength requirements and structural performance is intensified.

On the other hand, reinforced masonry walls are considered as one of the most common structural masonry elements that are broadly employed to undertake axial and lateral loads. Depending on the application and also the orientation of masonry walls, these elements can be submitted to out-of-plane bending actions arising from wind, soil pressure, or seismic excitations, in which situations, the role of flexural reinforcement is critically influential in flexural strength, behaviour, and serviceability of the walls. Masonry walls are vulnerable when subjected to considerable amounts of aforementioned lateral loads as a consequence of their inadequate ductility and tensile strength. Use of steel rebars has been established as the customary method to resolve these deficiencies similar to concrete structures.

Steel-reinforced masonry has been implemented in construction of different types of low-rise (up to four-story), mid-rise (five- to eight-story), and high-rise (more than eight-story) buildings. One of the most famous reinforced masonry buildings in North America is The Crittenden Court completed in 1995 in downtown Cleveland, Ohio (see Figure 1.1). The construction of this 17-story apartment building did not exceed seventeen weeks. Another example of modern reinforced masonry structures is The Renaissance Hotel, Springfield, Illinois (see Figure 1.2). The structure of this 12-story hotel comprises seven flours mainly constructed of load-bearing reinforced masonry walls, while steel and reinforced concrete are used in the other flours. These two examples as well as numerous reinforced masonry structures that are constructed in the last few years, demonstrate the popularity of steel-reinforced masonry as a low cost, less time consuming, and durable type of construction. However, when dealing with lateral loads of larger magnitudes (e.g. in seismic prone areas), steel reinforcement might lose its

suitability due to design constraints such as the upper limit of reinforcement defined by the balanced reinforcement ratio. This calls for methods of reinforcing the walls that can achieve higher flexural capacities while maintaining the dimensions of the walls.

Fibre-Reinforced Polymer (FRP) composites have been studied and used extensively to reinforce concrete structures as a new substitute for steel reinforcement for more than a decade. FRP bars have been proven to be an effective means to replace steel reinforcement in various concrete structures such as bridge deckings and parking garages. In addition to their superior durability, mainly due to outstanding non-corrosive characteristics, these composite materials have the benefits of high strength-to-weight ratio, considerable fatigue properties, and electromagnetic transparency. Moreover, their usage in concrete structures has been codified in the most recent Canadian Highway Bridge Design Code (CHBDC) (CSA S6 (2006)). Lower fire resistance and higher costs are considered as the disadvantages therein. However, the former is not an issue in the case of concrete masonry in that the minimum required cover for FRP-reinforced concrete (FRP-RC) structures, which is found to be 64 mm or less (Saafi (2002), Kodur and Bisby (2005), and CHBDC (2006)), is naturally fulfilled by the dimensions of masonry units. Moreover, the decreasing cost of FRP as well as lower transportation and handling costs of lighter materials are making the use of FRP in construction more competitive (Grace *et al.* (1998), and Kodur and Bisby (2005)). Significant amount of work has been directed to utilizing different types of FRP that are externally bonded or mounted on the surface of masonry walls for strengthening and rehabilitating reinforced and unreinforced masonry walls (URM). It is reported by several researchers that notably higher shear and flexural strength as well as sufficient ductility can be attained by adding

these external FRP systems to deficient masonry panels. On the contrary, to the author's knowledge, there is not much work corresponding to the use of FRP for reinforcing masonry walls and in particular, there have been no efforts to exploit FRP as interior reinforcement of masonry structural elements.

1.2 Significance of the Research

This research examines the use of Glass FRP (GFRP) rods as a new reinforcing technique in concrete masonry walls and its effect on their out-of-plane flexural behaviour through a comprehensive course of experiments, the outcomes of which are theorized by applying and introducing different methods of analysis and modeling. It is also intended to ensure that crucial criteria as per the serviceability of the walls (e.g. deformability) are maintained while higher load-bearing capacities are attained. Moreover, the use of GFRP rods as an alternative for steel rebars eliminates the most important durability related problem which is corrosion of the steel rebars. Another durability related concern is the fire resistance of the GFRP-reinforced masonry walls which is automatically resolved, since the cover is more than what is required. Finally, as mentioned earlier, due to less weight and more flexibility of the GFRP rods, handling and placement of the rods will be facilitated in construction.

The experimental program comprises tests on eight full-scale masonry walls, six of which were reinforced with GFRP rods. The GFRP rebars used in this study are known as V-ROD^{TM} and manufactured by Pultrall Inc located in Québec (Pultrall (2007)). The main parameter of the research is the ratio of GFRP reinforcement that varies for GFRP-reinforced specimens included in the experimental program. The effect of (not) filling the

cells, into which the longitudinal reinforcement is not positioned, has been considered as another aspect of this study that leads to a more efficient design. Test result of the unreinforced wall specimen proves the essential need of longitudinal reinforcement for masonry walls subjected to out-of-plane bending. The relative performance of the walls with different reinforcement ratios demonstrates the variation of their capacity with respect to their reinforcement ratio. The foregoing eventually verifies the proposed design diagram which can be used to get the proper amount of GFRP reinforcement for a given flexural demand similar to that of FRP-RC. In addition, the behaviour of the GFRP-reinforced specimens compared with the control specimens, unreinforced and steel-reinforced, exhibits the effectiveness of the suggested reinforcement method. It is intended to comprehend whether the possibility of over-reinforcing the section with GFRP, as opposed to steel, resolves the upper limit of flexural strength for a certain cross-sectional dimensions that confronts the designer when choosing steel as the reinforcing material for masonry. For this matter, an analogous steel-reinforced masonry wall, from the design point of view, is tested and compared with two of the GFRP-reinforced walls.

1.3 Scope of the Study

Based on the aforesaid, the need for an advantageous method of reinforcing masonry walls in order to achieve higher capacity for resisting lateral loads and improve durability as well as out-of-plane flexural response, motivates the study brought in this manuscript. The scope of the research, briefly, is to fulfill the following objectives:

- To introduce and utilize GFRP rods as the main internal reinforcement of concrete masonry walls for out-of-plane flexure,

- To demonstrate and compare the out-of-plane performance of unreinforced, steel-reinforced (as the accustomed reinforcing method), and GFRP-reinforced (as a new method) masonry walls,
- To reach a reliable method of predicting flexural strength of the walls based on available methods of section analysis for steel-reinforced masonry and FRP-RC, and validate and theorize the behaviour of the tested walls using the finest model,
- To evaluate the available methods of predicting the deflection and introduce a more accurate prediction for the forced-deformation response of the tested walls,
- To propose a design diagram based on the performance of the tested walls that is valuable in developing practical guidelines in designing GFRP-reinforced masonry elements in flexure,
- To investigate whether or not the GFRP-reinforced masonry walls exhibit acceptable responses with respect to deformability requirements.

It should be mentioned that this study is intended to examine the behaviour of specifically concrete masonry walls reinforced with FRP when subjected to out-of-plane lateral load, in particular. Therefore, nor the in-plane strength neither the shear behaviour of the walls is included herein. Besides, only single-wythe concrete wall structure is inspected in the course of the experiments and analyses. In addition, Anchorage strength of the longitudinal reinforcement is assumed to be sufficient in all analyses; and certain steps of current design codes may be excluded from the scope of this research. Moreover, strengthening existing masonry walls is not included in this thesis since it is intended to study the walls for new construction. The results of the experiments conducted in this research yield to a better perceptive of masonry walls' inelastic behaviour in out-of-plane

bending when reinforced with GFRP rods that can assist in theorizing a limit-states design methodology in future codes for masonry structures reinforced with FRP rods.

1.4 Organization of the Thesis

This thesis comprises seven chapters starting with chapter one, which delivers an introduction to the topic of the research, the main parameters that necessitate this research, and what this research has aimed to accomplish.

Chapter two reports a brief survey in the literature concentrating on reinforced masonry, use of FRP in strengthening masonry, and masonry reinforced with FRP.

The first part of Chapter three is devoted to the auxiliary tests accompanying the main tests on the walls. The second part of this chapter is meant to describe the main specimens, test setup, and instrumentation followed by procedure of the wall tests.

Chapter four reports the results of the tests on full-scale masonry walls. Photos of the tested walls along with the force-deformation and force-strain diagrams are enclosed herein. In addition, it presents a qualitative discussion on behaviour of the walls including comparisons between the specimens.

Chapter five includes different methods of analysis and numerical modeling focusing on two quantitative aspects of walls' response, flexural strength and deflections. In this chapter, efforts are made to establish finer methods of predicting walls' behaviour, closest to that of the tested walls.

Chapter six examines of a number of analytical methods for evaluating the performance of the GFRP-reinforced masonry walls in terms of deformability. Ductility of the masonry walls is of notable importance since steel is replaced with GFRP, known

as a brittle type of material; hence, in this chapter it is investigated whether or not the GFRP-reinforced walls function with sufficient deformability.

Chapter seven, lastly, summarizes this study, presents the conclusions derived based on the experimental results and analyses carried out in the course of this research, and recommends the areas to be studied further more.

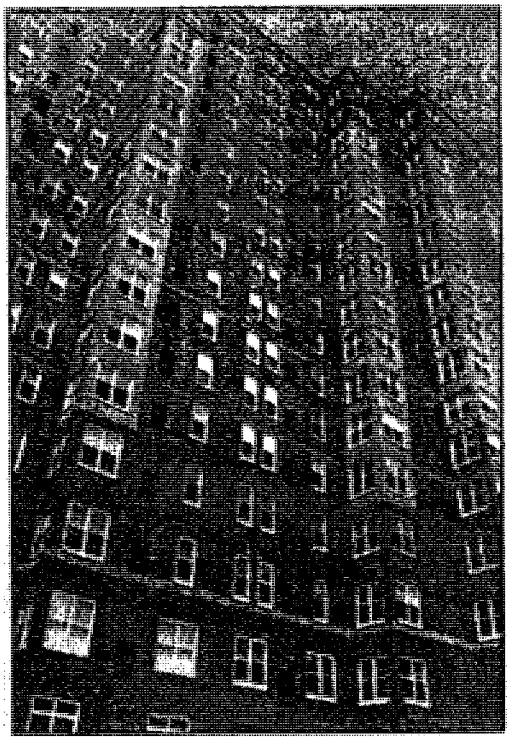

Figure 1.1. The Crittenden Court, 17-story reinforced masonry high-rise, Cleveland, Ohio (Taly (2001))

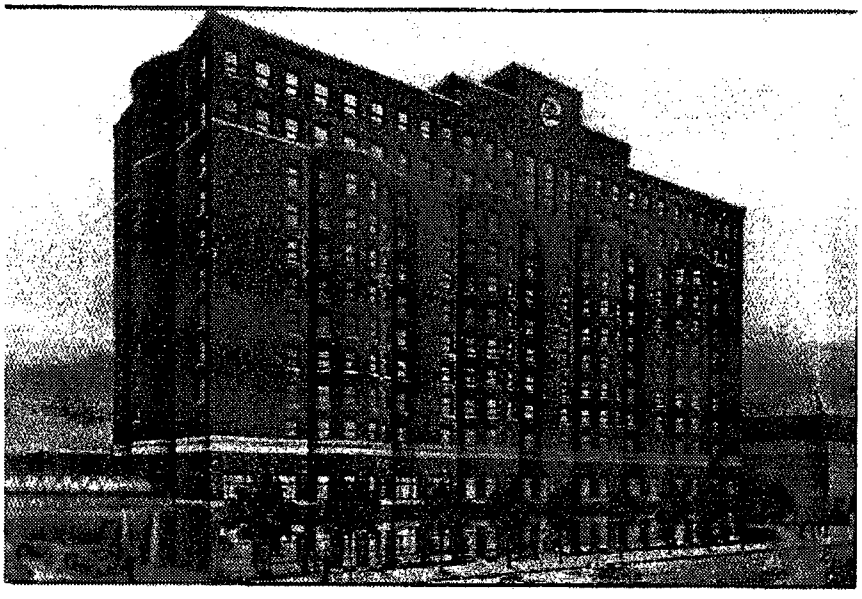

Figure 1.2. Renaissance Hotel, 12-story reinforced masonry building, Springfield, Illinois (Taly (2001))

CHAPTER 2

LITERATURE SURVEY

2.1 General

This chapter first delivers a review of the works that have been carried out in the field of reinforced masonry walls. In the following section, the use of FRP for strengthening and reinforcing masonry walls in previous literature is surveyed. Literature review indicates remarkable research with the purpose of improving the flexural capacity of unreinforced masonry and steel-reinforced masonry walls in terms of retrofitting and rehabilitation using new techniques and materials specifically FRP, while there is not much data available with regard to reinforcing new masonry walls with FRP to achieve higher level of lateral load-bearing capacity. Since concrete masonry walls are the subject of this research, the works conducted in the field of concrete masonry walls are mainly referred to herein.

2.2 Reinforced Masonry Walls

Similar to concrete, the major key to failure of masonry elements in flexure is the lack of sufficient tensile strength. Over the past four decades, considerable studies have been developed to assess and increase the resistance of masonry walls subject to lateral loads which mainly started by introducing steel rebars as the main reinforcing element to compensate for poor tensile strength in masonry assemblage.

Hamid *et al.* (1992) are amongst the first researchers that introduced internal reinforcement to masonry panels. They conducted a series of tests on five panels

reinforced with horizontal steel rebars spanning parallel to the bed joints. The effects of amount of horizontal steel reinforcement, type of joint reinforcement, and bond pattern (i.e. running bond vs. stack bond) on out-of-plane flexural behaviour of masonry walls were investigated in the course of this research. Crack patterns, cracking moments, load-deformation relationships, and flexural strengths of the panels were the parameters to be monitored during the tests leading to drawn comparisons and conclusions. Despite the fact that the joint reinforcement and bond pattern proved to be not influential on flexural strengths of the walls, the load-deflection curves were found to be a function of amount and type (i.e. ultimate tensile strength) of the horizontal steel reinforcement. It was the first time that the post-peak performance of horizontally reinforced masonry walls was inspected by experimental tests; however, the panels did not exhibit significant inelastic deformations.

Abboud *et al.* (1996) carried out full-scale out-of-plane bending tests thoroughly on steel-reinforced masonry walls as a part of the U.S.-Japan Coordinated Program on Masonry Building Research (TCCMAR) in which the post-yield behaviour and displacement ductility of the vertically reinforced masonry walls were inspected for the first time. The tested walls were designed to have different amounts of reinforcing steel rebar with different arrangements (i.e. centered vs. staggered) and also different extent of grouting (i.e. fully vs. partially grouted). Schematic drawing of tested walls as well as the test setup are shown in Figure 2.1. The reported post-yield load-deformation curves proved the significant effect of longitudinal reinforcement on improving the deficient flexural resistance of unreinforced masonry walls and justified its necessity. They decided to draw a parallel theoretical analysis on walls' response based on the Whitney

stress block using the common method of ultimate strength, which eventually established agreeable correlation with the experimental results. The amount of longitudinal reinforcement showed to have significant effect on ductility of the walls; so did the extent of grouting, the other major factor of the study. It was reported that panels with higher amounts of longitudinal reinforcement exhibited less ductile behaviour; whereas, partially grouted walls compared to the fully grouted specimens accomplished higher displacement ductility. Another important remark that could be concluded from the test results was that the mode of failure and also the shape of the load-deformation curve of the walls depend on the reinforcement ratio. As can be seen in Figure 2.2, the tensile forces at ultimate stage in the wall with relatively lower reinforcement ratio were not enough to cause failure in compression zone of the masonry and as a consequence, the steel rebars continued yielding and the wall kept on deflecting without any change in the applied lateral load. However, walls with higher ratios of steel reinforcement encountered crushing of the masonry after the yielding of the steel, sooner or later depending on the reinforcement ratio, and accordingly exhibited dissimilar load-deflection behaviour.

Liu (2002) inspected the beam-column behaviour of steel-reinforced concrete masonry walls through an experimental and theoretical program. The experimental part consisted of auxiliary laboratory tests and testing thirty nine full-scale masonry walls (three unreinforced and thirty six steel-reinforced walls) when subjected to axial load only and combined lateral and axial load. In the course of auxiliary tests, the effect of different Poisson ratios of masonry block and mortar was found to be influencing the mode of failure of the compressive masonry prisms. In some of the tests, the grouting was exposed intact after the face shell of the concrete block had spalled off at failure.

Strain of the masonry on both compression and tension sides of the walls were recorded during the tests and were used afterwards for calculation of curvature in developing moment-curvature diagrams which were eventually used to obtain the effective flexural rigidity (EI_{eff}) of the tested walls at the ultimate stage. Moreover, a finite element model was established taking into account the parameters and characteristics of the walls' constituents, such as compressive and flexural bond strength of the masonry, amount and position of the steel reinforcement, and specific stress-strain relationship of the masonry. This model was implemented to obtain the response of the walls as well as the effective flexural rigidity. Since the results of the finite element analysis showed consistency with the test results, a parametric study was performed to compare EI_{eff} for various modeled walls with values suggested by the Canadian masonry design code CSA S304.1 (2004). As a result, the code was found to be underestimating the rigidity of the walls leading to a more conservative design. In addition, it was concluded that for higher moment-to-axial force ratios, EI_{eff} reduces.

2.3 Concrete Reinforced with FRP Bars

Not until the mid-80's was FRP exploited as a new composite material to be utilized in structural engineering. However, the role of FRP in mechanical engineering and aerospace as well as auto industry had been proven to be indispensable earlier. FRP's have been examined and investigated in various applications of strengthening existing structures and reinforcing new structural components. Several research works conducted in the field of concrete and masonry structures illustrate their effectiveness in rehabilitation measures and retrofitting structures of insufficient strength. Moreover,

having several advantages compared to steel, such as higher durability and superior corrosion resistance, these composites have brought resolutions to the shortages that trouble the engineers when using steel, in particular, to reinforce concrete structural elements.

Brown and Bartholomew (1993) conducted a preliminary experimental study in order to examine the performance of concrete beams reinforced with GFRP bars. Six GFRP-reinforced concrete beams, also reinforced for shear using steel stirrups, were tested in a third-point loading setup monotonically up to failure. Pullout tests were carried out on twenty four specimens to investigate the GFRP-to-concrete bond strength. The flexural strength of the tested beams were tried to be predicted using Whitney stress block which had agreement with the experimental results. It was reported, based on the results of the tests, that the GFRP-reinforced beams exhibited a ductile behavior prior to failure, and in general, the response of the GFRP-reinforced concrete beams was quite similar to the behaviour pattern that is expected for steel-reinforced concrete beams. However, according to the results of the pullout tests, the FRP-to-concrete bond strength was approximately two third of that of steel rebars. Proper anchorage was suggested in this study to resolve this shortage, particularly when composites with higher tensile strengths are used in the design. Higher deflections at service stage (four times the deflection expected for steel-reinforced beams) due to lower modulus of elasticity of the GFRP was another deficiency of the new reinforcing bars.

Ehsani and Saadatmanesh (1996-b) carried out a research program inclusive of 102 specimens for the purpose of developing design guidelines for bond strength of GFRP bars. For this matter, forty eight beams were constructed to be tested along with

eighteen pullout specimens and thirty six hooked rebar specimens. Concrete compressive strength, cover, and cast depth, rebar diameter and embedment length, radius of bend, and tail length were considered to be the main parameters of the study. The pullout and hooked rebar specimens were subjected to tensile load that was gradually applied up to failure. The specimens were being monitored during the tests by measuring the slip between the GFRP and concrete at the loaded and free ends. The expected modes of failure were splitting of the concrete, rebar fracture, or rebar pullout failure. Based on the results of the tested specimens, design guidelines were developed for calculating the development length of the hooked and straight GFRP rods. In addition, new criteria were established to define the acceptable bond performance of the GFRP rods when used to reinforce concrete flexural members.

Laoubi *et al.* (2006) tried to investigate the creep effect and durability of GFRP bars when used to reinforce concrete flexural elements, by imposing individual and coupled presence of freeze and thaw cycles and sustained flexural stresses. For this purpose, twenty one concrete beams were designed to be reinforced with sand-coated GFRP bars and constructed to be exposed to different numbers of freeze and thaw cycles. The temperature ranged from -20 °C to +20 °C for each cycle. Some of the specimens underwent the cycles with no applied sustained load while the rest of the specimens were subjected to bending forces that produced stresses as mush as 27% of the ultimate tensile strength of the FRP bars. All the beams were tested, afterwards, in a four-point bending setup with a clear span of 1.5 m up to failure. The results of the beam tests showed that the effect of abovementioned conditionings was not significant on the flexural capacity of the GFRP-reinforced beams. Although the sustained stresses were fairly higher than the

suggested level of loading in ACI 440.1R (2006), the increase in the strain of the GFRP bars due to creep effect did not exceed 2.0% of its initial value. Furthermore, the equation introduced by ACI 440.1R (2006) for predicting the long-term deflections due to creep was proven to be overestimating the actual values found in the course of the conducted tests.

El-Ragaby *et al.* (2006) studied the fatigue characteristics of concrete bridge deck slabs, when reinforced with GFRP rebars. The experiments of this study included testing six full-scale slabs. These slabs were constructed to be subjected to different patterns of cyclic load up to the ultimate failure. Types, configuration and amount of GFRP reinforcing rebars were taken into consideration as the parameters of the program. Along with the experimental program, a thorough finite element analysis was carried out to inspect the effect of fatigue on the ultimate capacity of the GFRP-reinforced concrete slabs when subjected to static loads. It was also intended to develop a model that can predict the fatigue life of the slabs. The superior fatigue performance of the GFRP-reinforced slabs compared to steel-reinforced ones was the most important outcome of the experimental tests, which was attributed to the linear-elastic behaviour of the GFRP bars and also similar values for modulus of elasticity of concrete and GFRP rebars.

Thériault and Benmokrane (1998) investigated the effect of different FRP reinforcement ratios on the flexural performance of concrete beams by testing twelve GFRP-reinforced concrete beams. The compressive strength of the concrete was included in the study as the other major parameter. Cycles of unloading and reloading were carried out prior to failure at different stage of the applied lateral load. Beams of 1.5 m of clear span were tested in a four-point bending setup up to the ultimate failure. Tensile strain in

the GFRP bars, strain of the concrete, mid-span deflection, and crack widths and spacing were being recorded during the experiments. Based on the results of the tests and analyses performed on the response of the beams with regard to the deflection and crack width, the following equation was proposed for predicting the post-crack deflection of the beams:

$$\Delta_{mid-span} = \frac{3000L^2}{27E_c}\left(\frac{M_a}{I_m} - \frac{M_{cr}}{I_t}\right) + \frac{M_a}{20E_cI_g}\left(\frac{115L^2}{9}\right) \tag{2.1}$$

where I_m and I_t can be similarly calculated as such:

$$I_m = \frac{24I_{cr}I_{eff}}{8I_{cr}+15I_{eff}} \quad , \quad I_t = \frac{24I_{cr}I_g}{8I_{cr}+15I_g} \tag{2.2}$$

and I_{eff} is defined by this equation:

$$I_{eff} = I_{cr} + \left(I_g - I_{cr}\right)\left[1 - \left(\frac{M_{cr}}{M_a}\right)^3\right] \tag{2.3}$$

Moreover, it was suggested that the crack width can be predicted using this equation:

$$w_{crack} = 40.9 \times 10^{-5} f_{FRP} \frac{h-c}{d-c} \left(d_c A\right)^{1/3} \tag{2.4}$$

It was observed that for higher reinforcement ratios crack width (at the same level of applied moment) and residual crack width decrease. Cycles of the loading and unloading showed to have no significant effect on the stiffness of the beams. However, the GFRP reinforcement ratio seemed to have direct effect on the stiffness of the beams as the stiffness increased for higher amounts of reinforcement. Based on the strain distribution and crack pattern of the tested beams it was concluded that the GFRP bars used in reinforcing the tested beams exhibited acceptable bond behaviour with the surrounding concrete. Lastly, the deformability of the GFRP-reinforced beams was examined by

calculating the J-factor based on the experimental curvatures. The foregoing calculation proved that all the beams failed with sufficient ductility.

Benmokrane *et al.* (2006) published a brief report on designing and testing Morristown Bridge, located in Vermont, United States. The decking system of this bridge is consisted of continuous concrete slab of 280 mm thickness which was entirely reinforced with two identical layers of GFRP bars at the top and the bottom. The bridge was well instrumented and tested for standard service truck loads while the strain in the reinforcing bars and concrete as well as the deflections of the decking system were monitored. The strains recorded during the service load tests showed that the AASHTO (2000) flexural design method overestimates the service and ultimate design moments. It was also observed that the tensile strains in the concrete were maintained well bellow the cracking strains, meaning that the use of GFRP instead steel did not diminish the serviceability of the bridge. In addition to the aforesaid observations, it was highlighted by this report that transportation, handling, and placement of the GFRP bars on the site were more convenient compared to steel rebars.

Rasheed *et al.* (2006) presented a brief review on the available methods of deflection prediction for FRP-RC including the cracked section analyses and numerical methods of deflection calculation. Afterwards, a new method was proposed by the authors that estimates the deflection based on the distribution of the curvature of cracked and uncracked zones along the span of the beam. This method is established using an assumed function that defines a bilinear relationship for moment-curvature where the cracking differentiates the two segments of the moment-curvature diagram. The proposed model is developed for three particular common loading situations, four-point bending,

three-point bending, and uniform loading. Then, in order to verify the accuracy of the proposed method, experimental results of FRP-reinforced concrete beams tested by other researchers were compared to the predictions of the currently available methods and the proposed one. Figure 2.3 illustrates the comparisons for two beams with different reinforcement ratios. It can be seen that for higher amounts of reinforcement ratios, all the methods of deflection prediction provide very close results while for lower amounts of reinforcements the results of the predictions done by different methods are diverse.

Design manual number three of ISIS (2001) presents a comprehensive guideline for designing concrete structures reinforced with FRP's. This manual provides the codified methods of flexural and shear design, crack width calculation, and deflection prediction based on a cracked section effective moment of inertia. In addition, different serviceability criteria such as maximum allowable deflection and crack width and minimum required deformability are defined therein. Lastly, as one of the most important features of this design manual, a number of diagrams are included that can be used for flexural design of FRP-RC members. Figure 2.4 illustrates a sample design diagram for a specified type of GFRP rebar, where the reinforcement ratio that is needed for a given section in order to satisfy the required flexural strength can be found.

2.4 Use of FRP to Strengthen and Reinforce Masonry Walls

Ehsani *et al.* (1993) are considered to be the pioneers in the field of seismic retrofitting of URM walls using composite fibres. Six clay brick masonry beams with a clear span of 1.19 m, representing single-wythe clay masonry walls with stack bond, were built and afterwards strengthened with three different types of glass fabrics. Type of

fabrics, type of mortar, overall surface roughness of the walls, and age of the masonry units were taken into account as the major parameters of the research. Beams were tested in a four-point out-of-plane bending setup accordingly. Substantial improvement in flexural strength, as much as twenty four times the self-weight of the beams, and deflections, as much as 1/48 times the span, were of the outcomes of the experiments. Later, Ehsani and Saadatmanesh (1996-a) integrated the same technique to strengthen the existing masonry walls in shear by testing series of specimens that consist of three running bond clay bricks.

Mierzejewski *et al.* (2008) investigated the behaviour of strengthened URM walls made of hollow concrete blocks under out-of-plane bending. Different types of materials, including GFRP bars mounted in the pre-cut grooves and carbon-fibre reinforced polymer (CFRP) strips epoxy glued on the surface of the specimens were examined and compared to each other. Besides the significant increase in capacity and ductility, increasing the effective depth of the reinforcement by spreading them away from neutral axis and also avoiding grouting the cells were the other substantial advantages of the suggested methods. Near-surface mounted (NSM) reinforcement instead of internal reinforcement was also proposed as a new approach in constructing reinforced masonry providing that blocks with moulded grooves could be fabricated.

Comparable experiments were reported by Galati *et al.* (2006) in which they investigated the improved performance and modes of failure of URM walls strengthened with NSM FRP bars considering different composite materials (GFRP and CFRP), ratios, and shapes (circular and rectangular) as well as embedding details as the main parameters

of the study. It was proven that "flexural strengthening with FRP systems" enhances the flexural strength and pseudo-ductility of masonry walls to a great extent.

Turco *et al.* (2006) conducted a similar study that concerns the issue of retrofitting URM for shear and flexure walls with NSM FRP bars asserting the conclusions drawn by the aforementioned researchers.

Several researchers have carried out experimental studies that assess the use of externally bonded FRP whether it be sheets or fabrics of GFRP or CFRP (Gilstrap and Dolan (1998), Hamoush *et al.* (2001), Hamoush *et al.* (2002), Kiss *et al.* (2002), Galal *et al.* (2003), Ghobarah and Galal (2004), and Tan and Patoary (2004)). Remarkable boost to the out-of-plane load-carrying capacity and ductility of unreinforced and steel-reinforced masonry walls, despite the brittle behaviour of both FRP and masonry assemblage, is the common major outcome that can be found in all of them while parameters such as thickness of the layers, adhesive material, surface preparation method, and surface mounting approach were the decisive variables in the experiments.

As mentioned earlier, to the author's knowledge, there is not much work in the previous literature associated to reinforcing masonry walls using FRP and in particular, there have been no efforts to employ FRP as internal reinforcement in masonry structural elements.

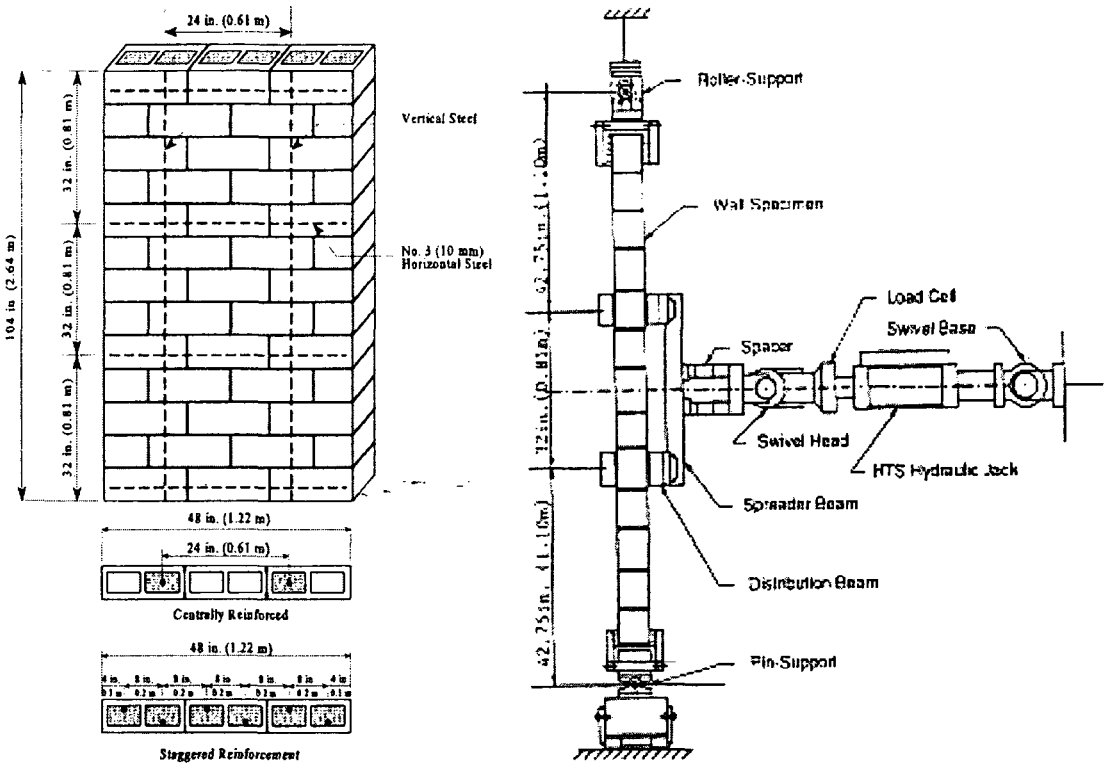

Figure 2.1. Steel-reinforced masonry walls tested under out-of-plane lateral load: (a) test specimen; (b) test setup (Abboud *et al.* (1996))

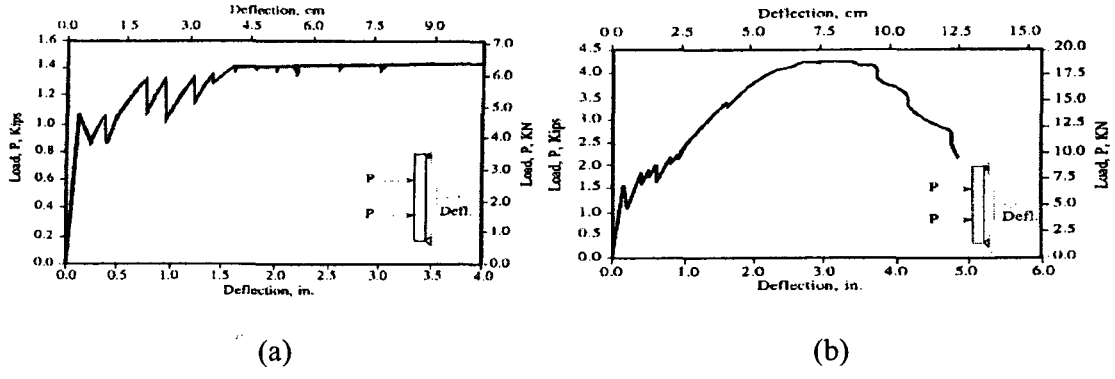

Figure 2.2. Load-deflection curves of tested steel-reinforced masonry walls with: (a) reinforcement ratio of 0.19%; (b) reinforcement ratio of 0.44% (Abboud *et al.* (1996))

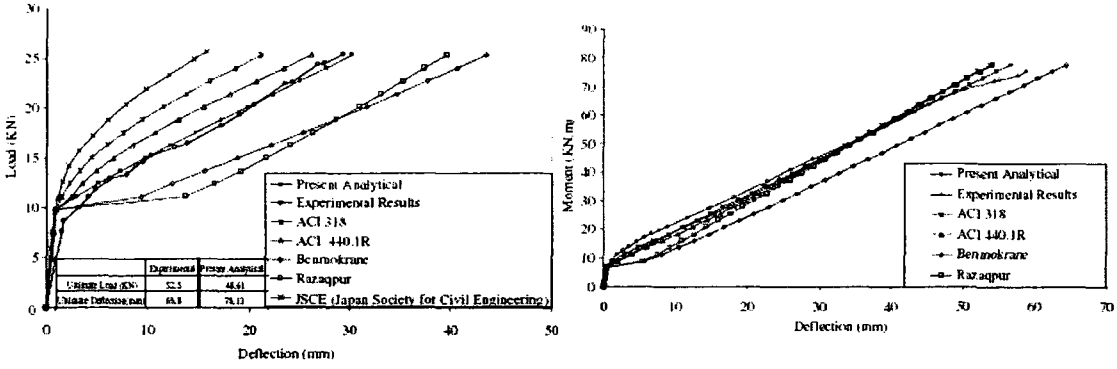

(a) (b)

Figure 2.3. Load-deflection prediction for FRP-RC flexural members by the currently available methods: (a) reinforcement ratio 0.23% (b) reinforcement ratio 0.40% (Rasheed *et al.* (2004))

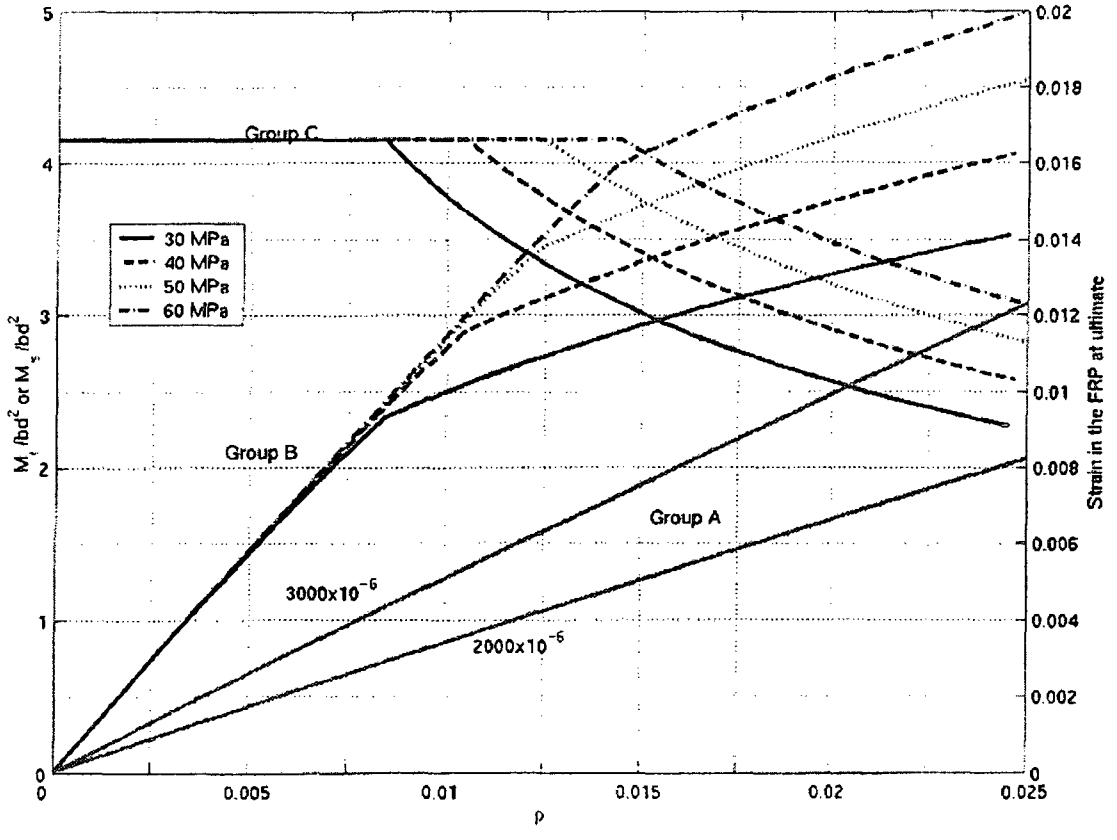

Figure 2.4. Sample capacity diagram for designing GFRP-reinforced concrete member for flexure ($f_{u,FRP}$ = 747 MPa, E_{FRP} = 45 GPa) (ISIS (2001))

CHAPTER 3

EXPERIMENTAL PROGRAM AND AUXILIARY TESTS

3.1 General

The experiments that are carried out as a part of this study mainly consist of two parts: a) the auxiliary tests that are meant to provide the structural characteristics of the construction materials and also the whole masonry compound, and b) main tests that include testing eight full-scale masonry walls that are GFRP-reinforced, steel-reinforced, and unreinforced. All the auxiliary specimens (masonry prisms) and full-scale walls were constructed by domestic professional masons (registered with l'Association des Entrepreneurs en Maçonnerie du Québec (AEMQ)) representing the current method of practice in Québec during four consecutive days.

3.2 Auxiliary Laboratory Tests

3.2.1 Concrete Masonry Units

The masonry unit that is used in this study is hollow concrete block available by domestic supplier (Simard-Beaudry (2008)) with nominal dimensions of 390×190×190 mm. The minimum nominal compressive strength of the unit is 15 MPa and the average net-to-gross area ratio is 0.54 as per the supplier's provided specifications.

3.2.2 Mortar

Type S mortar which is a mixture of 0.5 volumetric units Portland cement, one unit masonry cement, 2.9 units sand, and 0.7 units water was chosen after several trial

mixtures to be conforming with the requirements brought in ASTM C270 (2002) and CSA A179 (2004). Since the compressive strength of the mortar was highly sensitive for each day of construction a series of six mortar 50 mm cubes were sampled and tested at the age of 7 and 28 days according to ASTM C780 (2002). The average 7-day and 28-day compressive strengths obtained were 8.6 MPa and 20.7 MPa, respectively. The former should not be less than 7.5 MPa and the latter should not be less than 12.5 MPa according to CSA A179 (2004) and ASTM C270 (2002) for laboratory made mortar cubes.

3.2.3 Grout

The grout used in the program, categorized as "coarse grout" in accordance with CSA A179 (2004) and ASTM C476 (2002), was mixture of one volumetric unit Portland cement, 2.8 units fine aggregate (sand), two units coarse aggregates with the maximum size of 7 mm (¼"), and 0.9 units water. The average compressive strength at the age of 28 days was 21.6 MPa. Slump test of fluid grout was done every day of the construction period reporting 260mm to 280mm slump that assures the lower limit in the Canadian code (CSA A179 (2004)).

3.2.4 Compressive Strength of Masonry

In order to determine the compressive strength of the masonry assemblage a series of five unreinforced grouted prisms were tested as stated in ASTM C1314 (2002). It was decided to build five-block high and one-block wide prisms for this purpose to minimize the influence of slenderness by providing a central uniform stress zone so that the prism is a better representative of the real circumstances in the walls (Chen (2002), and

Drysdale and Hamid (2005)). The axial deformation over a gauge length of 600mm on both sides of each prism was acquired by displacement transducers (potentiometers) and recorded as well as the applied load continuously up to the failure point. Figure 3.1 shows the masonry prisms to be tested in compression and flexure. The summary of the related results are tabulated in Table 3.1 and the failures at ultimate as well as the axial load-strain curves for the tested prisms are shown in Figure 3.2 and Figure 3.3. The average compressive strength (f'_m) from the tests was 10.9 MPa with a coefficient of variation of 6.4% neglecting the result of the second prism. The Young's modulus (E_m) of the prisms is also determined to be 6.0 GPa based on a Secant line between 5% and 33% of average ultimate load. CSA S304.1 (2004) specifies E_m using 850× f'_m equal to 9.2 GPa which overestimates the reported value, so does MSJC (2005) using 900× f'_m giving 9.8 GPa. Typical splitting of the concrete blocks was observed as the dominant mode of failure initiated by cone and shear cracks. Previous studies has attested that the properties of the grout are of the major factors affecting the failure of grouted concrete masonry which may occur even at lower stress levels compared to ungrouted concrete masonry (Dhanasekar and Shrive (2002)). The relatively lower strength of the prisms of this program, compared to their constituents, can be attributed to the excess of grout expanding inside the cells that resulted in splitting the face shells. The grout cores that were found intact at the end of all five tests also account for this observable fact.

3.2.5 Flexural Bond Strength of Masonry

For the purpose of estimating the cracking moment of the walls, another series of five prisms were tested by third-point loading method described in ASTM E518 (2002).

Prisms with the height of seven blocks and width of one block were tested such as to locate the two point loads and supports in the middle of the block and also to provide for sufficient span-to-depth ratio (ASTM E518 (2002)). The mid-span deflection of the prisms was measured during each test using a potentiometer to establish the load-deflection curves in Figure 3.5. The average flexural bond strength of the prisms, also referred to as modulus of rupture (R), was found to be 1.11 MPa with a coefficient of variation of 9.5% disregarding the result of the last prism (see Table 3.2). Table 3.3 summarizes the properties of the masonry assemblage and its constituents. The failed prisms are depicted in Figure 3.4.

3.3 Tests on Full-Scale Masonry Walls

The main part of the experimental program in this study consists of testing eight full scale walls under out-of-plane bending.

3.3.1 Description of the Walls

Each specimen is a single-wythe masonry wall with nominal dimensions of 1m×3m that is made of 15 courses of two and a half concrete blocks with half running bond. Figure 3.6 contains photos of construction of the masonry walls that was done by AEMQ certified masons.

As shown in Table 3.4 and Figure 3.7, the first wall is unreinforced, the second wall is reinforced with customary steel rebars, and the other six walls are reinforced with different GFRP reinforcement ratios. The wall designation refers to: 1) type of reinforcement (Steel, GFRP, or Unreinforced), 2) number and size of the rebars, and 3)

the extent of grouting (Full or Partial). Wall G-3#13-P and G-4#13-P are identical, with regard to the reinforcement ratio, to wall G-3#13-F and G-4#13-F, respectively; yet they are only grouted at the locations of the longitudinal reinforcements, to study the effect of not grouting the empty cells. This is the common method of practice in construction of steel-reinforced concrete masonry walls; since, due to the height of the wall it is not practical to have the reinforcing rebars in place and pass the concrete blocks through, afterwards. Bed joint reinforcement that consisted of truss type 3.2 mm (⅛") gauge wire was placed in every other joint (with a spacing of 400 mm) for all the main specimens. The walls were designed to have adequate shear capacity in that a compression failure in concrete block due to flexural action was intended to be the dominant mode of failure. The longitudinal reinforcing bars were pushed into the grouted cells right after grouting the cells.

Table 3.5 shows the properties of the GFRP rods as provided by the supplier (Pultrall (2007)), and Figure 3.8 depicts the three different diameters used in the experimental program. 400 MPa steel rebars were used in reinforcing wall S-5M10-F. Walls were constructed, cured, and hardened vertically. Afterwards, they were transferred and laid horizontally on the setup using a steel braced frame designed for this purpose.

3.3.2 Test Setup and Instrumentation

The main specimens were tested in a third-point loading setup, shown schematically in Figure 3.9 and Figure 3.10, with an effective span of 2.4 m. Two point loads, at third spans, were applied and monotonically increased by a 15-ton hydraulic actuator, reacting against a rigid steel loading frame, up to the ultimate failure. Load was

transferred through the loading apparatus and applied over two 152.4 mm (6″) wide channels to avoid crushing the blocks due to stress concentration. The walls were tested while positioned horizontally on a hinge at one end and a roller at the other end (see Figure 3.11 and Figure 3.12), similar to previous tests on masonry walls performed by several researchers (e.g. Gilstrap and Dolan (1998), Kiss *et al.* (2002), Hamoush *et al.* (2002), Tan and Patoary (2004), and Galati *et al.* (2006)). The reason was that it was not as convenient and secure to test the walls vertically. Potentiometers were located to measure the displacement at ten different points of each tested wall (three at mid-span, six at third-spans and one at quarter-span), in order to obtain the longitudinal profile of the wall at various load levels and also to ensure that the wall is not tilted or twisted in width due to probable test setup imperfections. The maximum axial strain, assumingly in the mid-span, for every reinforcing rod (GFRP and steel) was recorded using strain gauges that had been installed on the rods before construction. Furthermore, the strain in two of the reinforcing rods for each reinforced wall at quarter-span was recorded.

3.3.3 Testing Procedure

Since the self-weight of the walls, compared to their nominal capacity, was considerable, walls were rested prior to the loading commencement properly over a set of temporarily wooden supports. These supports were removed after the data acquisition system had launched recording the applied load, deformations, and tensile strains (in the case of reinforced walls) so that the deformations and strains due to the own weight of the walls would not be missed. Afterwards, the out-of-plane lateral load was applied and increased monotonically until the ultimate failure of the wall occurred. After the failure

of four walls (including the steel-reinforced specimen), the load was removed to determine the permanent (i.e. inelastic) portion of total displacement. Three of them were reloaded gradually to examine the post-failure strength of the specimen. In order to avoid any unwanted incident, the unloading and reloading process was not done for all of the walls. Lastly, the failed walls were to be removed in a secure manner and the exact location of the reinforcing bars (in the cross section of the reinforced walls) at the section where failure had occurred were measured to aid the analyses.

Table 3.1. Summary of the test results for the compressive prisms

Prisms	Failure load (kN)	Compressive Strength (MPa)	Axial strain at max. compressive stress ($\times 10^{-6}$)
1	707.2	11.6	1680
2	538.3	8.9	1862
3	596.3	9.8	2041
4	687.0	11.3	2416
5	651.6	10.7	2044

Table 3.2. Summary of the test results for flexural auxiliary prisms

Prisms	Failure load (N)	Modulus of rupture (MPa)
1	11890	1.06
2	12232	1.09
3	14456	1.28
4	11120	0.99
5	8117	0.74

Table 3.3. Properties of the masonry assemblage and its constituents

Characteristic	Average (MPa)	C_v (%)
Compressive strength of masonry unit	15.0	—
Compressive strength of mortar	20.7	26.2
Compressive strength of grout	21.6	3.9
Compressive strength of masonry assemblage (f'_m)	10.9	6.4
Modulus of rupture of masonry assemblage (R)	1.11	9.5

Table 3.4. Matrix of the full-scale masonry walls

Wall	Reinforc. material	Average effective depth (mm)		Reinforc. ratio (%)		Extent of grouting
		Nominal	Measured	Nominal	Measured	
U-F	—	—	—	—	—	Fully
S-5M10-F	Steel	95	90	0.53	0.56	Fully
G-3#10-F	GFRP	95	95	0.25	0.25	Fully
G-3#13-F	GFRP	95	100	0.42	0.40	Fully
G-3#13-P	GFRP	95	105	0.50	0.45	Partially
G-4#13-F	GFRP	95	105	0.56	0.51	Fully
G-4#13-P	GFRP	95	125	0.61	0.46	Partially
G-3#19-F	GFRP	95	125	0.89	0.69	Fully

Table 3.5. Properties of the GFRP rods used in this program as provided by the supplier (Pultrall (2007))

Diameter (mm)	Tensile modulus of elasticity (GPa)	Ultimate tensile strength (MPa)	Ultimate tensile strain ($\times 10^{-6}$)
10	45.4	856	18900
13	46.3	786	17000
19	47.6	728	15300

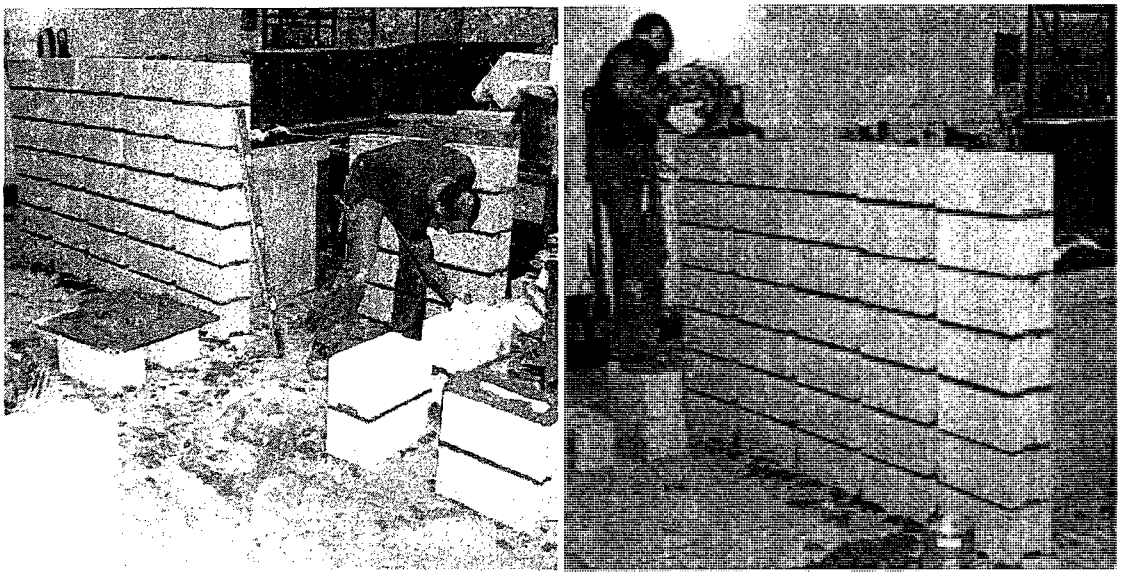

(a)

(b)

Figure 3.1. Masonry auxiliary prisms to be tested in compression and flexure: (a) construction of the prisms; (b) after construction

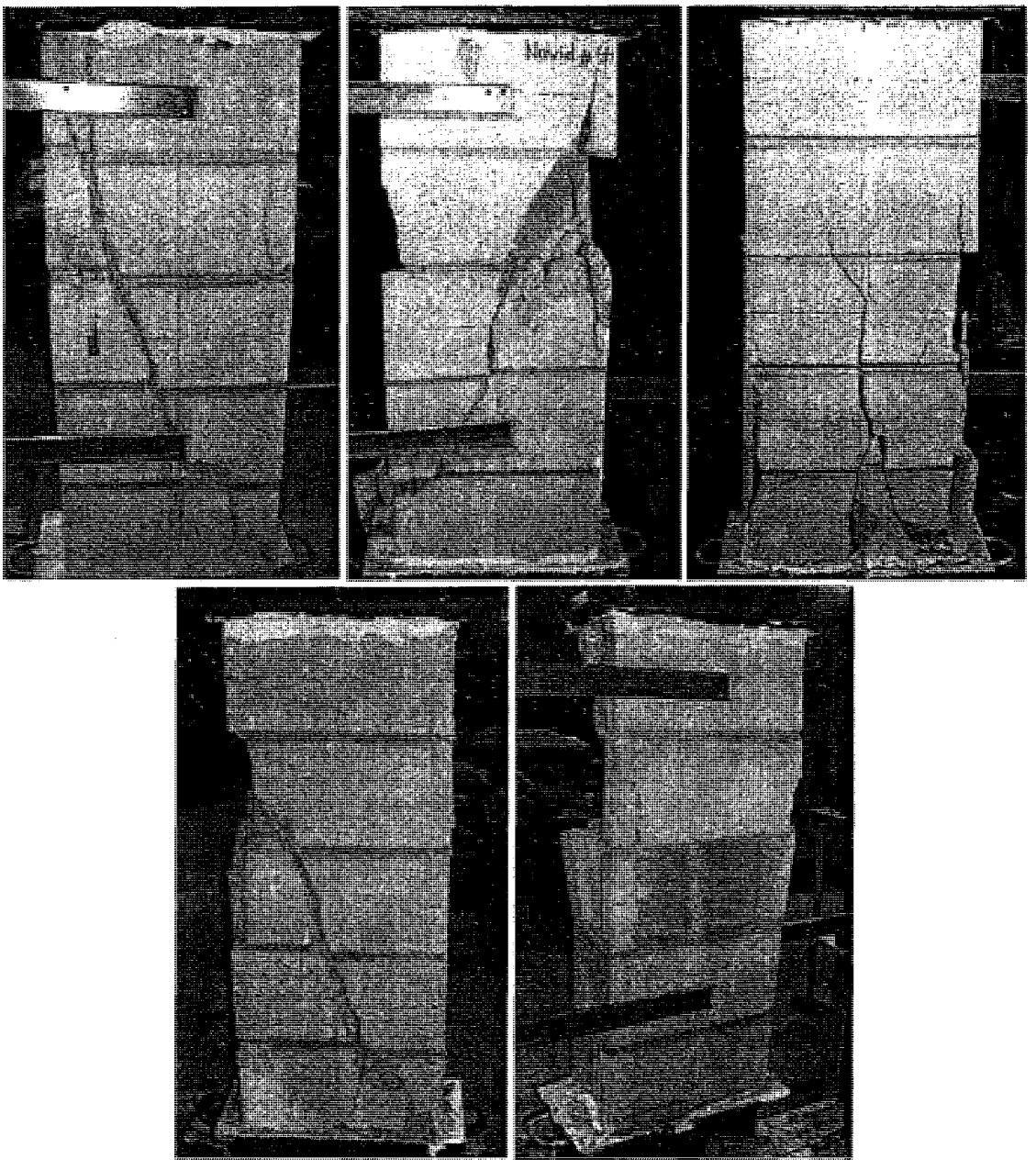

Figure 3.2. Compressive masonry prisms at failure

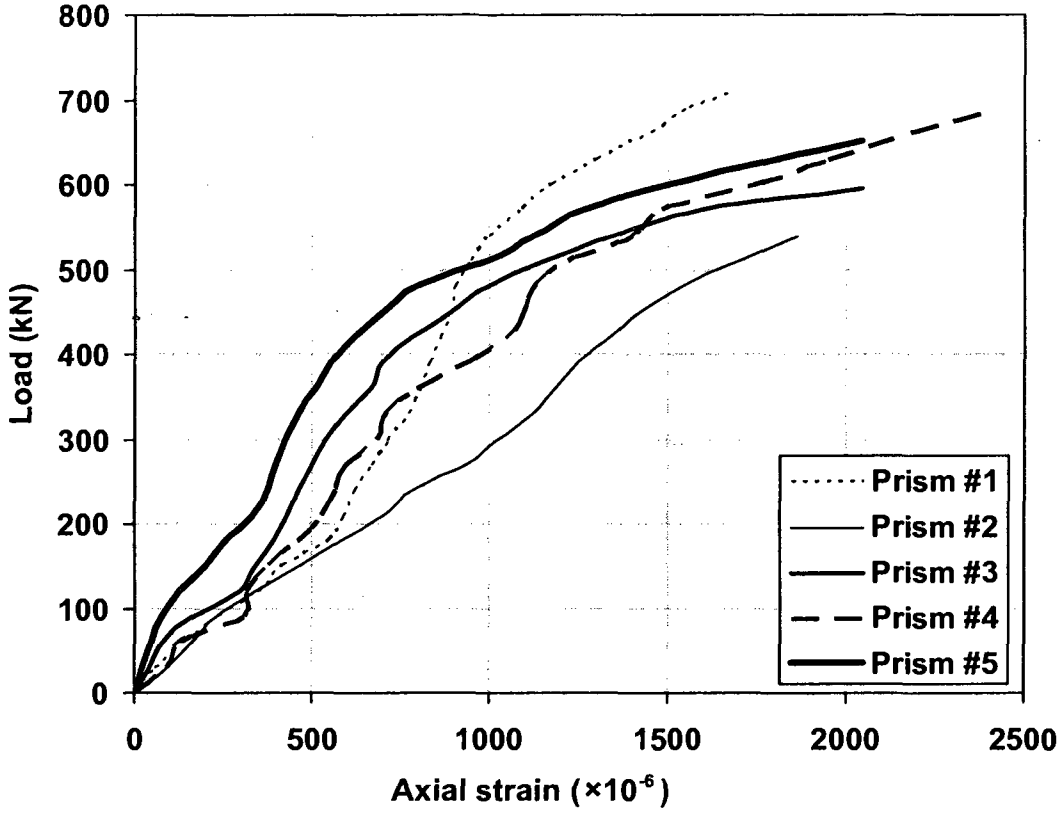

Figure 3.3. Results of the compressive masonry prisms

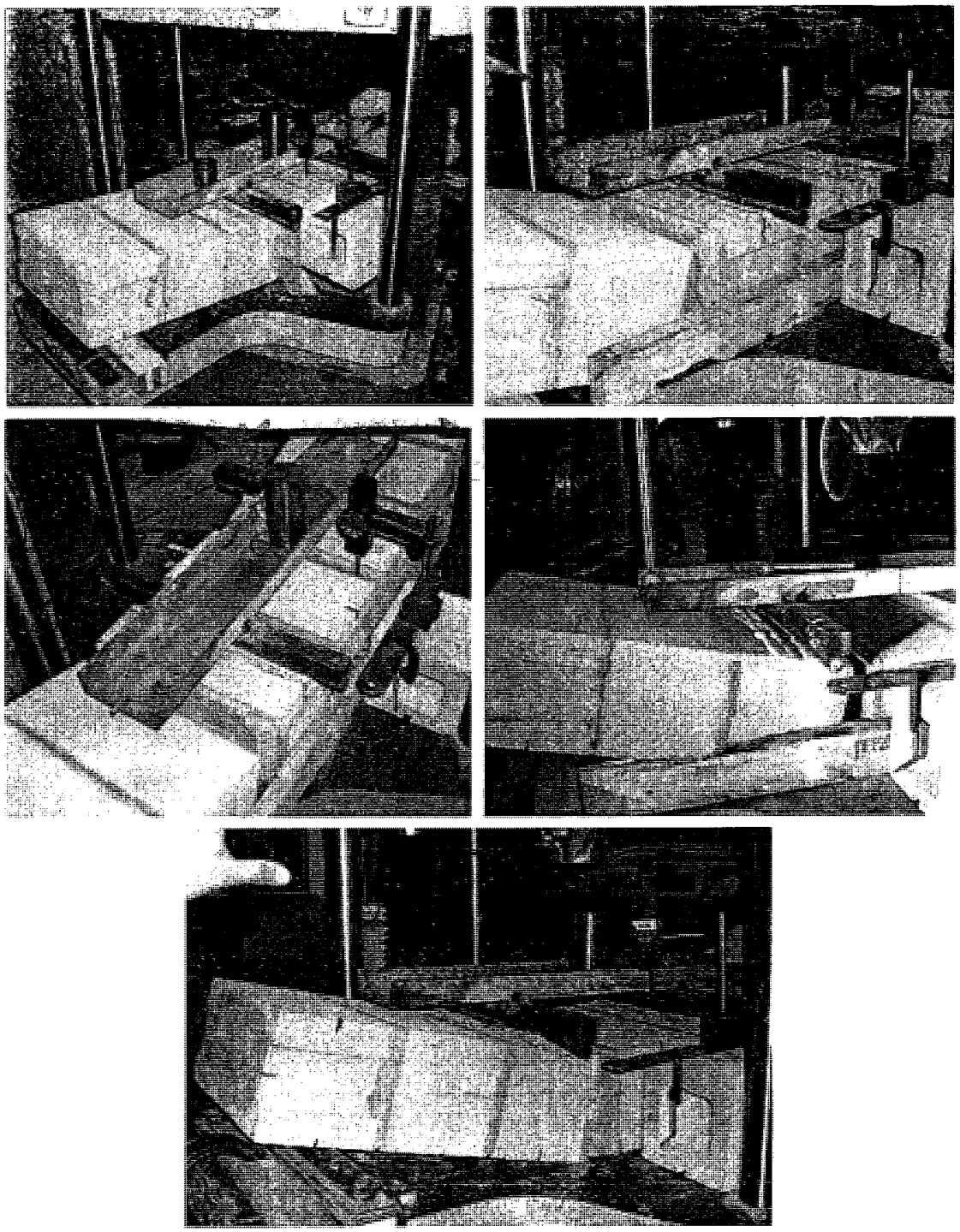

Figure 3.4. Flexural masonry prisms at failure

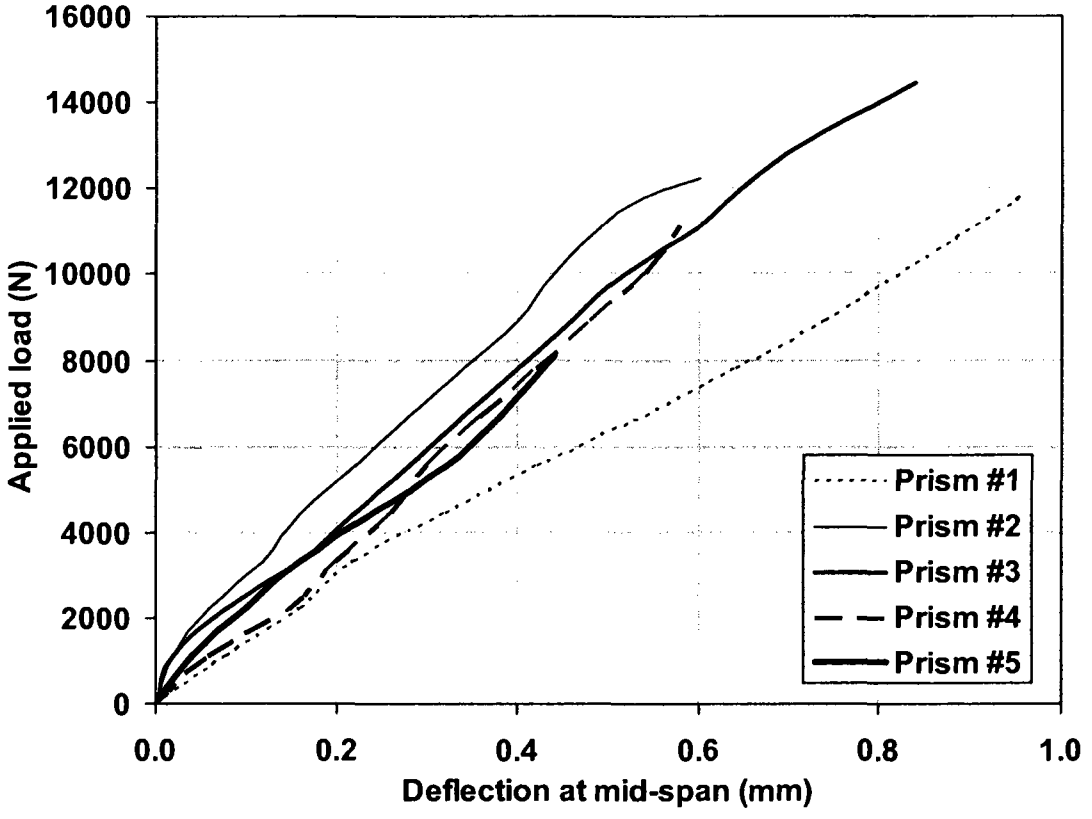

Figure 3.5. Results of the flexural masonry prisms

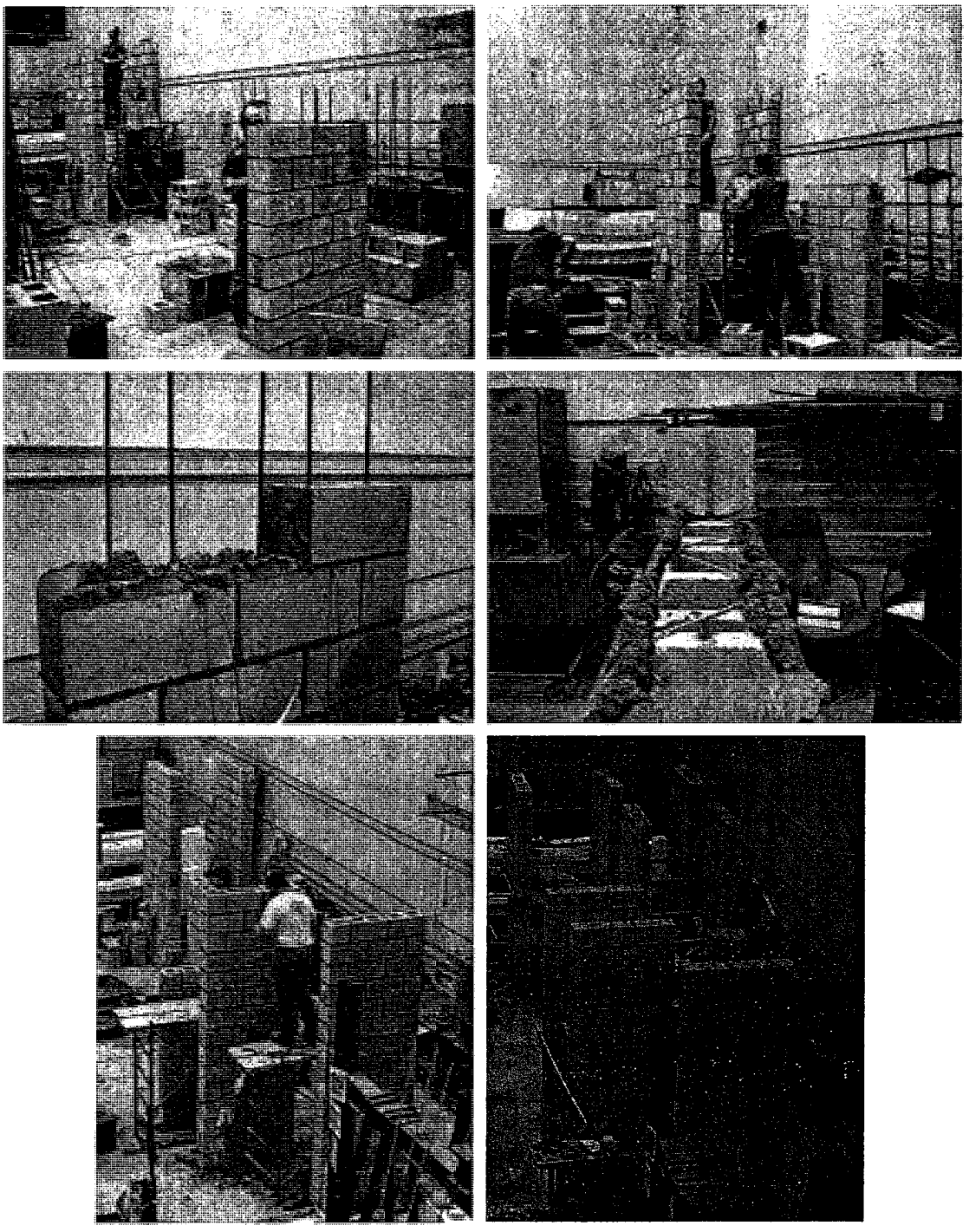

Figure 3.6. Construction of the full-scale masonry walls to be tested under out-of-plane bending

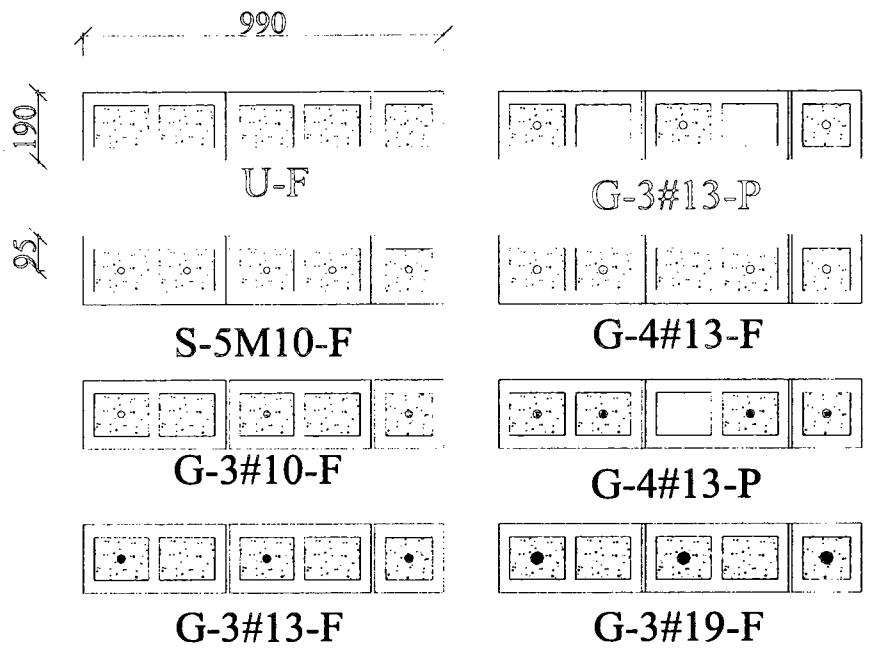

Figure 3.7. Cross-sections of the eight tested masonry walls

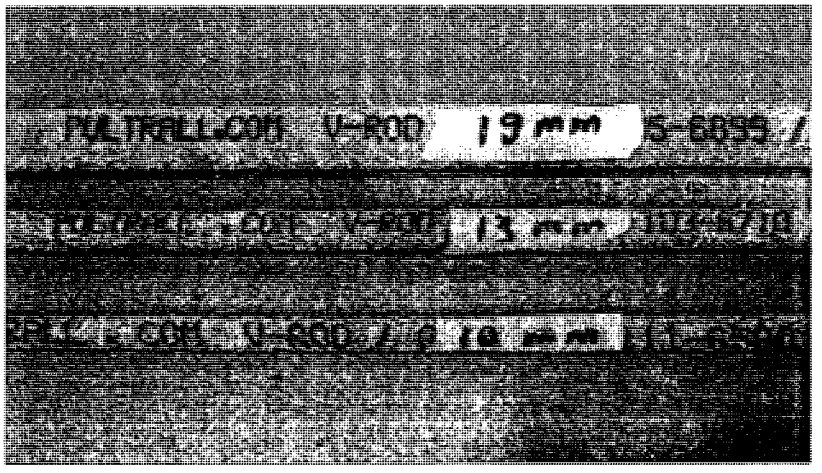

Figure 3.8. The GFRP rods used in this program

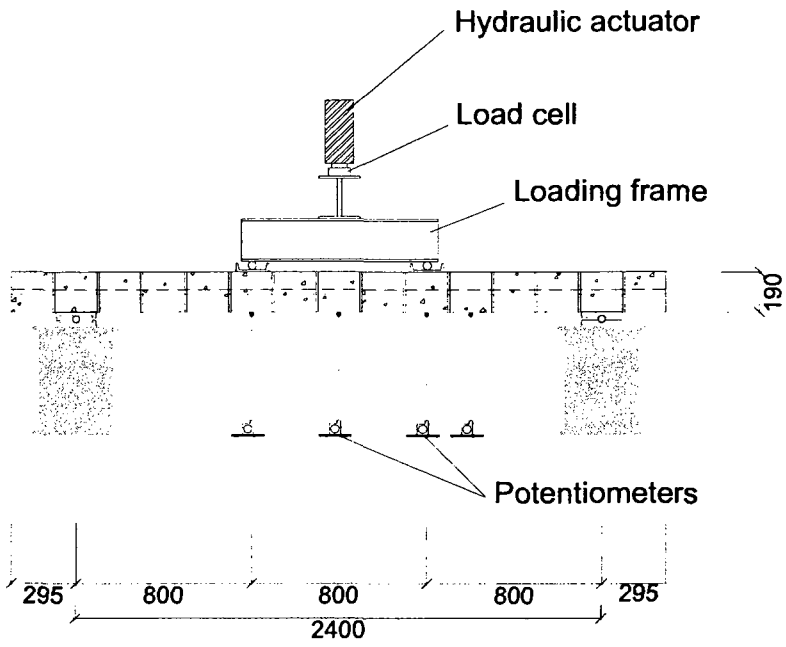

Figure 3.9. Schematic elevation view of the test setup for the eight tested walls

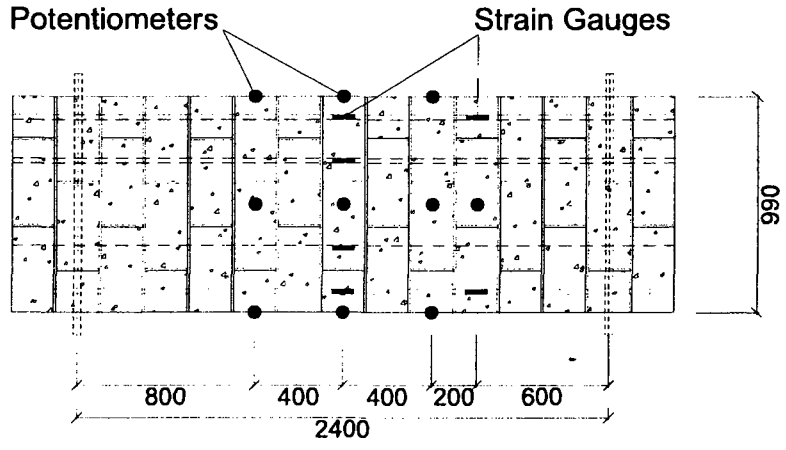

Figure 3.10. Schematic plan view of a typical wall reinforced with 4 rods, showing the instrumentation (i.e. 10 potentiometers and 6 strain gauges)

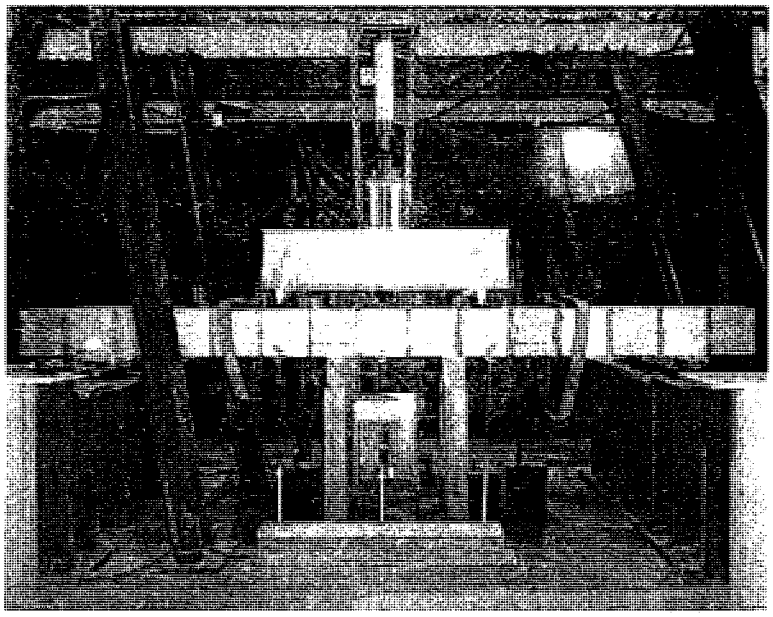

Figure 3.11. Elevation view of the test setup

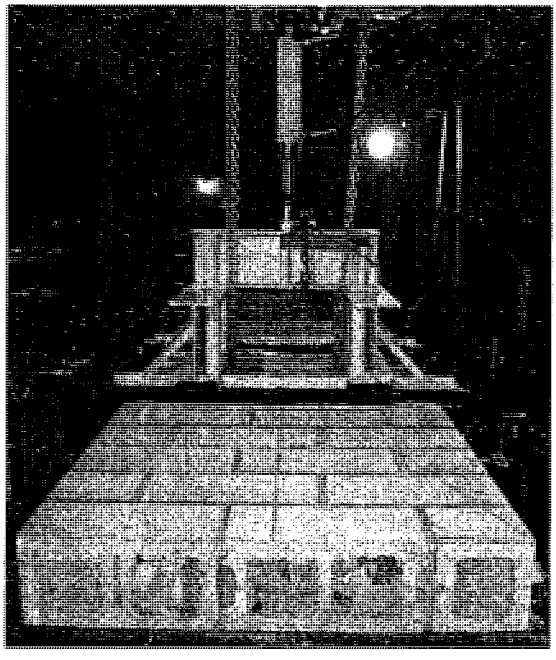

Figure 3.12. Side view of the test setup

CHAPTER 4

RESULTS OF THE WALL TESTS AND DISCUSSIONS

4.1 General

This chapter is divided into two main parts. The results and observations of the wall tests are described individually for each wall in the first part. The second part is allocated to the discussions and comparisons about the qualitative behaviour of the eight walls.

4.2 Results of the Eight Tested Walls

The test results of the eight full-scale masonry walls are presented in the following sections, starting with the control specimens and followed by the GFRP-reinforced ones (with ascending reinforcement ratio). Photos of the wall at different stages of loading and deformed longitudinal profiles of the wall prior to and at failure associated to each specimen as well as force-deformation and force-tensile strain curves (exclusively for reinforced panels) are shown.

During the tests, no notable relative deformation was observed along the width of the walls, nor did appear any sign of torsional deformations. Thus, the recorded displacement of mid-span, third-spans and quarter-span of the centerline were employed in developing the longitudinal profile of the walls. For the purpose of drawing the force-deformation curves, one of the three points in the mid-span (i.e. center and the sides) whose deflections were being measured continuously by the potentiometers was selected, based on the observations during the tests, to be the reference of the data; inasmuch as

different phenomena in some of the tests (e.g. local crushing, spalling, or separation) close to the failure, lead to misrepresenting the overall deformed shape of the wall in one of the three mid-span reading points. As for the force-strain curves, the mid-span strain of the rod that had the closest effective depth to the average effective depth of all the reinforcing rods was chosen to be the reference of the data. It should be mentioned that in the following sections, the term "deflection" is shortly referring to the deflection of the mid-span according to the referenced potentiometer of each wall.

The average self-weight of the fully-grouted walls was calculated, based on the weight of a portion of tested walls, to be 12.3 kN. This could produce the same moment as 10.2 kN of applied lateral load does. The self-weights of walls G-3#13-P and G-4#13-P were similarly found to be 6.9 kN and 11.0 kN, equivalent to 6.1 kN and 9.2 kN of applied lateral load, respectively. The weight of the loading apparatus and hydraulic actuator, total amount of 1.2 kN, is also included in calculating the equivalent dead load.

Table 4.1 contains the chronicled order of the tests of the eight masonry walls.

4.2.1 Wall U-F

Wall U-F was designed to have no reinforcement and completely grout-filled. It was expected to fail no sooner than the cracking moment was reached by the applied load added to the self-weight of the wall. A sudden failure took place at the total moment of 5.6 kN.m. Maximum applied lateral load of 3.8 kN at failure is only 0.4 times the equivalent dead load of the wall. The mid-span deflection of the wall at failure was 1.4 mm. Figure 4.1 illustrates wall U-F before and after failure, in addition to the failed section.

4.2.2 Wall S-5M10-F

This wall was reinforced with five 10M steel rebars (nominal reinforcement ratio of 0.53%), having one rebar in every cell of the cross-section. The first crack appeared when the moment reached 6.9 kN.m, in one of the mortar-to-block bed joints inside the maximum moment zone; the rebars started to yield at the moment of 14.4 kN.m and corresponding deflection of 15.5 mm; and lastly, the loading process was stopped, due to displacement restrictions of the setup, as the wall was experiencing 16.9 kN.m of moment and 143.2 mm of deflection. The flexural cracks in the bed joints were widely opened at that stage, as can be seen in Figure 4.2. Another interesting observation was that except the two bed joints next to the point load (with maximum shear forces), none of the joints outside the zero-shear region cracked, nor did occur any shear crack on the sides of the concrete blocks. The maximum applied lateral load of 32.1 kN represents 3.2 times the equivalent dead load of the wall. The reinforcement ratio based on the actual effective depth of the wall was found to be 0.56%.

The load was removed, later on, to obtain the elastic deflection of the wall. Aresidual deflection of 131.1 mm was obtained after the load removal. It was unnecessary to reload the wall; because, theoretically, steel-reinforced wall should achieve the same level of applied load. The lateral load versus the out-of-plane deformation and tensile strain of the steel rebars are shown in Figure 4.3. It also depicts the deformed shape of the wall early after yielding to the point the loading stopped.

4.2.3 Wall G-3#10-F

The first wall to be tested was the one with the least amount of GFRP reinforcement, three 10-mm GFRP rods (nominal reinforcement ratio of 0.25%). This specimen was fully grouted and the rods were located in the middle cell, as well as the cells on the sides of the section. The flexural cracks in the constant moment zone set off after the wall encountered bending force of 6.0 kN.m. Significant opening in one of the joints was followed by crushing the upper face shell of the blocks (see Figure 4.4) at bending moment of 14.2 kN.m accompanied by 111.4 mm of deflection. The final lateral load of 25.4 kN is 2.5 times the equivalent dead load of the wall. The actual reinforcement ratio happened to be the same as expected. The load-deflection and load-strain performances of the wall can be seen in Figure 4.5. It also depicts the deformed shape of the wall early after the first cracks up till the ultimate failure.

4.2.4 Wall G-3#13-F

The number and location of the reinforcing bars of wall G-3#13-F, with nominal reinforcement ratio of 0.42%, were similar to those of wall G-3#10-F, while the diameter of the GFRP bars used here was 13 mm. This specimen was also fully grouted. Not until the wall underwent 7.6 kN.m of bending moment did the flexural cracks start to appear. Notable shear cracks in the masonry blocks were propagated outside the constant moment region prior to the failure. As shown in Figure 4.6, a long and fairly wide crack grown diagonally on top of the wall between the point loads manifested the failure of the wall at the moment of 18.3 kN.m with corresponding deflection of 107.4 mm. The final lateral

load of 35.4 kN is approximately 3.5 times the equivalent dead load of the wall. The actual reinforcement ratio was found to be 0.40%.

100 mm of deflection was maintained after the applied load was removed. Afterwards, the wall was reloaded gradually and reached the maximum bending moment of 6.3 kN.m. The lateral load versus the out-of-plane deformation and tensile strain of the GFRP rods are shown in Figure 4.7. It also displays the deflected shape of the wall at different stages of the test.

4.2.5 Wall G-3#13-P

Identical to wall G-3#13-F, wall G-3#13-P was only grout-filled in the cells accommodating the three 13-mm GFRP rods (i.e. the middle and side cells). First crack in the bed joints was initiated once the wall reached 4.3 kN.m of bending moment. Less shear cracks on the sides of the blocks were monitored, compared to the previous panel. Compressive failure was preceded by one side of the wall breaking off completely along the constant moment region (see Figure 4.8). Failure moment and deflection were reported 17.9 kN.m and 108.5 mm, respectively. The final lateral load of 38.6 kN is approximately 6.3 times the equivalent dead load of the wall. The actual reinforcement ratio was found after measuring the average effective depth to be 0.45% while the nominal reinforcement ratio was meant to be 0.50%

After unloading the wall 66.7 mm of deflection was still residual; and, the total bending moment did not exceed 8.3 kN.m when the lateral load was applied again to the wall gradually. The corresponding load-deflection and load-strain curves are illustrated in

Figure 4.9. The deformed shape of the wall early after the first cracks untill the ultimate failure can be seen as well.

4.2.6 Wall G-4#13-F

Wall G-4#13-F was designed to have 0.56% of reinforcement ratio, provided by four GFRP rods of diameter of 13 mm. Although the middle cell was not accommodating any rod, it was filled with grout as well as the other four cells. The first bed joint cracked in the same way in the constant moment zone after the wall encountered bending force of 5.8 kN.m. The very same joint had widened remarkably just before the typical compressive failure of the masonry manifested itself (see Figure 4.10), once the bending moment of 21.7 kN.m and deflection of 108.9 mm were attained. The final lateral load of 44.0 kN is just as much as 4.3 times the equivalent dead load of the wall. The actual reinforcement ratio was eventually found to be 0.51%. The lateral load versus the out-of-plane deformation and tensile strain of the reinforcing GFRP rods are demonstrated in Figure 4.11. It also depicts the deformed longitudinal profile of the wall early after initial cracks until the ultimate failure of the wall.

4.2.7 Wall G-4#13-P

Wall G-4#13-P, analogous to the previous specimen, was only grouted partially. The reinforcement ratio was designed to be 0.61%. Despite the fact that the first crack was detected when the bending moment was 4.5 kN.m, the slope of the force-deformation curve was diminished after the wall undertook 5.9 kN.m of bending force. As displayed in Figure 4.12, similar to wall G-3#13-F, a diagonal crack on the upper side of the wall

exhibited the compressive failure of the masonry at the moment of 30.3 kN.m with corresponding deflection of 94.3 mm. Trivial shear cracks were observable on the sides of the blocks close to failure. The final lateral load of 66.5 kN is about 7.2 times the equivalent dead load of the wall. The actual reinforcement ratio was found to be 0.46% after measuring the actual depth of the rebars. The load-deflection and load-strain curves associated to wall G-4#13-P are demonstrated in Figure 4.13. It also displays the deformed shape of the wall at three different levels of loading including the ultimate failure.

4.2.8 Wall G-3#19-F

Wall G-3#19-F, with the highest amount of GFRP reinforcement, was reinforced with three 19-mm rods in the middle and side cells. It was also fully grouted and designed to have 0.89% of GFRP reinforcement ratio. Cracking moment and the ultimate bending capacity of the wall were found to be 6.2 and 39.3 kN.m, respectively. The maximum deflection that was recorded before the failure was 93.6 mm. While the wall failed due to crushing of the blocks in the constant moment zone, the only notable observation was the considerable width of the shear cracks in the blocks. The maximum bending moment corresponds to the applied lateral load of 88.2 kN which represents 8.6 times the self weight of the wall.

After the load was removed, the remaining deflection was reported 60.1 mm. The post-failure flexural strength of the wall was found to be 18.6 kN.m once the wall was reloaded. Pictures corresponding to this wall test are gathered in Figure 4.14, while

Figure 4.15 shows the force-deformation and force-strain diagrams as well as the deflected profile of the wall.

4.3 Discussions on the Qualitative Behaviour of the Eight Tested Walls

The following sections discuss the qualitative behaviours of the eight tested walls; and useful comparisons are made between the walls concerning different aspects of their behaviour. To begin with, crack patterns and deformed shape of the tested walls will be discussed. The second part is expressing the relative performance of the walls in which both lateral deflection and tensile fibre strain versus the applied load are demonstrated in different series of comparison. Lastly, walls' behaviour at ultimate and also after failure will be discussed in the third part. Table 4.2 contains a summary of the test results of the eight full-scale masonry walls.

4.3.1 Cracks and Deformations

Based on flexural bond strength of the tested auxiliary prisms, no cracking was expected to occur due to the self weight of the walls. The first crack was generated in the constant moment zone as the applied moment reached the vicinity of the expected cracking moment. More flexural cracks as well as shear cracks outside the constant moment zone started to appear by increasing the applied moment beyond the cracking moment which also deepened and widened the existing cracks gradually. All the cracks were initiated primarily from the bottom of the section at the interface of masonry unit and mortar and developed upward in the grout. Each crack resulted in separating the

block from mortar along the lower face shell at one instant and as a result the deflections increased dramatically.

The threshold of flexural strength was preceded by big opening in one of the block-mortar joints between the two point loads and cracks in the concrete blocks that culminated in crushing of the masonry units in compression. In all the tested walls, that block-mortar (bed) joint was noticed to have shear reinforcement. In some of the tests, the mortar in the section of the cracked bed joint spalled off the compression side. The unreinforced wall experienced a sudden failure that followed a crack formed in one of the joints in the constant moment region.

For the steel-reinforced wall, the shear cracks appeared, after the rebars had yielded, in two bed joints which underwent the maximum shear force (see Figure 4.2 (b) and (d)). The relatively higher contribution of steel reinforcement in shear strength compared to GFRP can be concluded. On the other hand, the less wide cracks in the GFRP-reinforced walls underline the superior bond characteristics of this type of reinforcement compared to steel.

Another finding was the effect that the extent of grouting had on the cracking load. The partially grouted walls cracked at fairly lower levels of applied load when compared to their analogous companions. However, it can be stated that type of the reinforcement (steel vs. GFRP) had not a significant effect on the onset of cracking, nor did it on the immediate width of the cracks.

4.3.2 Load-Deformation and Load-Strain Relationships

It should be mentioned that in order to take into consideration the self weight of the walls (between 6.9 and 12.3 kN), the equivalent load (dead load) that produces the same moment as the distributed self weight over the wall does, was added to the recorded live load which was applied by the hydraulic actuator. This was done without missing any useful information; in view of the fact that, as mentioned before, the expected cracking moment (6.6 kN.m) was larger than the moment produced by the own weight of the walls (between 2.5 and 4.1 kN.m). Furthermore, a pair of temporary supports were fabricated to carry the weight of the walls and removed after having launched the data acquisition system, so that the strains and deflections due to the self weight of the walls would not be missed either. Having the equivalent dead load and its corresponding deflection and strain, the initial portion of the force-deformation and force-strain curves was superimposed to that of live load.

The drastic drops in the recorded loads correspond to cracks' occurrence, while the tiny drops can be associated with the existing cracks widening or extending in depth which also happened intermittently. It is observed that after each drop the load has caught up to a higher level but with a diminished stiffness. It illustrates how the section approaches to the cracked section properties progressively. Figure 4.16 shows the applied lateral load versus the deflection at mid-span of the GFRP-reinforced walls along with the steel-reinforced and unreinforced ones.

The remarkably poor strength and deformation of the wall U-F simply depicts the drastic effect that the use of even smallest amount of GFRP reinforcement can have on the flexural performance of the masonry walls. More importantly, the sudden failure is

replaced with ample deformation of the walls after the first crack. Another notable observation is that G-3#19-F with the largest reinforcement ratio, when compared to S-5M10-F, shows that we can reach higher capacities with acceptable deformability that could not be achieved by steel-reinforced masonry walls due to the constraint of not exceeding the balanced reinforcement ratio.

As one of the intentions of this study, the relative performance of the steel-reinforced wall is also demonstrated compared with that of the specimens which were designed to have comparable amounts of GFRP reinforcement from the design point of view. In other words, the product of reinforcement area and guaranteed design tensile strength (considering the reduction factors for steel and FRP (CHBDC (2006))) for these two walls (G-4#13-F and G-4#13-P) were intended to be close to that of the steel-reinforced wall. This product was calculated for wall G-4#13-F and S-5M10-F respectively as shown below:

$$\begin{aligned} A_{FRP}\Phi_{FRP}f_{u,FRP} &= \left(4\times126.7\ mm^2\right)\left(0.5\right)\left(708\ MPa\right) = 179\ kN \\ A_s\Phi_s f_y &= \left(5\times100\ mm^2\right)\left(0.85\right)\left(400\ MPa\right) = 170\ kN \end{aligned} \tag{4.1}$$

It can be seen that the GFRP-reinforced walls reached relatively higher strengths. Although the S-5M10-F experienced more deformation, the GFRP-reinforced walls had adequate deflections to forewarn the failure. Looking at the same graph, it can be concluded that grout-filling the empty cells does not have a positive effect on the general performance of the walls. Wall G-4#13-P exhibited significantly higher strength compared to wall G-4#13-F; this could be attributed to the actual location of the GFRP rods inside the cells which was determined for the walls after the tests. The average

effective depth of the bars for wall G-4#13-P was found to be 125 mm, whereas that of wall G-4#13-F was found 105 mm.

Figure 4.17 illustrates the change in tensile strains of the longitudinal reinforcements with applied lateral load. Since the reinforcing rods are in the vicinity of the neutral axis of the gross section, there is not much stress and consequently strain recorded before the occurrence of the first crack, at which stage the neutral axis is raised up significantly. The effect of the cracks can similarly be detected herein. In general, the curves show that the tensile strain and accordingly the tensile stress increase linearly with the applied load up to the failure of the walls. The maximum recorded strains highlight the fact that the GFRP rods did not fail until the compressive crushing in masonry induced the failure of the walls.

4.3.3 Modes of Failure and Post-Failure Behaviour

The unreinforced wall encountered a sudden failure right after the first flexural crack formed. For the reinforced walls, the failure was always in compression zone of the masonry compound even though it was preceded by different phenomena. G-3#10-F failed after the joint next to the point load inside the moment zone had opened up significantly and the top face shell of one cell next to the same bed joint was crushed (see Figure 4.4 (c) and (d)). Same response occurred in G-3#13-F, G-4#13-F, G-4#13-P, and G-3#19-F; however, there were some diagonal cracks detected on the side of the blocks next to the failed joints. G-3#13-P failed after a strip of 3 consecutive grouted cells separated on one side of the wall inside the constant moment zone (Figure 4.8 (d)). A half block on one side was separated and misaligned before the failure of G-4#13-F (Figure

4.10 (d)). For the case of G-3#19-F, the cracks in the masonry units were relatively wide. G-3#13-F, G-4#13-P, and G-3#19-F experienced shear cracks on the side of masonry units outside the constant moment region. For G-3#13-F, these cracks joined a mortar-block interface next to the point load which widened considerably, nevertheless the failure was induced by a long and wide crack on the top surface of the wall that was diagonally developed over the constant moment zone (Figure 4.6 (c) and (d)). The steel-reinforced wall simply failed after the joint cracks were widened and compressive cracks had appeared on the compression side of the blocks, although no shear crack was detected on the masonry units. This could be attributed to the dowel action of the steel rebars.

G-3#13-F, G-3#13-P, G-3#19-F, and S-5M10-F were unloaded and all but the last one were reloaded after the failure in order to investigate their post-failure strength and inelastic deformation. It was not practical to reload the steel-reinforced wall due to its substantial deformation. Their inelastic deformations as percentages of their total deformations were found to be 7.8%, 39%, 36.5%, and 7.3%, respectively. The post-failure resistances corresponding to the first three were found to be 34.4%, 46.6%, and 47.3% of the ultimate flexural capacity, respectively. It can be concluded that the larger amounts of GFRP reinforcement increase both parameters significantly. The notable observation therein is that not only did the post-failure strength of the FRP-reinforced walls exceed their dead loads, but also it helped to encounter considerable amount of applied live load.

Another important characteristic to mention herein is the ratio of flexural capacity of the walls to their own weight. Table 4.2 contains this ratio for all the tested walls

which ranges from 1.4 (for the unreinforced wall) to 9.6 (for the wall with highest GFRP reinforcement area). The importance of this ratio is intensified when seismic response of the lateral load bearing structural element is of the design concerns. In general, the total seismic load exerted to the structural system is a function of the self-weight of the whole structure, a considerable part of which is constituted by walls. While the poor flexural strength of the unreinforced wall proves that this type of the walls is unsuitable when dealing with considerable lateral loads, the results of the GFRP-reinforced walls highlight the fact that higher flexural capacity, for the same cross-sectional dimensions and consequently weight, is reachable when FRP reinforcement. In addition, this ratio was magnified 62% and 55%, respectively, for G-3#13-P and G-4#13-P compared to their analogous panels (i.e. fully grouted ones) which, again, underlines the effectiveness of this approach of designing reinforced concrete masonry walls.

Table 4.1. Chronicled order of the wall tests

Number	Wall	Date of the test
1	G-3#10-F	06/20/2008
2	U-F	18/07/2008
3	G-4#13-F	29/07/2008
4	G-4#13-P	01/08/2008
5	G-3#19-F	21/08/2008
6	G-3#13-P	05/09/2008
7	G-3#13-F	12/09/2008
8	S-5M10-F	30/09/2008

Table 4.2. Summary of the test results for the eight full-scale masonry walls

Wall	M_{cr} (kN.m)	M_n (kN.m)	$\frac{M_n}{M_{self\text{-}weight}}$	Max. defl. (mm)	Max. tensile strain ($\times 10^{-6}$)	Mode of failure
U-F	5.6	5.6	1.4	1.4	—	Tensile in bed joint
S-5M10-F	6.9	16.9	4.2	143.2	—	↑
G-3#10-F	6.0	14.2	3.5	111.4	14002	↑
G-3#13-F	7.6	18.3	4.5	107.4	11218	Compressive
G-3#13-P	4.3	17.9	7.3	108.5	9997	in masonry
G-4#13-F	5.8	21.7	5.3	108.9	9613	↓
G-4#13-P	5.9	30.3	8.2	94.3	10235	↓
G-3#19-F	6.2	39.3	9.6	93.6	8440	↓

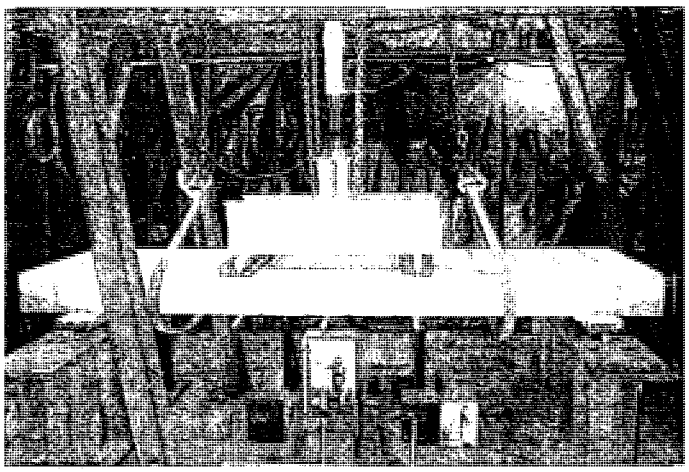

(a)

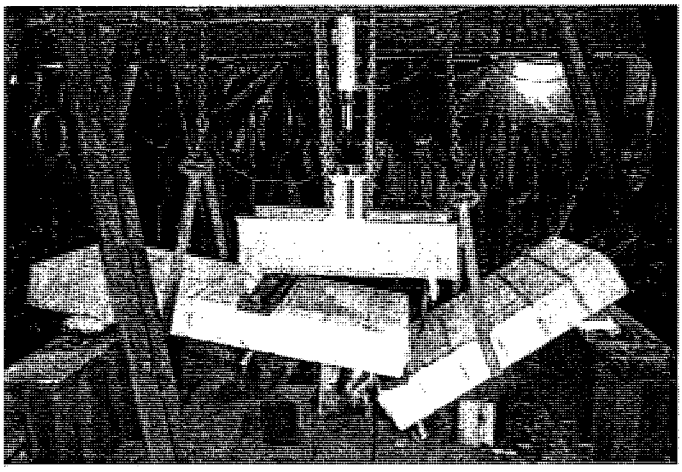

(b)

(c)

Figure 4.1. Wall U-F: (a) wall before the loading was started; (b) wall after the sudden failure; (c) failed section

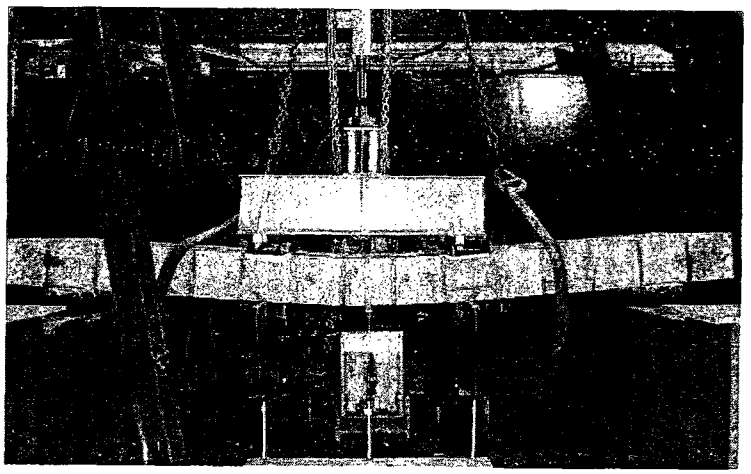

(a)

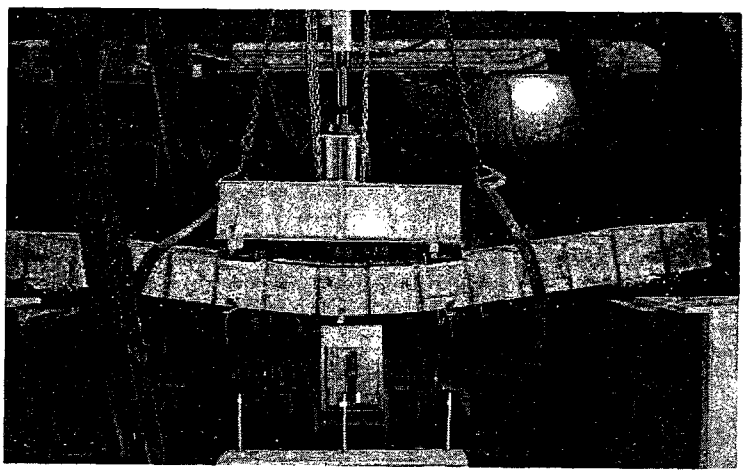

(b)

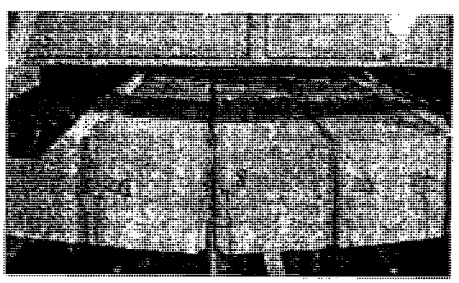

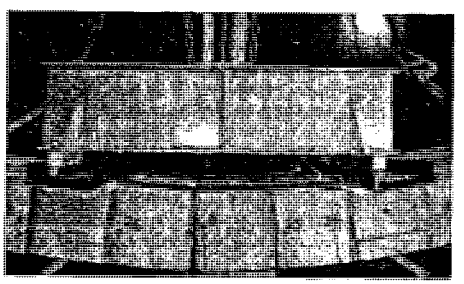

(c) (d)

Figure 4.2. Wall S-5M10-F: (a) wall after cracking; (b) wall close to failure; (c) significant width of the flexural cracks; (d) cracked joints when the loading stopped

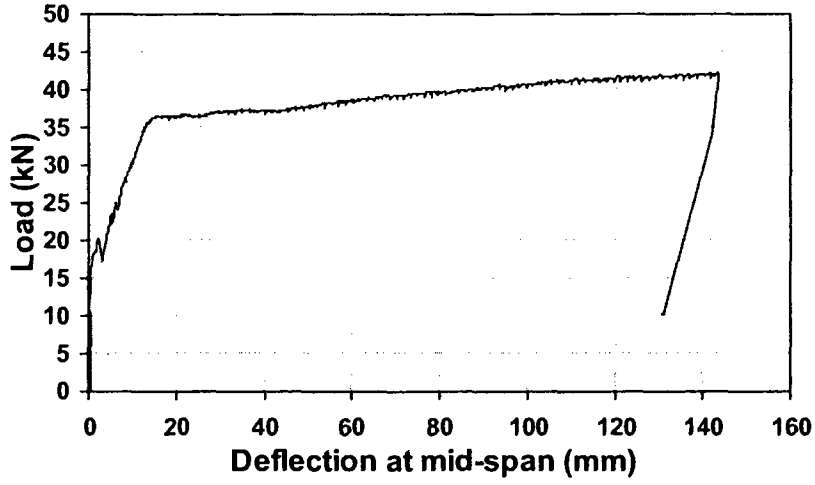

(a)

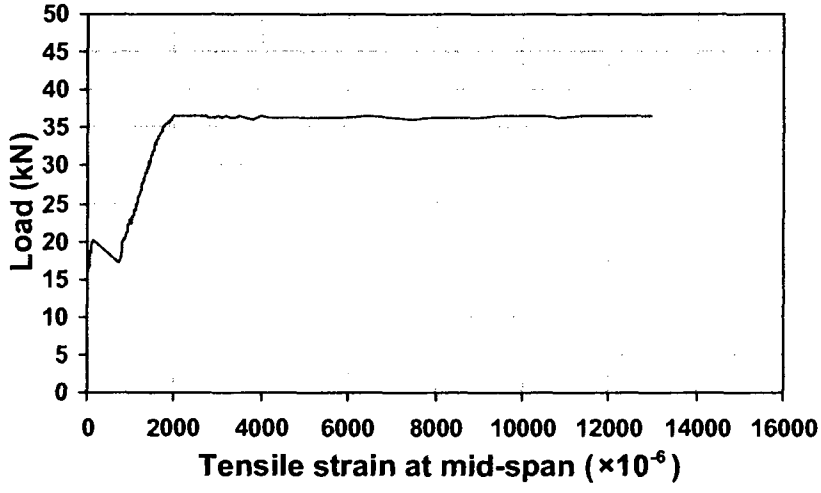

(b)

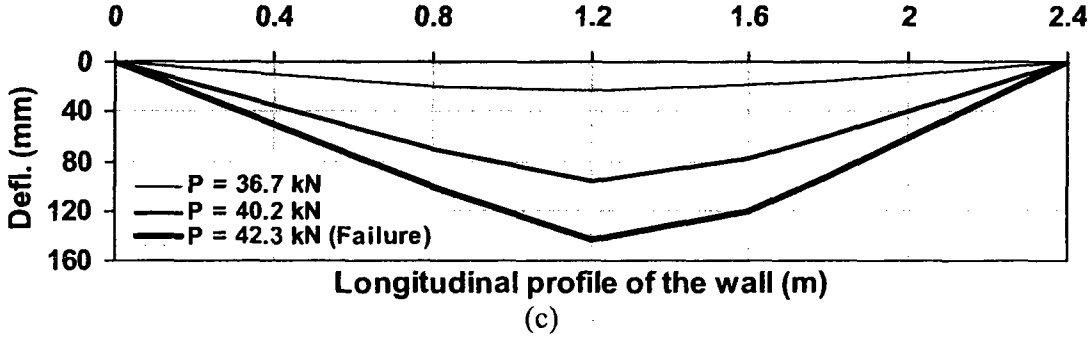

(c)

Figure 4.3. Test results of wall S-5M10-F: (a) load-deflection at mid-span; (b) load-strain at mid-span; (c) deformed shape at three different stages

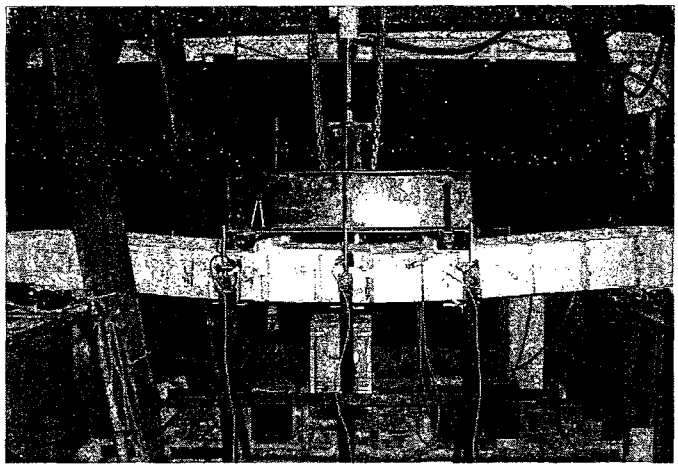

(a)

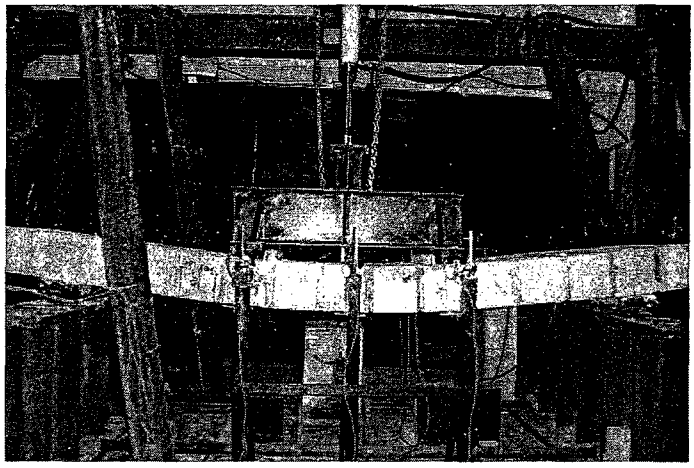

(b)

(c)

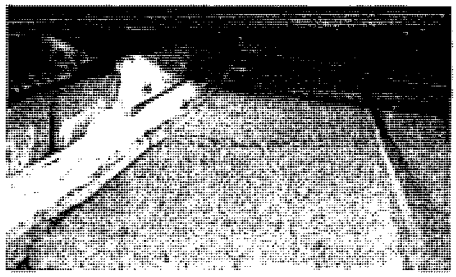

(d)

Figure 4.4. Wall G-3#10-F: (a) wall after cracking; (b) wall close to failure; (c) the widely opened joint next to the failed section; (d) compressive failure in masonry

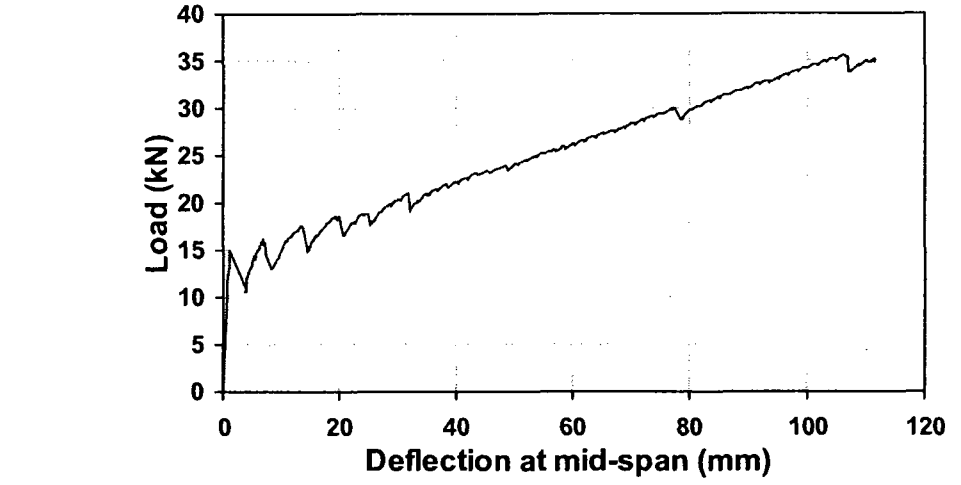

(a)

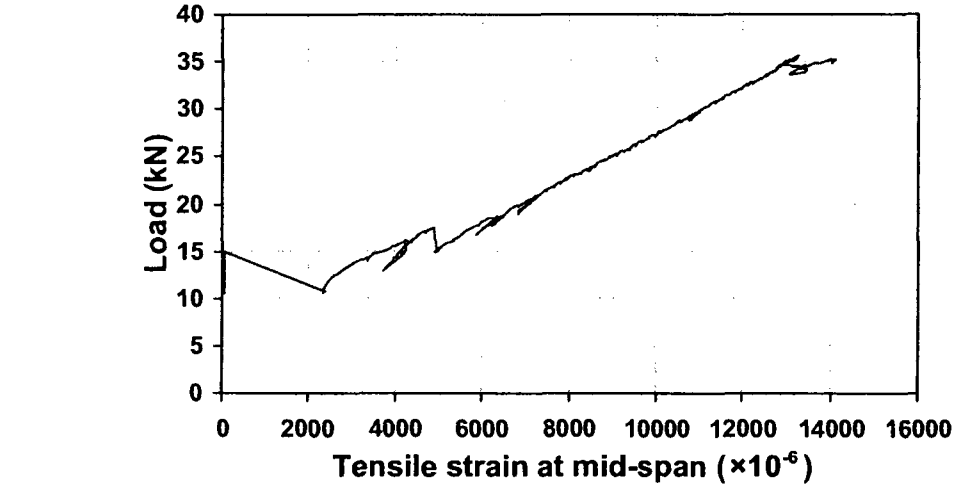

(b)

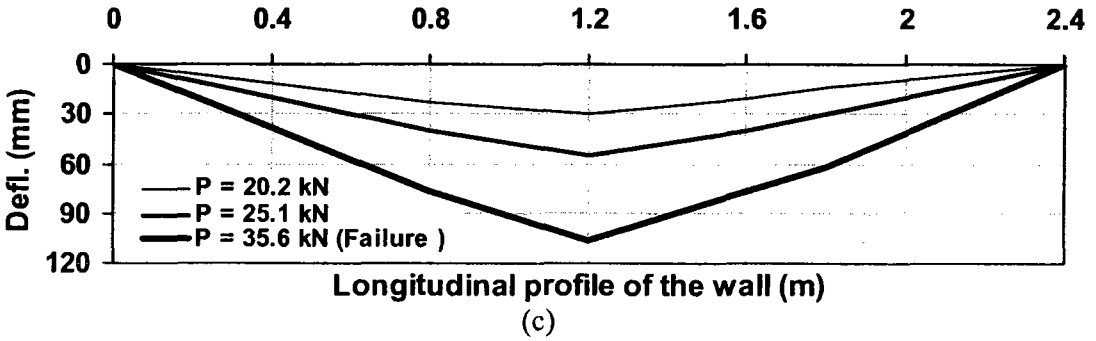

(c)

Figure 4.5. Test results of wall G-3#10-F: (a) load-deflection at mid-span; (b) load-strain at mid-span; (c) deformed shape at three different stages

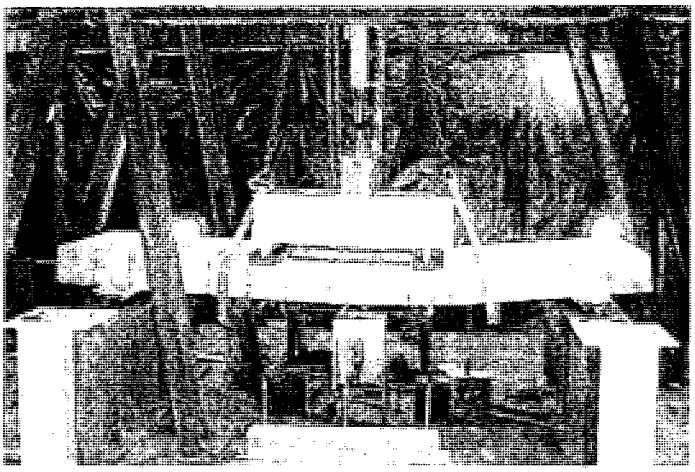

(a)

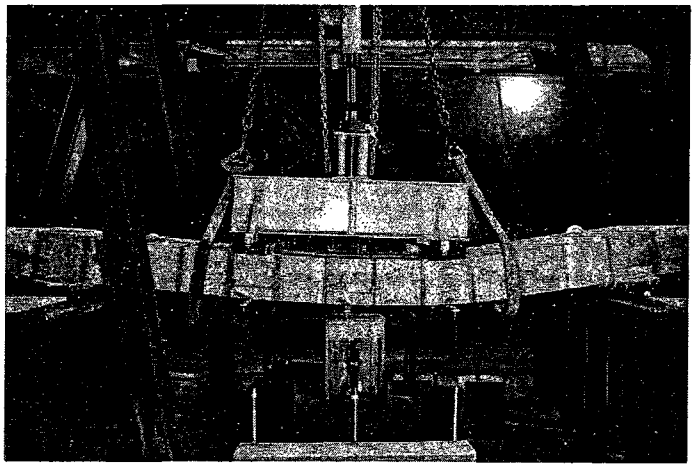

(b)

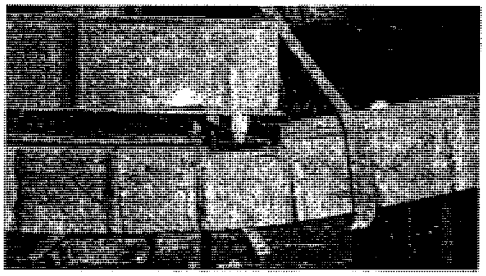

(c)

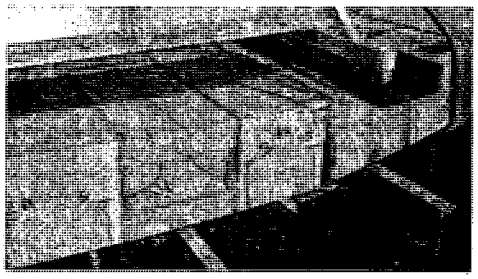

(d)

Figure 4.6. Wall G-3#13-F: (a) wall after cracking; (b) wall close to failure; (c) the shear cracks; (d) wide long crack manifesting the compressive failure in masonry

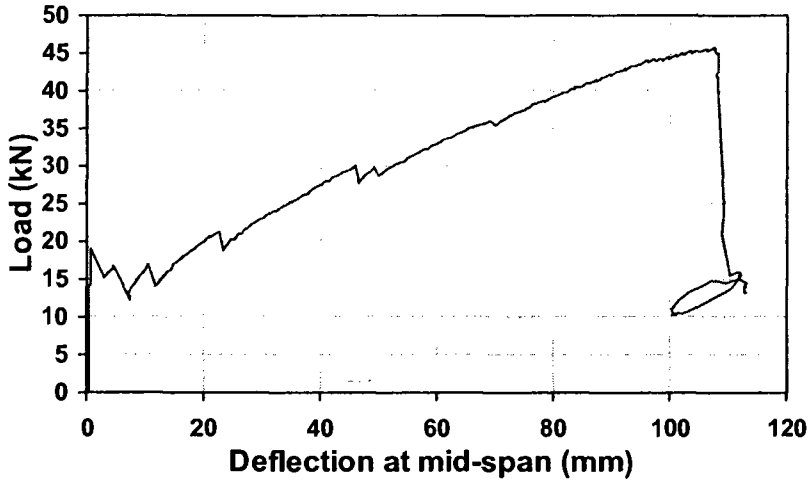

(a)

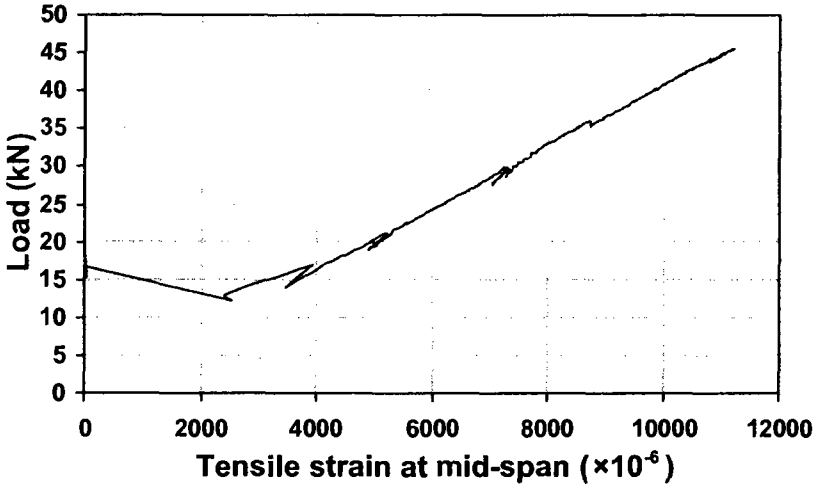

(b)

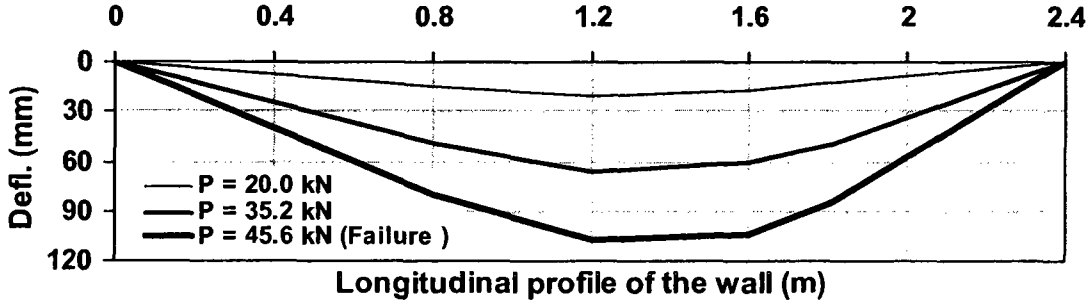

(c)

Figure 4.7. Test results of wall G-3#13-F: (a) load-deflection at mid-span; (b) load-strain at mid-span; (c) deformed shape at three different stages

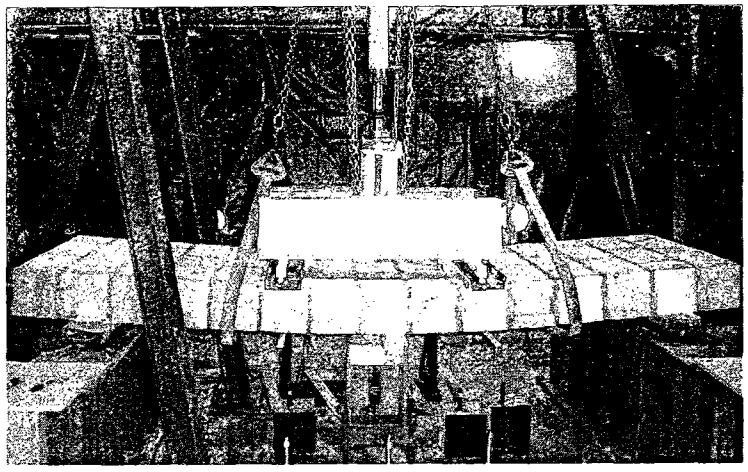

(a)

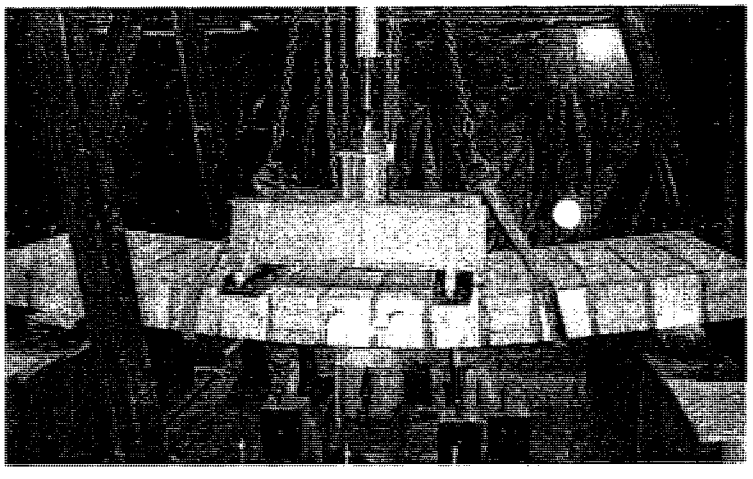

(b)

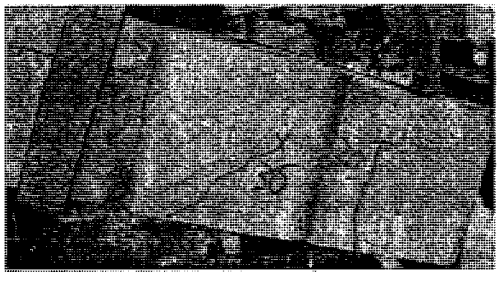

(c)

(d)

Figure 4.8. Wall G-3#13-P: (a) wall after cracking; (b) wall close to failure; (c) the shear cracks; (d) a strip of grouted blocks separated from the wall (rear view)

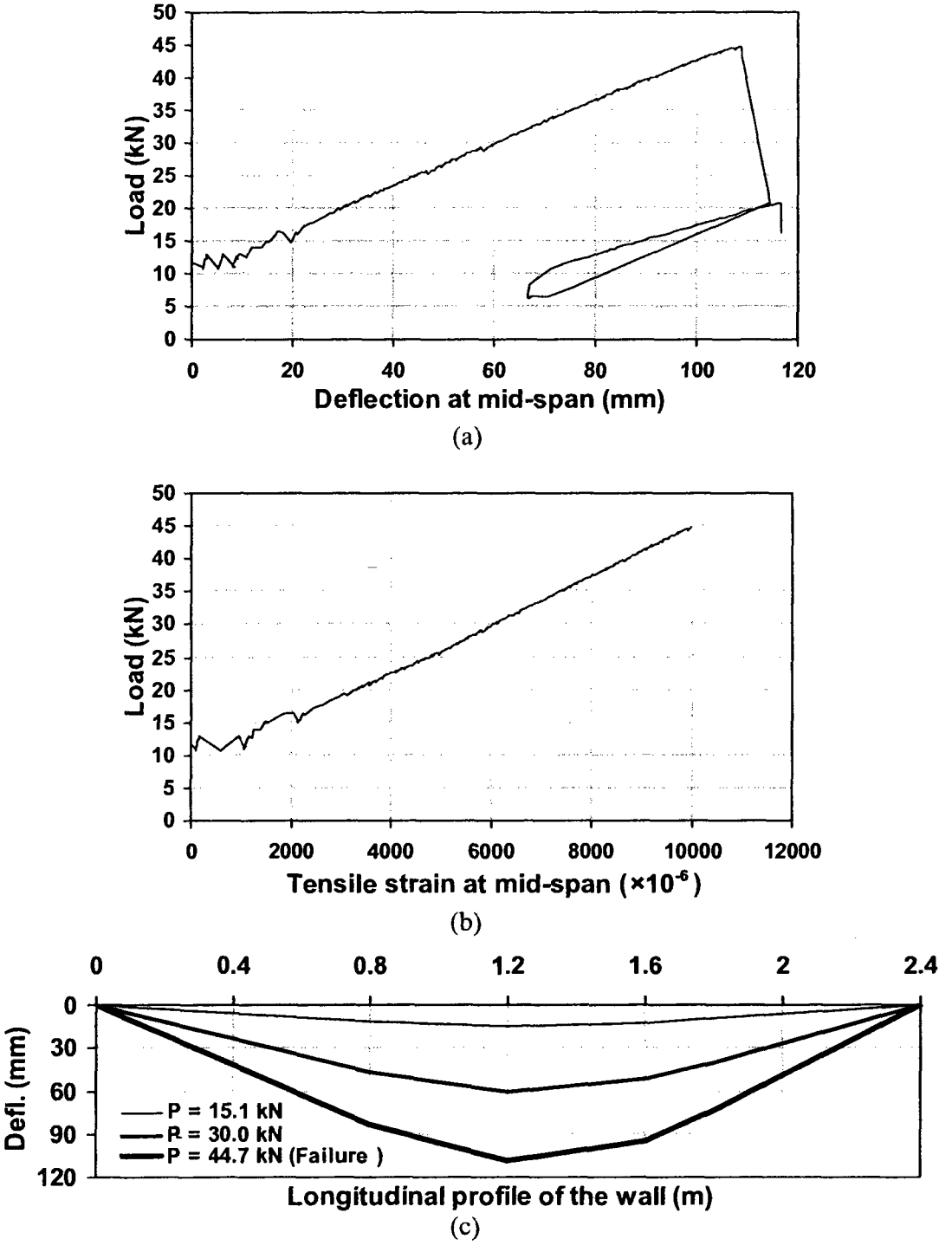

Figure 4.9. Test results of wall G-3#13-P: (a) load-deflection at mid-span; (b) load-strain at mid-span; (c) deformed shape at three different stages

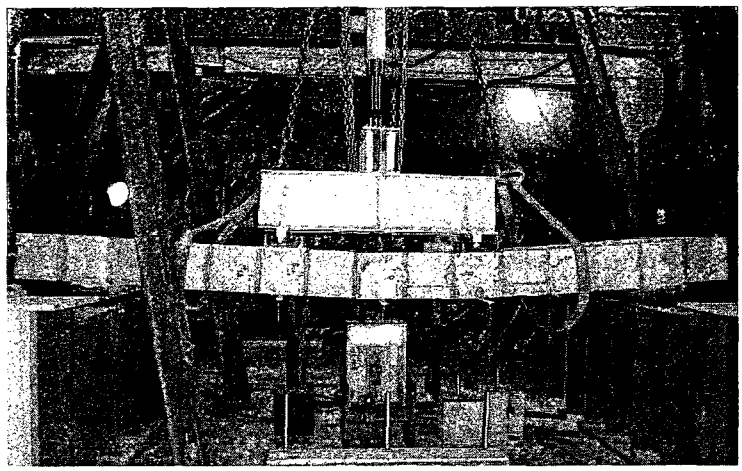

(a)

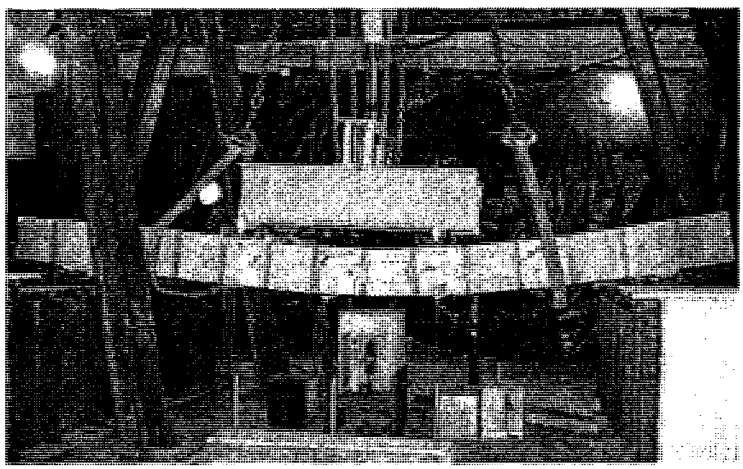

(b)

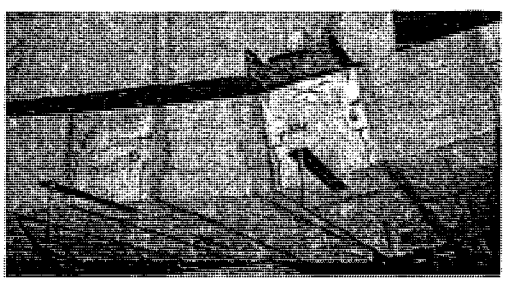

(c)

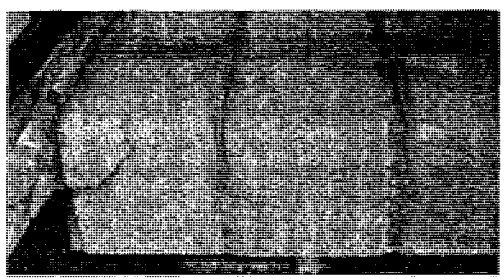

(d)

Figure 4.10. Wall G-4#13-F: (a) wall after cracking; (b) wall close to failure; (c) the widely opened joint next to the failed section; (d) compressive failure (rear view)

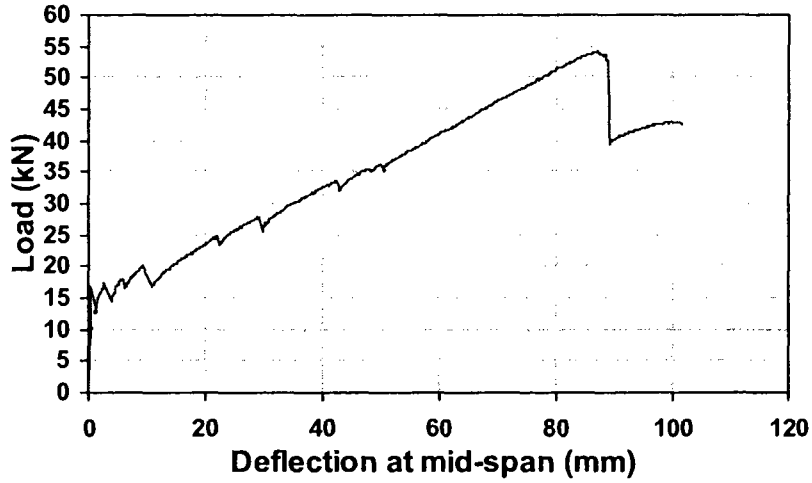

(a)

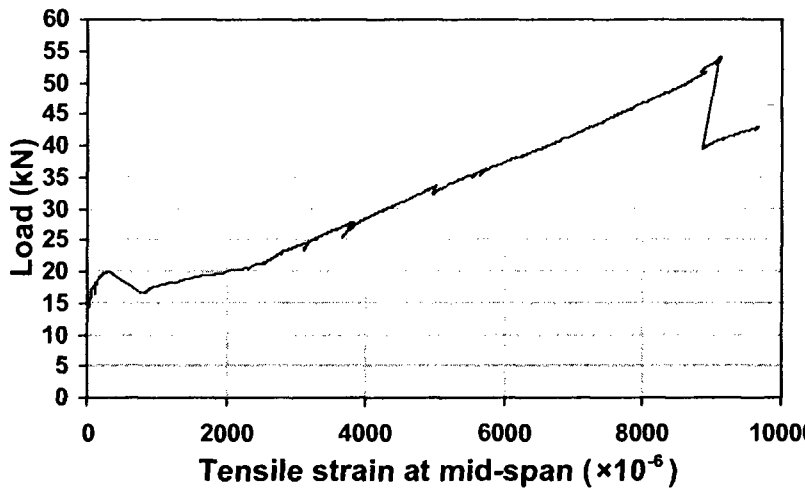

(b)

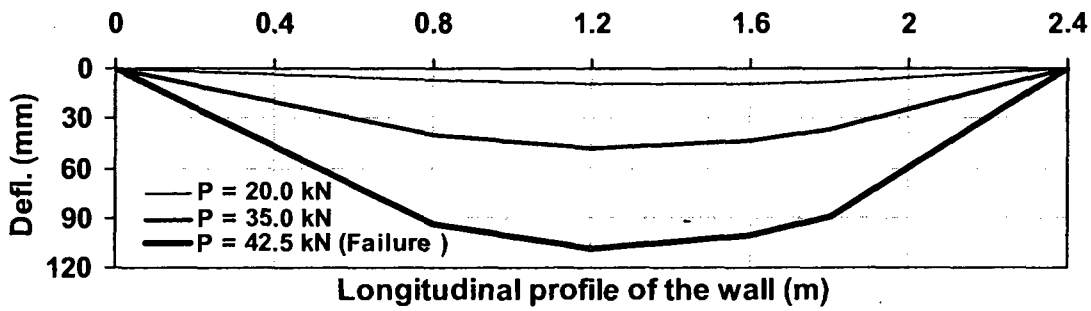

(c)

Figure 4.11. Test results of wall G-4#13-F: (a) load-deflection at mid-span; (b) load-strain at mid-span; (c) deformed shape at three different stages

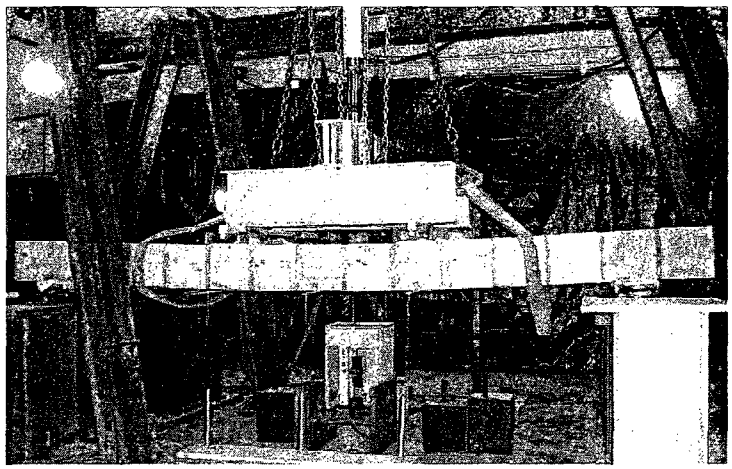

(a)

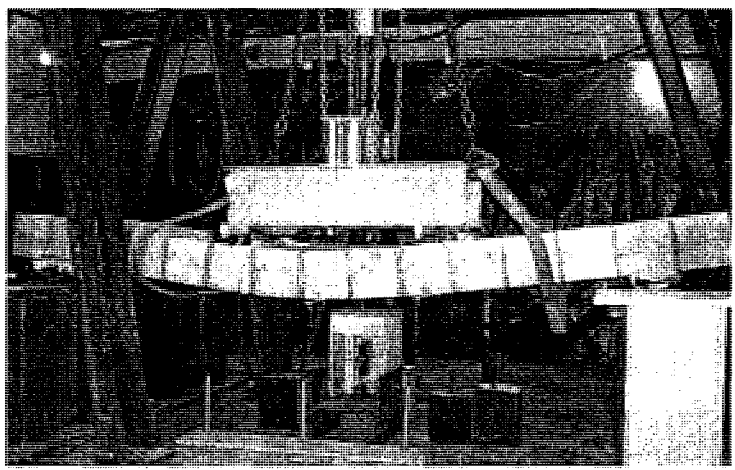

(b)

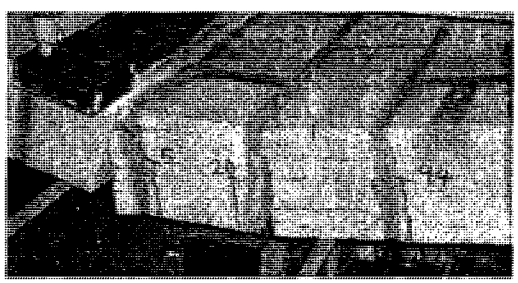

(c)

(d)

Figure 4.12. Wall G-4#13-P: (a) wall after cracking; (b) wall close to failure; (c) the widely opened joint next to the failed section; (d) compressive failure in masonry

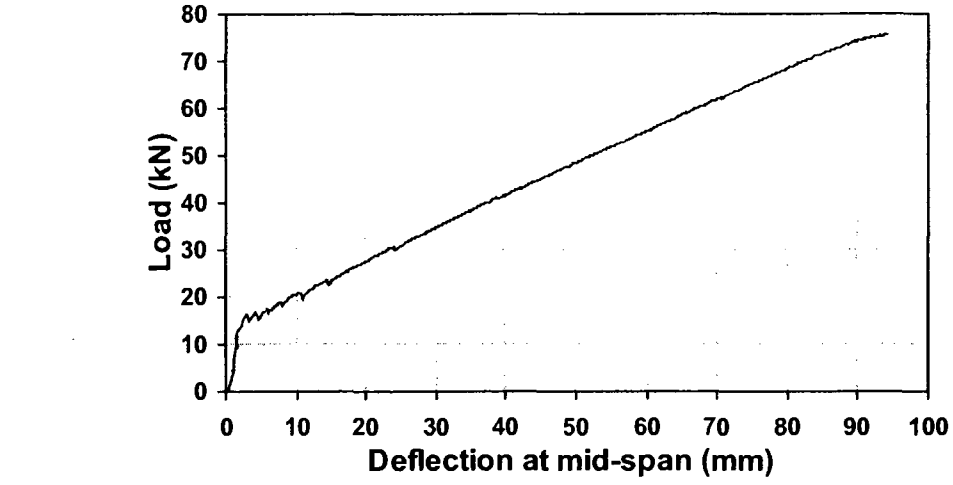

(a)

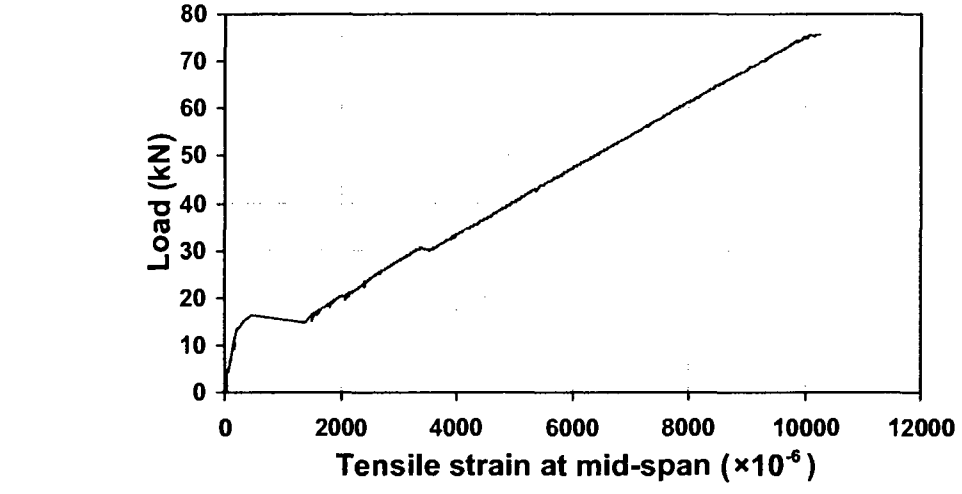

(b)

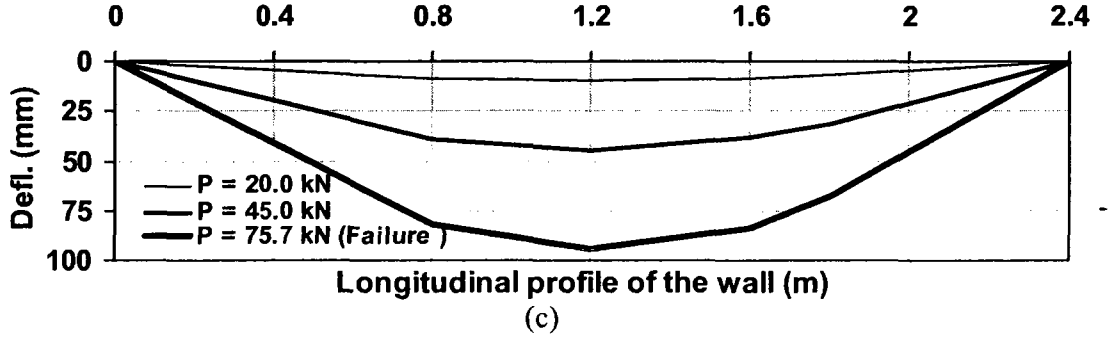

(c)

Figure 4.13. Test results of wall G-4#13-P: (a) load-deflection at mid-span; (b) load-strain at mid-span; (c) deformed shape at three different stages

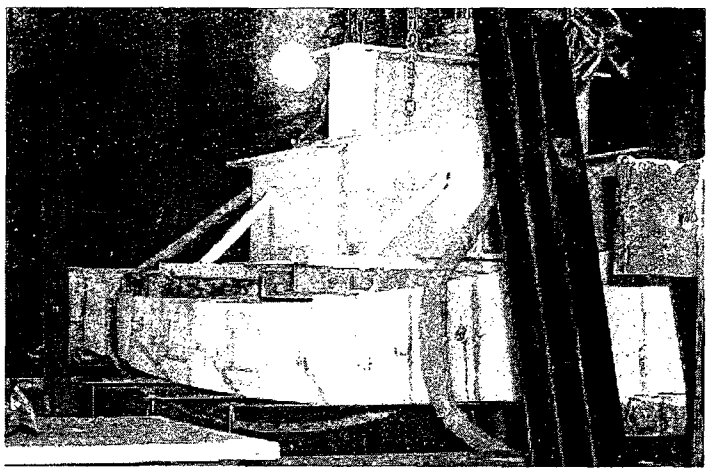

(a)

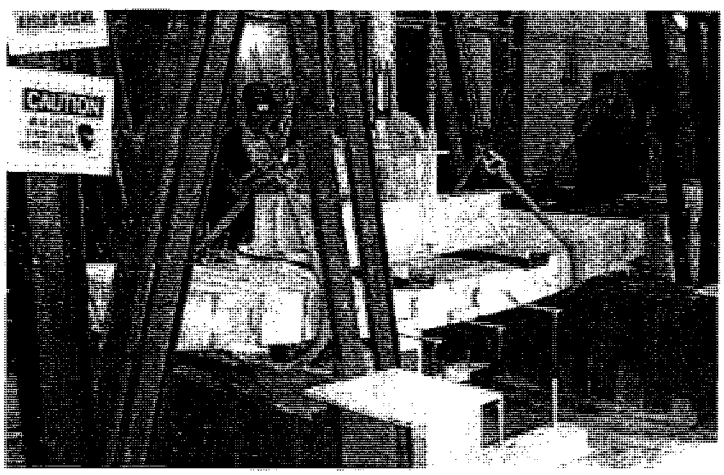

(b)

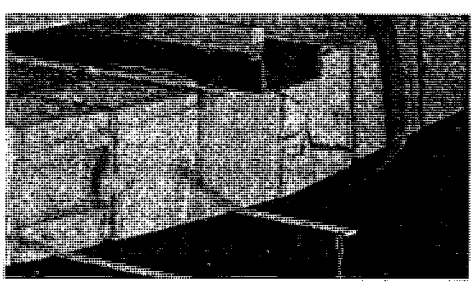

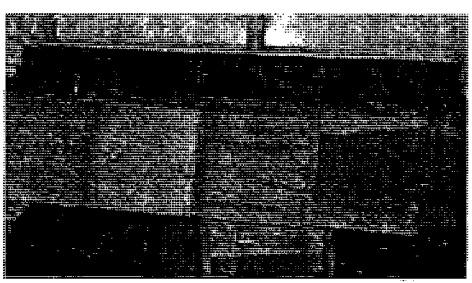

(c) (d)

Figure 4.14. Wall G-3#19-F: (a) wall after cracking; (b) wall close to failure; (c) the shear cracks; (d) wide long crack manifesting the compressive failure in masonry

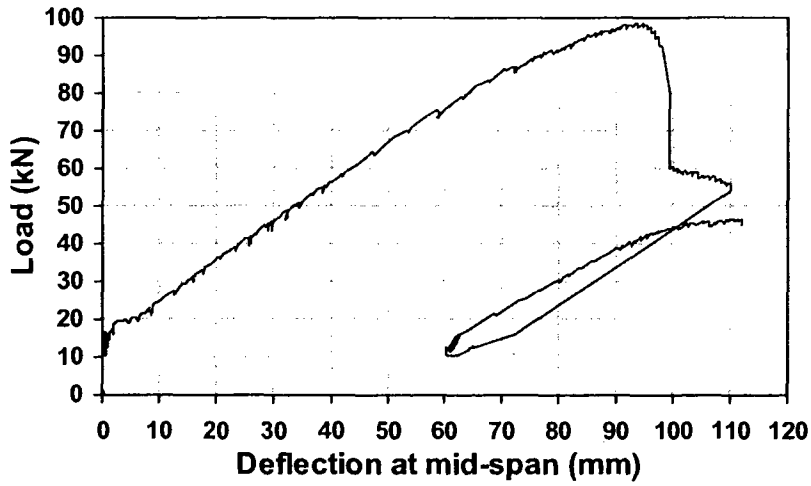

(a)

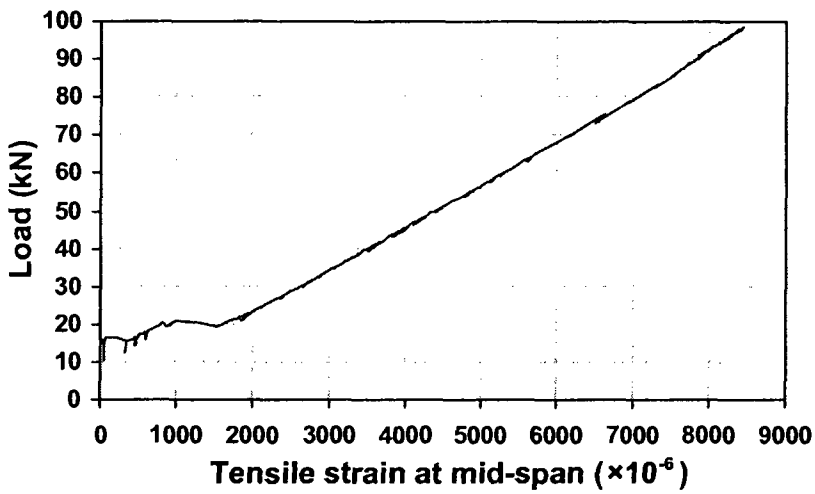

(b)

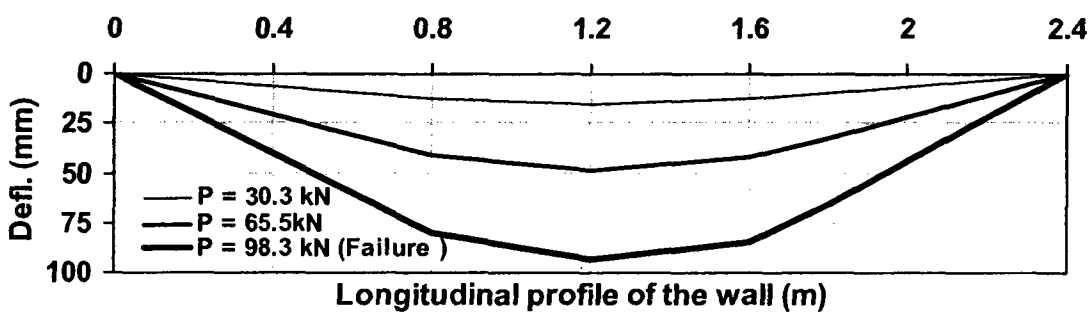

(c)

Figure 4.15. Test results of wall G-3#19-F: (a) load-deflection at mid-span; (b) load-strain at mid-span; (c) deformed shape at three different stages

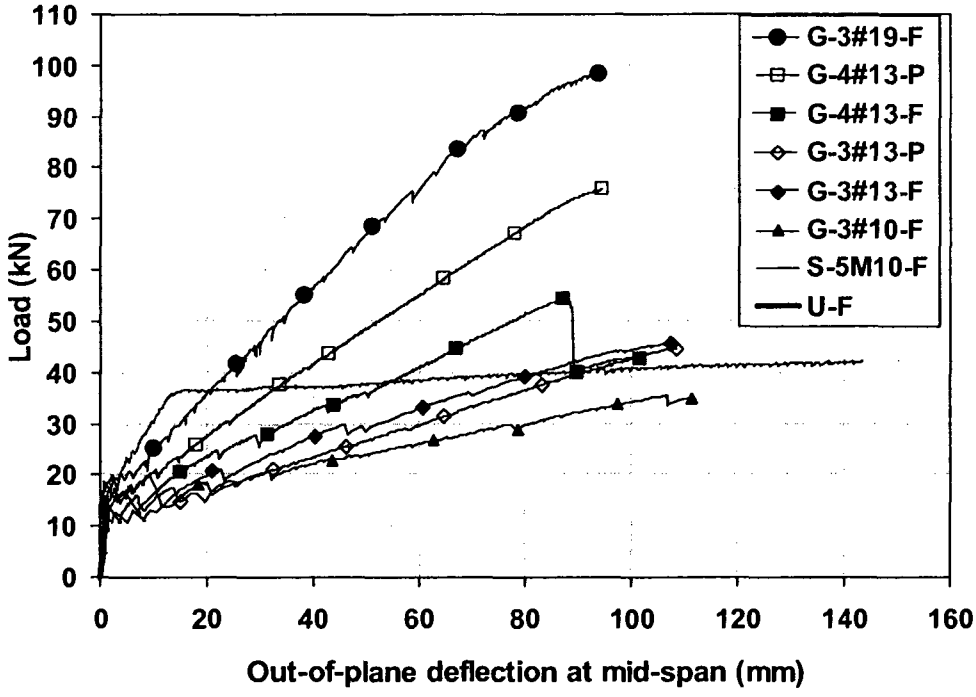

Figure 4.16. Load-deflection relative performance of the eight tested masonry walls

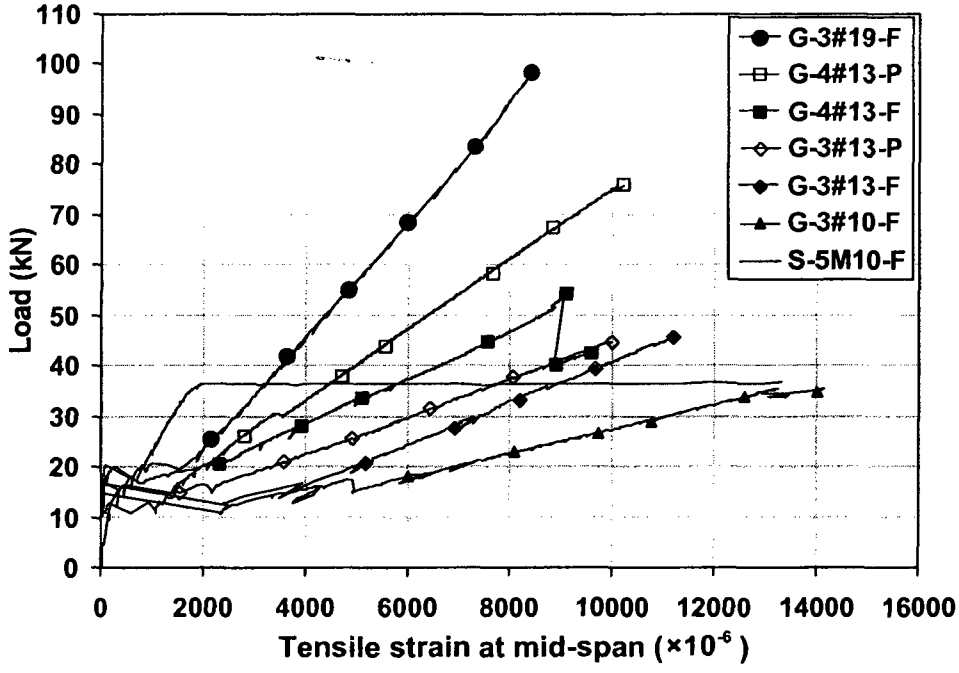

Figure 4.17. Load-strain relative performance of the eight tested masonry walls

CHAPTER 5

QUANTITATIVE BEHAVIOUR AND NUMERICAL MODELING

5.1 General

In this chapter efforts are made to set up numerical models that are capable of predicting quantitative aspects of response of FRP-reinforced masony walls, flexural capacity of the section and load-deflection relationship, to an acceptable level of accuracy. As such, it is intended to present analytical models that correlate with test results of the walls and based upon which, the outcome of the wall tests can be theoretically quantified and predictable. It can be asserted, afterwards, that the same methods of analysis can be used to theorize a limit-states design methodology for designing masonry elements in flexure when reinforced with FRP rods. For this purpose, the methods of analysis and numerical models that are already available for steel-reinforced masonry and FRP-RC are utilized to incorporate the presence and effects of FRP as the reinforcing material in concrete masonry. Concrete masonry is known to have similar structural characteristics to concrete, notwithstanding the fact that it is not a uniform material but a composite, formed by different cementious components; since, the main components are concrete block and grout (i.e. low strength concrete). Therefore, it is only reasonable to try to establish methods of analysis for FRP-reinforced concrete masonry analogous to those of FRP-RC.

5.2 Section Analysis in Flexure

The tested walls' section analysis is conducted using the common method of ultimate strength conditions that is adopted in CSA S304.1 (2004). For the case of GFRP-reinforced sections, necessary modifications are adopted to the procedures in accordance with ISIS (2001). The approach employed in this part is assumed to be appropriate, in that all the tested walls failed due to the compressive failure of the masonry.

The analysis is carried out assuming that 1) plane sections remain plane, 2) the strain varies linearly in the depth of the section, 3) deformations are small, 4) tensile strength in the masonry and compressive strength of composites are negligible, 5) the GFRP rods bond with concrete with no interfacial slippage, 6) the ultimate compressive strain of the masonry compound is 0.003 as suggested in CSA S304.1 (2004), and 7) all the GFRP-reinforced sections fail due to masonry crushing as they were designed to be over reinforced. The ultimate fibre tensile strains were to be checked against the fibre rupture strains ultimately to verify the last assumption. The choice of 0.003 as the ultimate masonry strain (with 0.002 as the strain corresponding to the peak stress) agrees with the strain corresponding to the peak stress for the compressive masonry prisms which ranged from 0.0017 to 0.0024 (see Table 3.1). Moreover, the recorded strains in the GFRP rods of the tested walls were well below their ultimate tensile fibre strain, which shows that the sections were over reinforced. As for the GFRP rods, the stress-strain relationship is presumed to be linear elastic up to the point where the rupture happens. Their tensile properties, as can be seen in Table 3.5, vary slightly for different diameters. Although the rods were initially intended to be placed in the middle of the unit cells with an effective depth (d) of 95 mm, after the failure of each wall the actual d of

the rods were measured at the failed section to have a more precise analysis. The average measured d ranged for the walls from 100 mm to 125 mm.

5.2.1 Customary Method Based on Whitney Stress Block

According to CSA S304.1 (2004), the two stress block factors that specify the Whitney uniform stress block, α_1 and β_1, are respectively 0.85 (constant) and 0.8 for concrete masonry using the following equation:

$$\beta_1 = 0.8 - 0.10\left(\frac{f'_m - 20}{10}\right) \leq 0.80 \tag{5.1}$$

For the over reinforced walls, the equilibrium equations of internal forces were solved to find the tensile stress in the GFRP at ultimate state directly as shown below:

$$f_{FRP} = 0.5E_{FRP}\varepsilon_{m,u}\left[\left(1+\frac{4\alpha_1\beta_1 f'_m}{\rho_{FRP}E_{FRP}\varepsilon_{m,u}}\right)^{\frac{1}{2}} - 1\right] \tag{5.2}$$

where ρ_{FRP} is the actual GFRP reinforcement ratio of the wall (after the measurement of the depth of the rods), E_{FRP} is the modulus of elasticity of the GFRP rod that varies for the three different diameters slightly (Pultrall (2007)), and $\varepsilon_{m,u}$ is the ultimate compressive strain of the masonry compound. Having the expected stress of the GFRP rods at ultimate, the expected flexural strength of the wall, then, was found as such:

$$M_n = f_{FRP}A_{FRP}\left(d - \frac{\beta_1 c}{2}\right) \tag{5.3}$$

In the foregoing equation, A_{FRP} and f_{FRP} are, respectively, the reinforcement area and the expected stress of the GFRP rods at ultimate. Besides, the depth of the compressive block (c) can be found using the equilibrium of compressive and tensile forces in the section:

$$c = \frac{f_{FRP} A_{FRP}}{\alpha_1 \beta_1 f'_m b} \tag{5.4}$$

The outcomes of the numerical evaluations state that the theoretical prediction is fairly conservative, since the ratio of experimental to theoretical ultimate strength varies from 1.13 to 1.28. The corresponding results are tabulated in Table 5.1.

5.2.2 Section Analysis Based on Stress-Strain Models for Masonry

In order to have a more accurate prediction, in lieu of equivalent Whitney stress block, three different stress-strain models that account for more realistic stress-strain behaviour of concrete masonry were adopted in the aforesaid procedure. Dhanasekar and Shrive (2002) have proposed two stress-strain curves, defined by a simple and a refined equation:

$$\sigma_m = f'_m \left(\frac{u_0 x}{1 + x^{u_1}} \right) \qquad \text{(Simple)} \tag{5.5}$$

where u_0 and u_1 are constants, taken as 2.0 and 2.0 respectively for grouted concrete masonry and 1.4 and 2.6 for ungrouted concrete masonry, and x is the ratio of strain to the strain at maximum stress.

$$\sigma_m = f'_m \left(\frac{\left(1 + u_0 \left(1 + u_1\right)\right) x}{u_0 \left(1 + u_1 x\right) + x^{1+u_0}} \right) \qquad \text{(Refined)} \tag{5.6}$$

where u_0 and u_1 are 1.5 and 1.0 respectively for grouted concrete masonry and 2.1 and 0.1 for ungrouted concrete masonry. These two models have been developed based on stress-strain equations for concrete proposed by, respectively, Desayi and Krishnan (1964) and Loov (1991). Dhanasekar and Shrive found their proposed model reliable for predicting

flexural behaviour of reinforced masonry (Dhanasekar and Shrive (2002) and Assa and Dhanasekar (2002)).

In an earlier research, Priestley and Elder (1983) had suggested the use of another model for concrete masonry based on modified Kent-Park curve for concrete (Park *et al.* (1982)). This stress-strain relationship for masonry is defined as such:

$$\sigma_m = 1.067 f'_m \left[\frac{2\varepsilon_m}{0.002} - \left(\frac{\varepsilon_m}{0.002} \right)^2 \right] \qquad \varepsilon_m \le 0.0015$$
$$\sigma_m = f'_m \left[1 - Z_m \left(\varepsilon_m - 0.0015 \right) \right] \qquad \varepsilon_m \ge 0.0015 \tag{5.7}$$

Where Z_m is:

$$Z_m = \frac{0.5}{\left(\frac{3 + 0.29 f'_m}{145 f'_m - 1000} \right) - 0.002} \tag{5.8}$$

Figure 5.1 illustrates the curves for these three stress-strain models. All the three curves were integrated into the walls' section analysis leading to closer estimate of strengths, even though still slightly conservative. Theoretical flexural strength of the sections based on the stress-strain models were evaluated in the same fashion but using the two stress block factors α_1 and β_1 calculated for the presented stress-strain curves by means of these two integrals:

$$\beta_1 = 2 - \frac{2 \int_0^{\varepsilon_{m,u}} \sigma_m \varepsilon_m d\varepsilon_m}{\varepsilon_{m,u} \int_0^{\varepsilon_{m,u}} \sigma_m d\varepsilon_m} \quad , \quad \alpha_1 = \frac{\int_0^{\varepsilon_{m,u}} \sigma_m d\varepsilon_m}{\varepsilon_{m,u} f'_m \beta_1} \tag{5.9}$$

The model most conforming to the results of the tests was found to be the refined equation proposed by Dhanasekar and Shrive (2002). Furthermore, this stress-strain relationship estimates the modulus of elasticity of masonry equal to 10.7 GPa based on a

Secant line between 5% and 33% of f'_m. Lastly, the ratio of experimental to theoretical ultimate strength using the chosen stress-strain curve varies from 1.01 to 1.15. The results of section analyses are summarized and compared with those of the wall tests in Table 5.1.

5.2.3 Discussion

One valuable finding of abovementioned analyses is that the use of Whitney block factors α_1 and β_1 culminated in underestimating the nominal flexural capacity of the concrete masonry walls; whereas, the use of stress-strain models specified for concrete masonry provided us with more precise evaluation of walls' strength.

The relatively lower theoretical values, in general, can be attributed to a number of causes. Concrete masonry as an assembly of nonhomogeneous compounds could not be accounted for perfectly by the same approach that is used for concrete unless its stress-strain relationship is established properly. In addition, the structural properties of the masonry assemblage are influenced by labor and materials; hence, they acquire notable discrepancy from day to day of the construction period.

Another parameter conducive to the results mismatch can be the presence of grout cores inside the hollow concrete blocks. The theoretical analysis is carried out assuming that, according to the results of auxiliary tests, f'_m is 10.9 MPa. For the prisms tested under compression, the grout expansion was of major reasons initiating the failure, whereas for the walls tested under out-of-plane bending the grout is not subjected to compression, thus not expanding, since the depth of the compression zone (c), except for G-3#19-F, is always less than the face shell thickness. Therefore, the masonry compound

can undertake larger amounts of stress in the compression zone leading to higher flexural resistance for the walls. Furthermore, it can be concluded that grouting the cells with no reinforcement is not necessarily effective, as seen before in the results of the wall tests, since the grout is not contributing to the flexural strength of the section.

5.3 Force-Deformation Prediction

As another facet of response of the walls to out-of-plane bending, it is invaluable to have the ability of foreseeing their force-deformation relationship up to the ultimate failure. To begin with, various models that have been proposed for predicting deflection in FRP-RC and masonry members are inspected and put on display in comparison to the results of the wall tests. Later on, a computer program is utilized for the same purpose; and accordingly, efforts have been made to come up with a finer numerical method of evaluating this characteristic of GFRP-reinforced walls based on the results and observations of the wall tests.

Compressive strength and modulus of rupture used in calculating the deflections are the ones obtained in the course of the auxiliary tests, while for the modulus of elasticity it was decided to use the one corresponding to the stress-strain model defined by Dhanasekar and Shrive (2002). The mid-span deflections of tested walls before the cracking moment are calculated using the gross section properties. The post-crack deflections are tried to be calculated using the effective moment of inertia (I_{eff}) method such that the tension-stiffening below the neutral axis between the uncracked and cracked grout is taken into account.

5.3.1 Available Methods of Cracked Section Analysis

CSA S304.1 (2004) defines an equation to calculate I_{eff} for steel-reinforced masonry similar to steel-reinforced concrete. Thus, it is an appropriate approach to use the proposed I_{eff} for FRP-RC members in calculating the deflections of the GFRP-reinforced walls. There are various ways of determining I_{eff} which are proposed and verified by several researchers (Faza and GangaRao (1992), Benmokrane *et al.* (1996), Brown and Bartholomew (1996), Thériault and Benmokrane (1998), Gao *et al.* (1998), Abdalla (2002), and Mota *et al.* (2006)). Moreover, Horton and Tardos (1990) have suggested another way of predicting the post-crack deflection for masonry members, in particular. It was observed in the course of analysis and also can be detected by comparing Figure 5.2 and Figure 5.3 that different methods yield to diverse results for lower amounts of reinforcement while they converge for higher reinforcement ratios. However, all the different available numerical methods of deflection evaluation underestimate the out-of-plane deformation of the walls in view of the fact that they are either not taking the special characteristics and differences of concrete masonry into account or they have been developed based on a limited knowledge of FRP's bond characteristics. The methods proposed for FRP-RC would not completely be capable of explaining the significant openings that are imposed to take place in the bed joints of the maximum moment zone. Moreover, these models mostly contain parameters that are found by curve fitting the results of limited test specimens, reinforced by particular types of FRP, which need further experiments to be generalized. The ones that are specialized for reinforced masonry, on the other hand, could not be representative of the special characteristics of FRP. For instance, Lee (2001) predicted only 67% (and less) of the

experimental deflection of FRP-strengthened masonry walls with cracked section analysis which was explained to be due to local bond failure of the FRP that can not be accounted for in the available methods of analysis. The load-deflection relationships of the wall predicted using I_{eff} defined by Gao *et al.* (1998) has been picked herein, as the commonly acknowledged method, to be illustrated and compared with the test results; since, it has been recognized by ISIS M03 (2001) to be used for predicting the deflection of FRP-RC members in flexure. It is calculated using this equation:

$$I_{eff} = I_{cr} + (\beta_b I_g - I_{cr})\left[1 - \left(\frac{M_{cr}}{M_a}\right)^3\right] \tag{5.10}$$

In which, I_{cr} and I_g are the moment of inertia of the cracked and gross section, M_{cr} and M_a are the cracking moment and applied moment of the section at each stage, and lastly, β_b depending on the properties of the composites is calculated as follows:

$$\beta_b = 0.5\left[1 + \frac{E_{FRP}}{E_{steel}}\right] \tag{5.11}$$

The load-deflection performances of the GFRP-reinforced walls predicted in this last-mentioned fashion are compared with test results in Figure 5.4 to Figure 5.9.

5.3.2 Force-Deformation Prediction Using Response 2000

In addition to the numerical evaluation, the tested walls were modeled in Response-2000 Version 1.0.5 (Bentz (2000)) which is a freely available specialty program for RC section analysis developed at the University of Toronto, based on the modified compression field theory. It has the ability to be given the full axial stress-strain curve of the masonry (i.e. the refined model proposed by Dhanasekar and Shrive (2002))

as well as the tensile properties of steel and GFRP reinforcements for modeling the wall sections. The load-deformation responses of the walls using the analysis program are also shown in Figure 5.4 to Figure 5.9. It can be observed that the load-deformation curves given by the program are a finer evaluation of the experimental results for the walls with lower reinforcement ratios, although still underestimating.

5.3.3 Proposed Method for Force-Deformation Prediction

In general, it is concluded that all the methods that have been developed to predict the load-deformation behaviour of reinforced masonry members are underestimating the post-crack deformations. One of the potential reasons, that was observed in the course of the tests of the masonry walls, can be the considerable width of the flexural cracks occurring at the mortar to block interface which magnifies the deformed shape of the wall. In other words, the total displacement of the wall is also comprised by the displacement caused by cracking pattern, which is not accounted for by current methods of predicting the deflection.

$$\Delta_{total} = \Delta_{analytical} + \Delta_{crack} \tag{5.12}$$

A simple approach is proposed here in order to improve the predictions of load-deformation behaviour of masonry walls reinforced with GFRP by adding the effect of wide cracks to the deflections predicted by cracked section analysis (introduced in ISIS (2001)). The width of the cracks can be calculated similar to FRP-RC as stated in ISIS (2001):

$$w_{crack} = 11 \times 10^{-6} \frac{E_{steel}}{E_{FRP}} k_b f_{FRP} \frac{h-c}{d-c} \left(d_c A\right)^{1/3} \tag{5.13}$$

In this equation, h is the thickness of the cross-section of the wall (i.e. 190 mm), d_c is the cover for the reinforcing rods, A is the effective tension area surrounding the reinforcing rods divided by the number of the rods, E_{steel} is the modulus of elasticity of the steel rebars, and k_b is a bond dependent coefficient that is found by Gao *et al.* (1998) to be 0.71, 1.00, and 1.83 for GFRP bars with superior, similar, and inferior bond properties when compared to steel (ISIS (2001)). k_b equal to 0.71 is employed in the calculation of crack width for the GFRP-reinforced walls in this research for two reasons; firstly, it was observed in the course of the experiments that the GFRP-reinforced walls experienced less wide cracks than the steel-reinforced wall at the same level of loading, and lastly, Ahmed *et al.* (2006), who conducted an experimental investigation on a total ninety sand-coated GFRP V-ROD™ specimens (i.e. the type that is utilized in the experimental program of this research) with respect to their bond behaviour, concluded that the required embedment length for the sand-coated V-ROD™ is $10d_b$, which is considerably less than that of steel rebars.

The additional deformation due to the crack width is then calculated based on the rotation of the wall at the cracking point assuming that 1) the cracks are imposed to occur at the interface of blocks and mortar, 2) the width of the cracks in all the joints inside the constant moment zone are the same, 3) the effect of shear cracks are neglected, 4) the crack width and depth increase linearly from zero, at the stage of cracking moment, to the maximum value at failure, and 5) maximum depth of the crack is the depth of the tension zone (i.e. h - c). The rotation due to each crack is calculated as such:

$$\theta = k_{crack} \frac{w_{crack}}{d_{crack}} \tag{5.14}$$

w_{crack} and d_{crack} are the width and depth of the crack and k_{crack} is the ratio of the depth of the crack to the depth of the cross-section which represents the resistance of uncracked zone. The deflection due to θ is the moment at mid-height of the conjugate structure of the wall, when a point load equal to θ is applied at the location of the crack. Therefore, the total deflection of the wall at each post-crack stage of the loading is the superimposition of the deflection found by the cracked-section analysis and the extra deflection due to the excessive width of the cracks in the maximum moment zone. Figure 5.4 to Figure 5.9 illustrate that the load-deformation performance of the GFRP-reinforced walls predicted by this new method introduced herein, shows agreeable consistency with the experimental result. The outcomes of the load-deflection analyses are also tabulated in Table 5.2.

5.4 Proposed Design Diagram

One of the main objectives of this research was to assure a facilitated approach to design the masonry walls for out-of plane bending when reinforced with GFRP rebars. For designing FRP-RC members in flexure, design charts are provided by ISIS (2001) for a given cross-sectional dimensions. The reinforcement ratio required for a certain amount of resistant moment can be chosen simply by following the proper curves of the charts. Having the results of the tested walls (i.e. the nominal flexural capacity and ultimate FRP tensile strain at failure) for different reinforcement ratios, a similar attempt has been made to propose a design diagram illustrated in Figure 5.10. The theoretical predictions are based on f'_m equal to 10.9 MPa and corresponding properties for different diameters of GFRP rods. However, in order to simplify the use of this type of diagrams, they can be

achieved eventually based on the average properties of the composites regardless of their slight variations due to the chosen diameters in design. The results of the tested walls seem to have consistency with the predicted values, that is to say the methods of analysis presented herein can be relied on to design this type of structural members. However, the author believes that further studies and experiments on FRP-reinforced masonry are required in order to validate and generalize the outcomes of this study.

Table 5.1. Summary of the section analyses for the full-scale masonry walls

Wall	Flexural capacity (kN.m)			$\frac{M_{n,exp.}}{M_{n,Whitney}}$	$\frac{M_{n,exp.}}{M_{n,Dhanasekar}}$
	Test results	Whitney block	Dhanasekar and Shrive		
U-F	5.6	6.4	6.6	0.89	0.85
S-5M10-F	16.9	16.6	16.2	1.01	1.05
G-3#10-F	14.2	12.8	13.1	1.15	1.09
G-3#13-F	18.3	15.9	17.7	1.15	1.03
G-3#13-P	17.9	15.8	17.6	1.13	1.02
G-4#13-F	21.7	19.2	21.4	1.13	1.01
G-4#13-P	30.3	24.5	27.3	1.23	1.11
G-3#19-F	39.3	30.6	34.2	1.28	1.15

Table 5.2. Summary of the load-deflection prediction for the full-scale masonry **walls**

Wall	Max. deflection at failure (mm)				$\frac{\Delta_{(1)}}{\Delta_{Exper.}}$	$\frac{\Delta_{(2)}}{\Delta_{Exper.}}$	$\frac{\Delta_{(3)}}{\Delta_{Exper.}}$
	Test result	(1) ISIS (2001)	(2) Response 2000	(3) Proposed method			
G-3#10-F	111.4	19.1	86.0	103.4	0.17	0.77	0.93
G-3#13-F	107.4	32.8	73.8	96.7	0.31	0.69	0.90
G-3#13-P	108.5	35.0	74.5	85.6	0.32	0.69	0.79
G-4#13-F	108.9	42.5	61.7	89.4	0.39	0.57	0.82
G-4#13-P	94.3	49.2	57.3	81.4	0.52	0.61	0.86
G-3#19-F	93.6	43.7	48.0	72.7	0.47	0.51	0.78

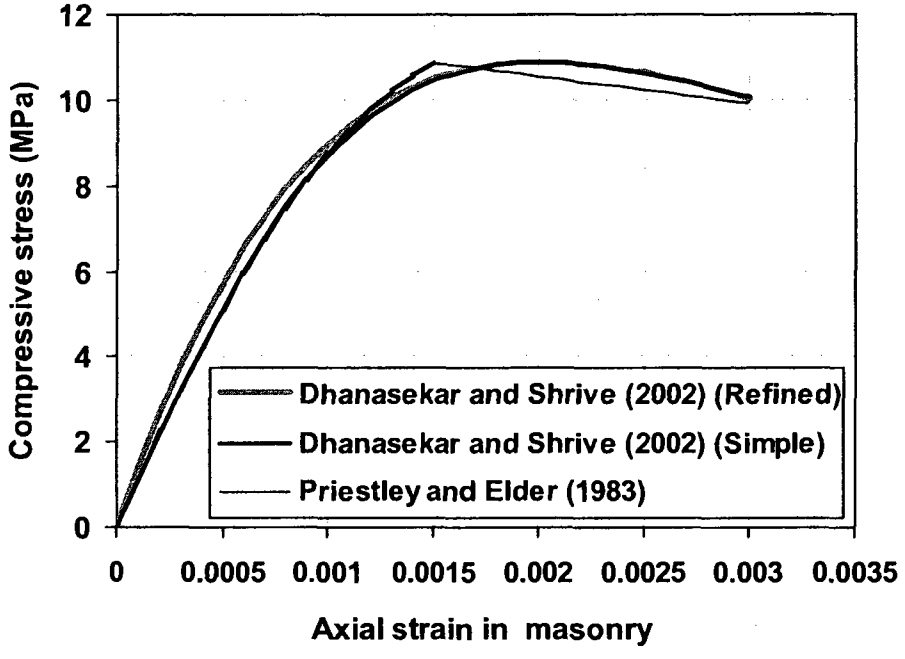

Figure 5.1. Stress-strain relationships for concrete masonry using three different models

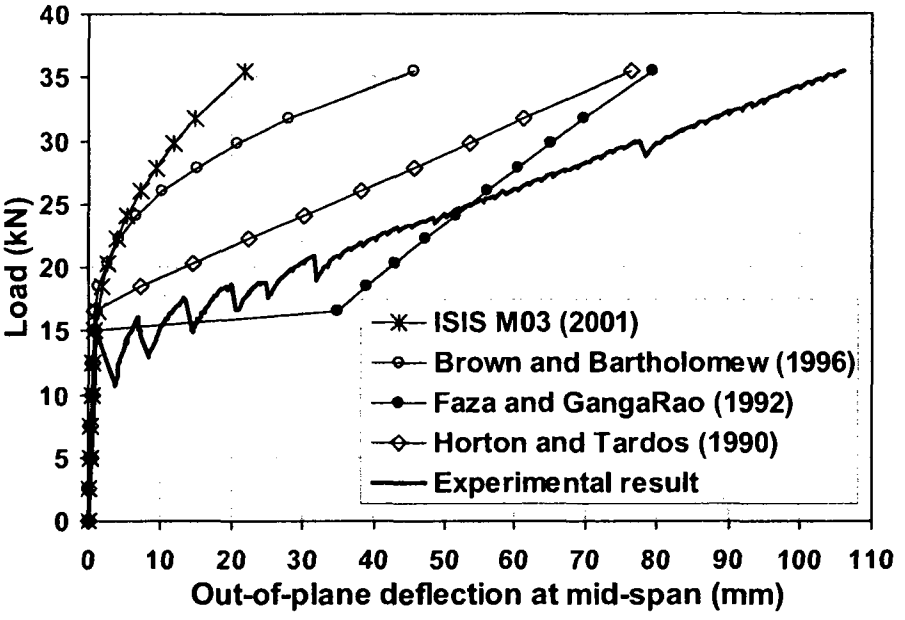

Figure 5.2. Load-deflection prediction for wall G-3#10-F using different methods of cracked section analysis

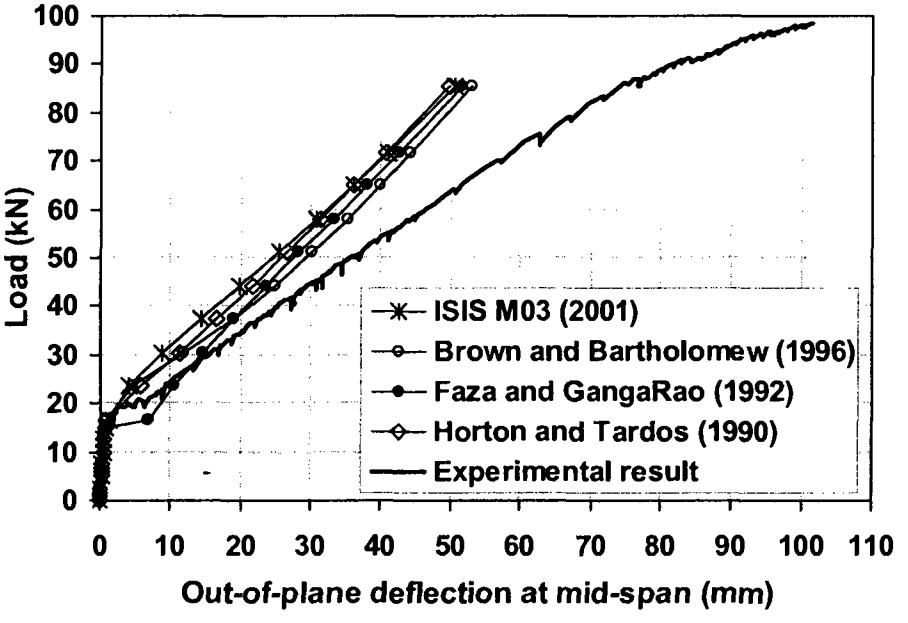

Figure 5.3. Load-deflection prediction for wall G-3#19-F using different methods of cracked section analysis

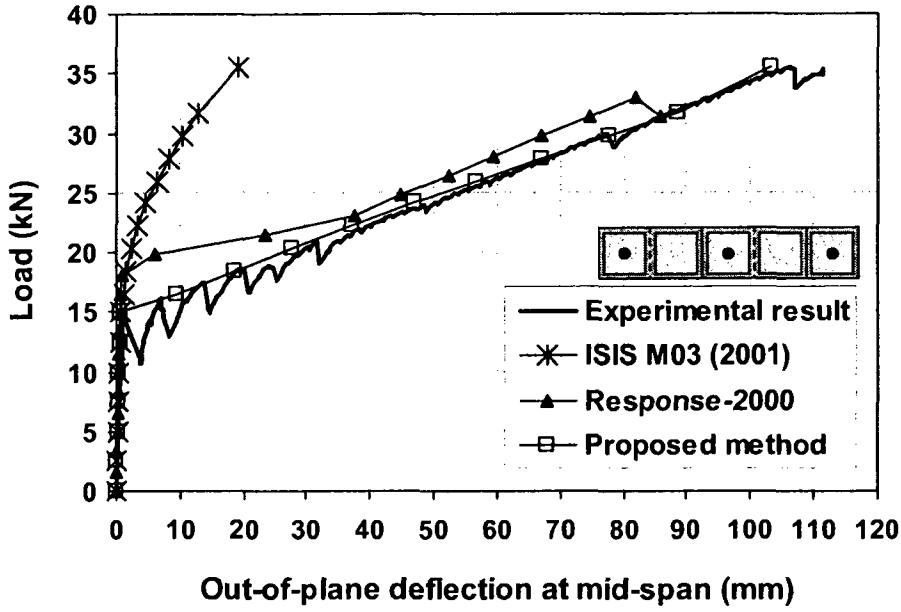

Figure 5.4. Load-deflection prediction for wall G-3#10-F

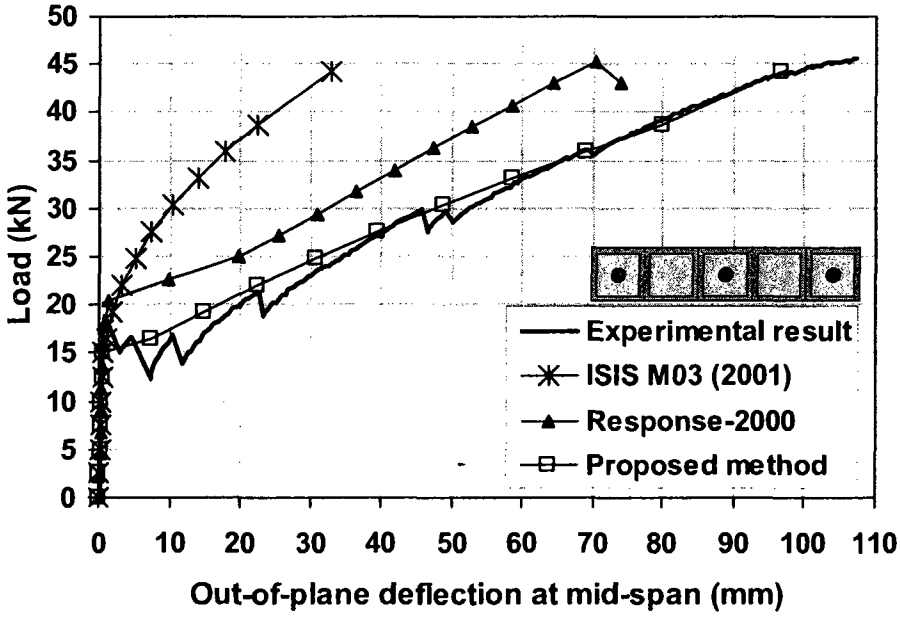

Figure 5.5. Load-deflection prediction for wall G-3#13-F

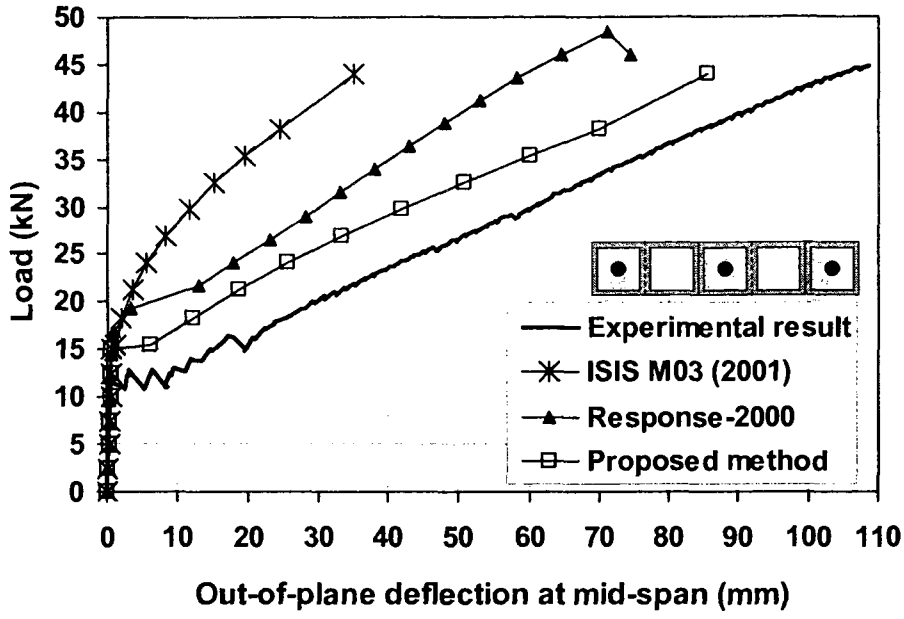

Figure 5.6. Load-deflection prediction for wall G-3#13-P

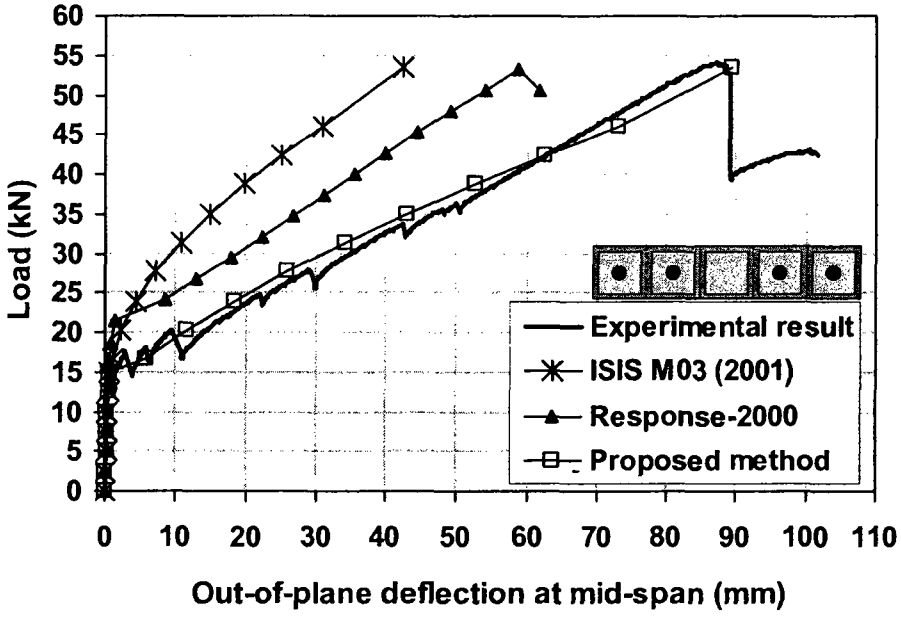

Figure 5.7. Load-deflection prediction for wall G-4#13-F

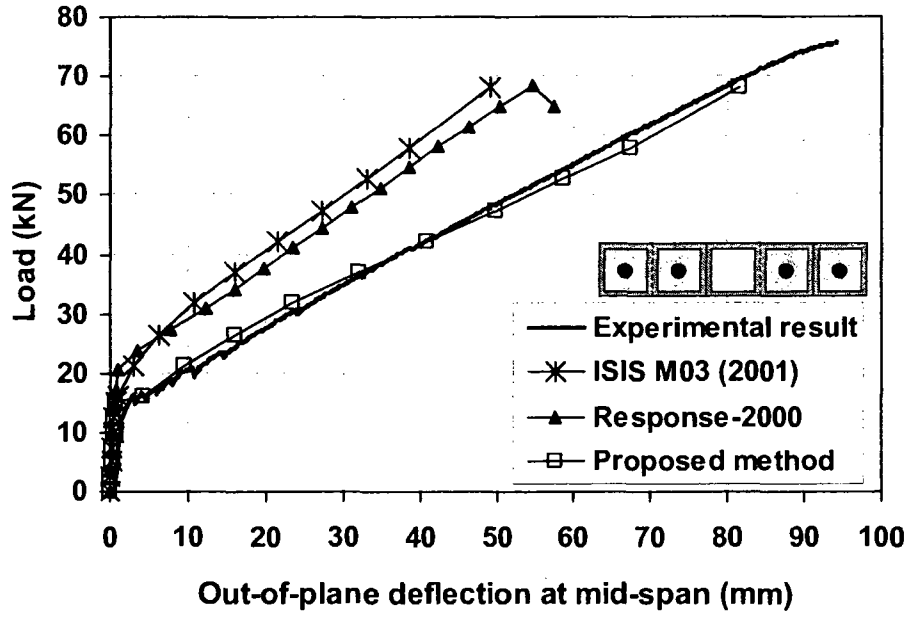

Figure 5.8. Load-deflection prediction for wall G-4#13-P

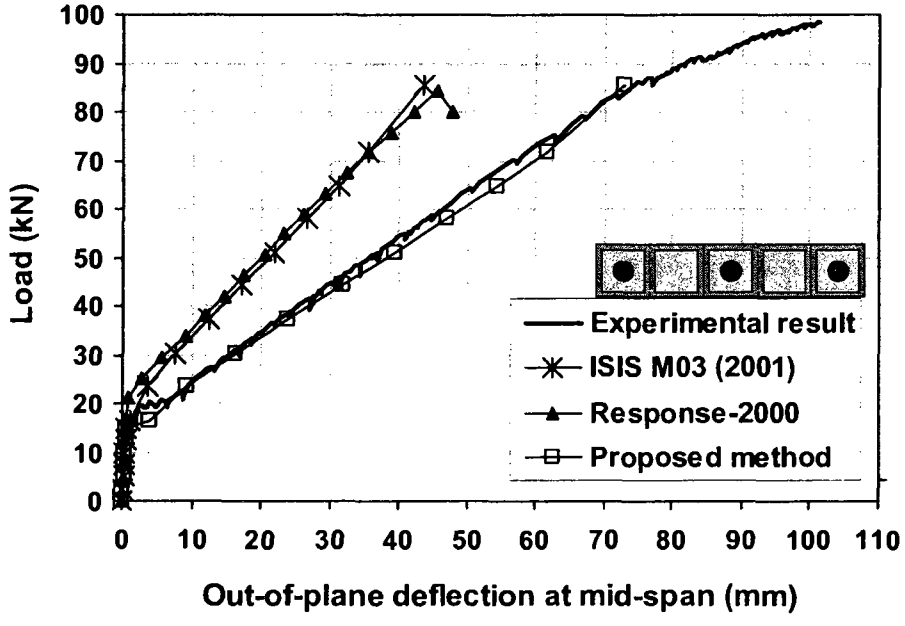

Figure 5.9. Load-deflection prediction for wall G-3#19-F

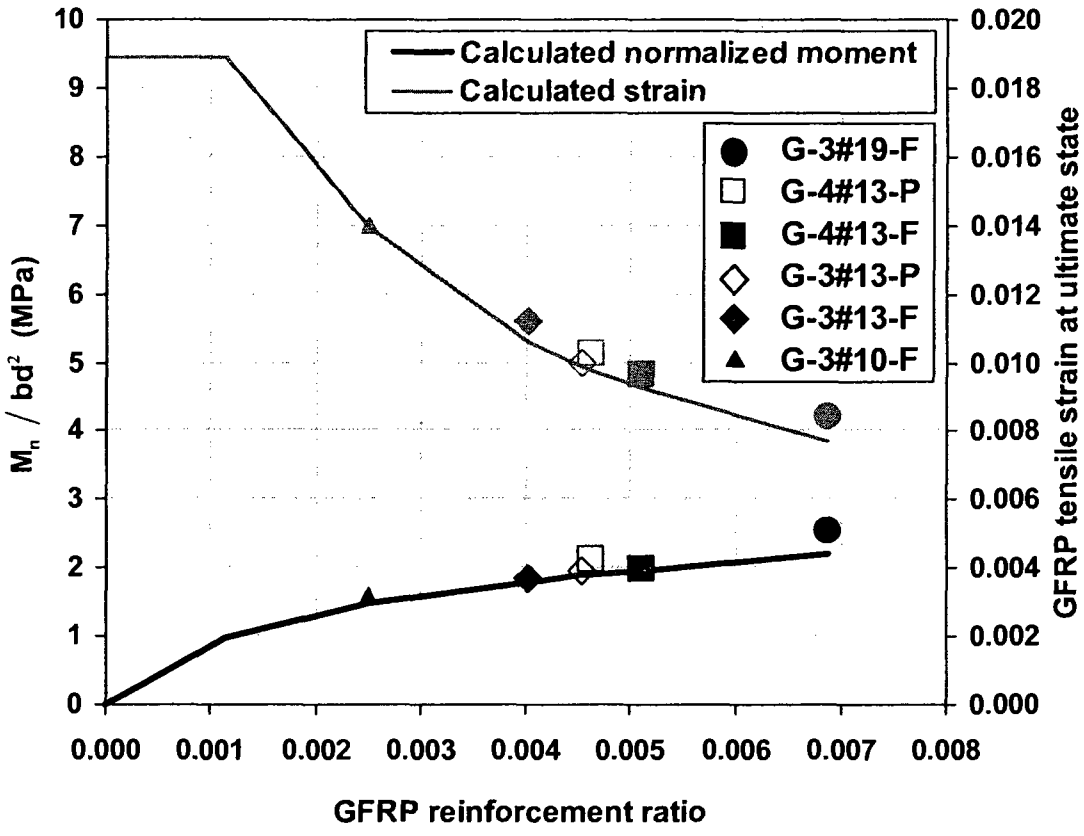

Figure 5.10. Proposed capacity chart for designing masonry walls reinforced with GFRP rods (f'_m = 10.9 MPa, $f_{u,FRP(ave.)}$ = 790 MPa, $E_{FRP(ave.)}$ = 46.4 GPa)

CHAPTER 6

DEFORMABILITY

6.1 General

When steel rebars are substituted with FRP ones whose behaviour is linearly elastic up to the sudden rupture, the ductility of the walls arises as a concern affecting their performance before failure. For steel-reinforced elements, conventional definition of deflection ductility as the ultimate-to-yield deformation ratio ($\mu_\Delta=\Delta_u/\Delta_y$) determines whether or not the members have sufficient ductility; however, for FRP-reinforced elements ductility should be defined apparently in a fashion that is independent of reinforcement yield point. In order to evaluate the ductility of GFRP-reinforced masonry walls two different approaches have been utilized based on different aspects of the load-deformation performance of the walls.

6.2 Curvature-Based Deformability Factor

One method is to calculate the deformability factor or J-factor proposed by Jaeger *et al.* (1995), which is modified to be introduced as a criterion for FRP-RC members in ISIS (2001), and calculated based on the curvature of the walls at ultimate and service load as such:

$$Deformability\ factor = \left(\frac{\psi_u M_u}{\psi_s M_s}\right) \tag{6.1}$$

where the s index refers to the service load that was primarily designated by Jaeger *et al.* (1995) to be the load at which point the compressive strain in concrete is 0.001. However,

ISIS (2001) associates it with a load due to which the tensile strain in the outermost FRP rebars reaches 0.002. The curvature therein was calculated based on the experimental deformed shapes of the walls. In other words, the absolute value of the second derivative of the deformed shape with respect to the length of the wall at each stage was considered as the curvature. This factor, which is required by ISIS (2001) to be more than 4 for all sections in flexure, is calculated for the tested GFRP-reinforced masonry walls to investigate their ductility (see Table 6.1).

6.3 Energy-Based Ductility

The second method that was used for evaluating the ductility of the GFRP-reinforced walls is based on the energy absorption capacity. Having the load-displacement diagram, the total absorbed energy by the wall can be calculated as the area under the curve. The permanent (i.e. inelastic) deformation and the unloading curve differentiate the elastic and inelastic energies. That is to say the dissipated energy by permanent deformations is represented by the inelastic portion of the area (i.e. the area surrounded between the loading and unloading curves). Given the fact that the more inelastic energy, the more ductile behaviour, the ductility of the walls can be evaluated based on the ratio of inelastic energy to total energy (energy ratio). Jeong (1994) expressed the ductility of FRP-RC members, disregarding the existence of yielding phenomenon although based on the same concept of deflection ductility, with a new ductility index (the Naaman index) using the energy ratio (see Figure 6.1 (a)):

$$\mu = \frac{1}{2}\left(\frac{E_{total}}{E_{elastic}} + 1\right) \tag{6.2}$$

where μ is the Naaman index, and E_{total} and $E_{elastic}$ are respectively the total and elastic absorbed energy by the wall.

A ductility index of 2.5, which has been adopted in structural codes (e.g. ACI (2008)) as the accepted level of ductility for steel-reinforced members, was considered to be adequate by Jeong (1994), since this new index was derived from the conventional definition of deflection ductility. Grace *et al.* (1998) have also categorized the flexural members with energy ratio of 75% and higher to have ductile behaviours. This energy ratio results in a ductility index of 2.5 and higher which was set to be the limit by Joeng (1994).

6.3.1 Experimental Unloading Curves

Three of the GFRP-reinforced walls (namely G-3#13-F, G-3#13-P, and G-3#19-F) were unloaded after the ultimate failure, for which the energy ratio can be found based on the experimental results (see Figure 6.3 to Figure 6.5). As shown in the figures, removal of the load does not change the deformed shape of the walls up to a certain limit, from which point, the deflection starts decreasing with a slope close to that of the post-crack loading curve. Table 6.2 contains the calculated energy ratios based on the experimental results for the foregoing GFRP-reinforced walls.

6.3.2 Numerical Method

Joeng (1994) proposed a method to predict the unloading part of the load-deflection curve based on the loading part. In this method the slope of the unloading part is the weighted average of three different segments of the loading curve (see Figure 6.1

(b)). Grace *et al.* (1998), as shown in Figure 6.2, made some modifications to the foregoing method, such that it takes into account mode of failure (β), type of reinforcement (γ), and properties of the FRP that is used as the flexural reinforcement. The slope of the unloading curve is consequently found by the following equation:

$$S = \beta\gamma \frac{E_{FRP}}{E_s} \times \frac{f_y}{f_{u,FRP}} \times \frac{P_1 S_1 + (P_2 - P_1) S_2 + (P_3 - P_2) S_3}{P_3} \qquad (6.3)$$

In which β for compressive failure is 1.0 and γ for GFRP is 4.0. P_1, P_2, and P_3 are the loads corresponding to three different points of the loading curve where the slope of the load-deflection curve changes notably. S_1, S_2, and S_3 are the slopes associated to three parts of the loading-curved that are differentiated with P_1, P_2, and P_3. The theoretically predicted unloading curves for the tested GFRP-reinforced masonry walls are illustrated in Figure 6.6 to Figure 6.11. The permanent deflections (after unloading) as a result of the proposed equation conform adequately with the results of the three unloaded walls (see Figure 6.7, Figure 6.8, and Figure 6.11), even though the predicted unloading curves underestimate the inelastic portion of total energy leading to a conservative evaluation of ductility of the walls. Table 6.2 categorizes the behaviour of the tested GFRP-reinforced walls based on their energy ratio that is calculated using the unloading curves predicted by the aforesaid method.

6.3.3 Proposed Method

Although the method that was introduced by Joeng (1994) and developed by Grace *et al.* (1998) for predicting the slope of the unloading part of load-deflection diagram has proven to be capable of foreseeing the unloading behaviour of the FRP-RC

members, the performance of the three GFRP-reinforced walls, of all the tested walls, that were unloaded after the failure, revealed that a different type of behaviour with two evident characteristics could be attributed to the GFRP-reinforced masonry walls.

According to the performance of the abovementioned GFRP-reinforced walls, it can be stated that there exists a post-failure residual capacity after the failure occurs for the GFRP-reinforced masonry wall. Hence, when the loading stopped (due to failure of masonry), the recorded applied load decreased to a lower level which was partly due to the presence of the GFRP rebars which had not failed and were still capable of undertaking tensile stresses. The load and deflections would start to decrease from that point with a slope which is almost equal to the slope of the post-crack loading curve, as opposed to FRP-RC, if the wall was to be unloaded gradually. Thus, the residual capacity and the slope of the unloading curve are the main features of the unloading behaviour of the GFRP-reinforced masonry walls that differentiate them from FRP-RC.

Based on the results of the walls that were unloaded gradually after failure, a simple method is proposed here to predict unloading behaviour of the GFRP-reinforced masonry walls assuming that the post-failure residual capacity is only 50% of the post-crack strength of the wall and the slope of the unloading branch of the curve is equal to the slope of the post-crack loading diagram. These two parameters can be calculated as such:

$$Residual\ Capacity = 0.5\left(M_n - M_{cr}\right) \tag{6.4}$$

and

$$S = \frac{M_n - M_{cr}}{\Delta_u - \Delta_{crack}} \tag{6.5}$$

S is similarly the predicted slope of the unloading part of the load-deflection curve. The numerically predicted unloading curves are shown in Figure 6.6 to Figure 6.11. Moreover, Table 6.2 includes the energy ratios calculated using the proposed method, based on which the bahaviours of the walls are categorized.

6.4 Discussion

The deformability factor of the GFRP-walls not only satisfies the lower limit set by ISIS (2001), but also this factor is fairly higher than the limit for all of the tested walls. This can be accounted for by the fact that the out-of-plane deflection and accordingly the curvature of the deformed shapes are trivial before the section is cracked. However, the presence of the GFRP reinforcing rods supplies for notable deformation prior to the ultimate failure. The deflection of the wall at the stage of cracking, in some cases, was less than one percent of the deflection at failure. The ratios of deflection at the cracking stage to deflection at ultimate for the tested GFRP-reinforced walls are listed in Table 6.1.

The experimental unloading curves express that the energy ratio for the GFRP-reinforced walls is satisfactory since the permanent deflections compared to the total deflections of the walls are not significant. The theoretical unloading curves found by the approach proposed for FRP-RC (Joeng (1994), and Grace *et al.* (1998)) affirm the same conclusion. Regardless of the fact that this method does not account for the initial part of the load removal, due to which no deflection is recovered, it can be seen that the theoretical elastic deformation is closed to that of the walls that were unloaded during the tests.

The shapes of the predicted and experimental unloading curves in Figure 6.7, Figure 6.8, and Figure 6.11, and also the energy ratios calculated using the proposed predictions compared to the experimental energy ratios (see Table 6.2) proved that the method which is proposed herein for GFRP-reinforced masonry walls is capable of expressing the unloading performance of the tested GFRP-reinforced masonry walls more specifically and closer to the actual behaviour of the tested walls. The pre-failure behaviour of all the tested GFRP-reinforced masonry walls can be considered to have adequate deformability based on the numerically calculated energy ratios using the proposed model.

Overall, despite the fact that the use of GFRP instead of steel diminishes the ductile behaviour of the masonry walls, the investigations and analyses carried out in this chapter showed that all the GFRP-reinforced walls have exhibited acceptable deformability.

Table 6.1. Classification of the GFRP-reinforced walls according to their curvature based deformability factor

Wall	$\frac{\Delta_{crack}}{\Delta_u}$ (%)	Curvature Factor	Moment Factor	Deformability Factor	Type of Behaviour*
G-3#10-F	0.90	13.7	3.3	45.5	Ductile
G-3#13-F	0.75	6.2	3.7	22.9	Ductile
G-3#13-P	2.82	5.8	2.7	15.8	Ductile
G-4#13-F	2.45	14.8	2.0	29.8	Ductile
G-4#13-P	3.20	10.1	3.8	37.9	Ductile
G-3#19-F	0.53	7.4	4.1	30.6	Ductile

* *Based on deformability factor limit of 4 for ductile behaviour of FRP-RC members (ISIS 2001).*

Table 6.2. Classification of the GFRP-reinforced walls according to their energy based ductility

Wall	Experimental		Grace *et al.* (1998)		Proposed method	
	$\frac{E_{inelastic}}{E_{total}}$	Type of behaviour*	$\frac{E_{inelastic}}{E_{total}}$	Type of behaviour*	$\frac{E_{inelastic}}{E_{total}}$	Type of behaviour*
G-3#10-F	—	—	0.94	Ductile	0.90	Ductile
G-3#13-F	0.91	Ductile	0.80	Ductile	0.89	Ductile
G-3#13-P	0.81	Ductile	0.82	Ductile	0.86	Ductile
G-4#13-F	—	—	0.92	Ductile	0.88	Ductile
G-4#13-P	—	—	0.57	Brittle	0.84	Ductile
G-3#19-F	0.76	Ductile	0.66	Brittle	0.83	Ductile

* *Based on minimum energy ratio of 75% for ductile behaviour of FRP-RC members (Grace et al. (1998)).*

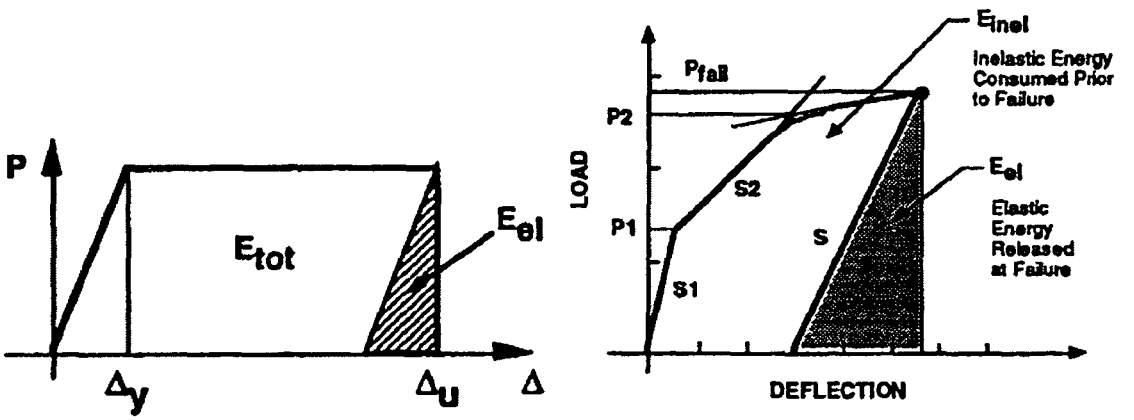

(a) (b)

Figure 6.1. Energy based ductility index: (a) definition of energy ratio based on the conventional deflection ductility; (b) prediction of unloading curve (Jeong (1994))

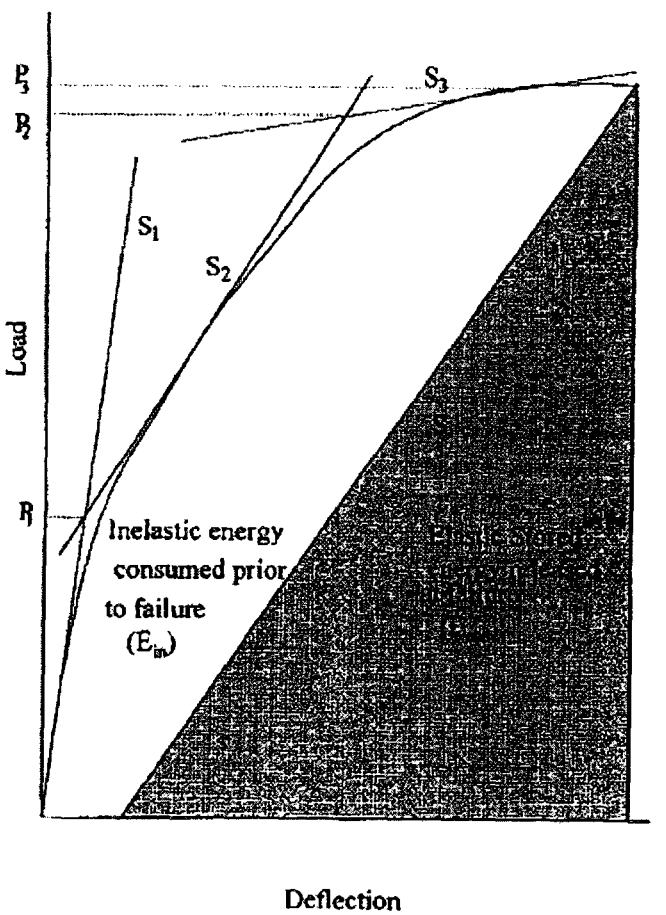

Figure 6.2. Prediction of unloading curve (Grace *et al.* (1998))

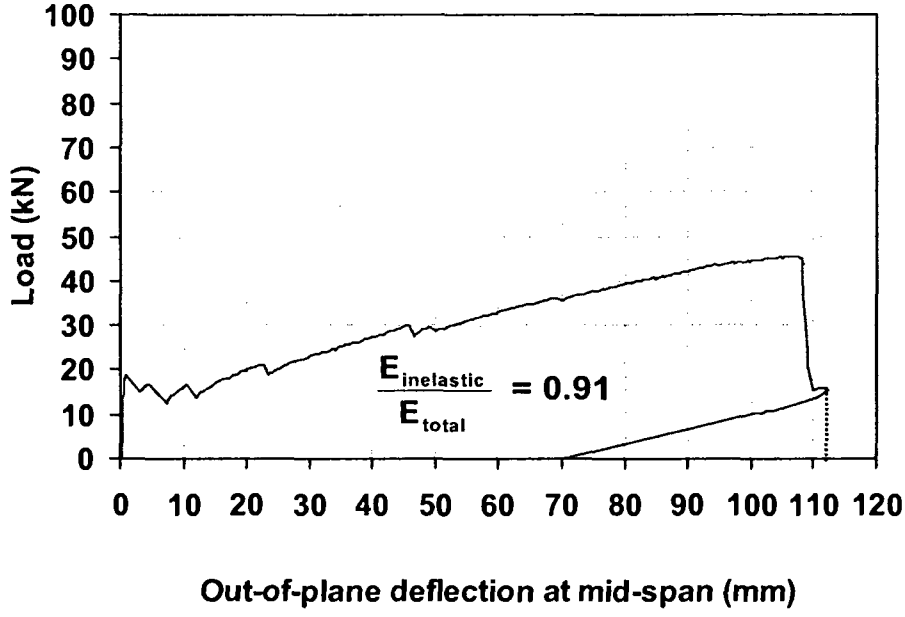

Figure 6.3. Experimental energy ratio for wall G-3#13-F

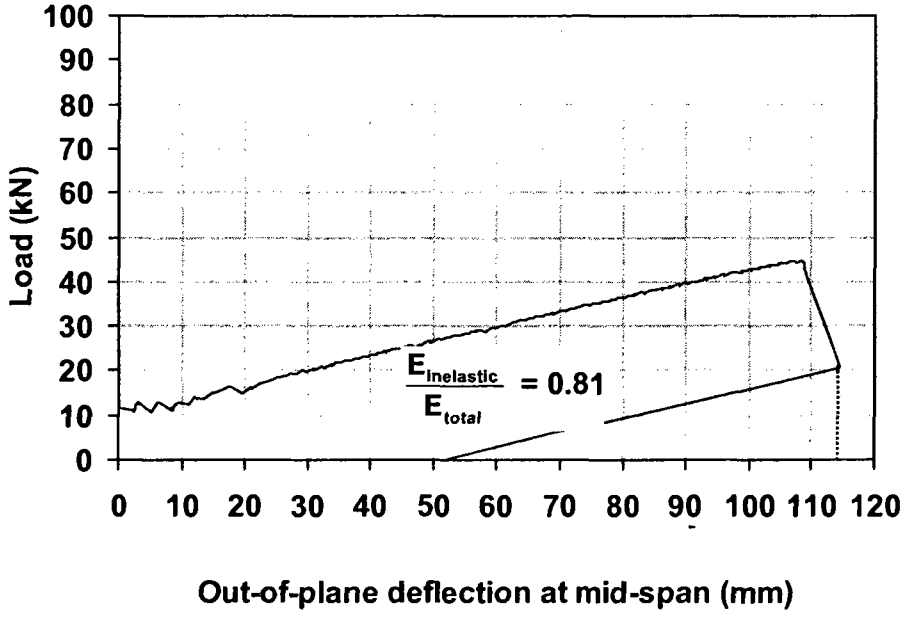

Figure 6.4. Experimental energy ratio for wall G-3#13-P

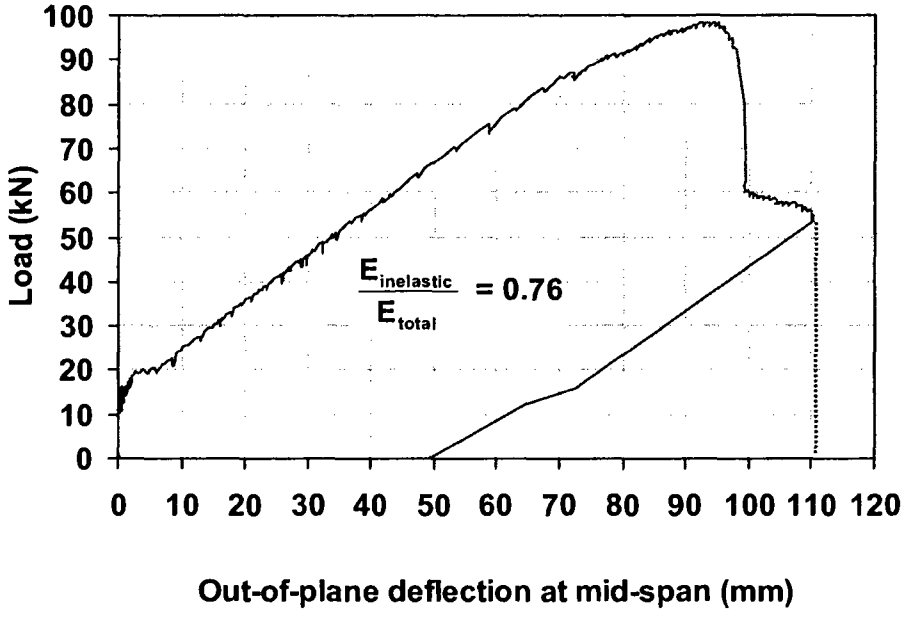

Figure 6.5. Experimental energy ratio for wall G-3#19-F

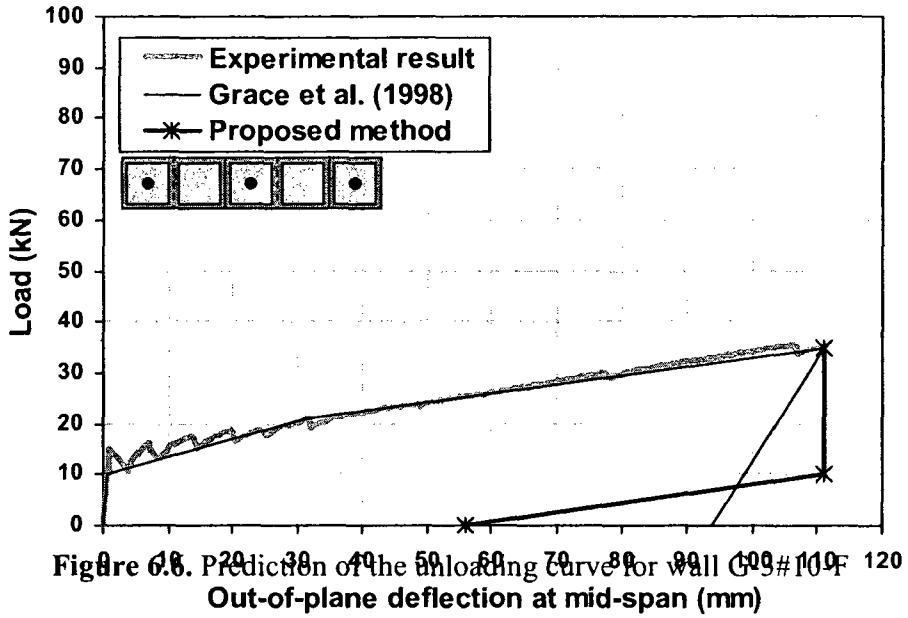

Figure 6.6. Prediction of the unloading curve for wall G-3#10-F

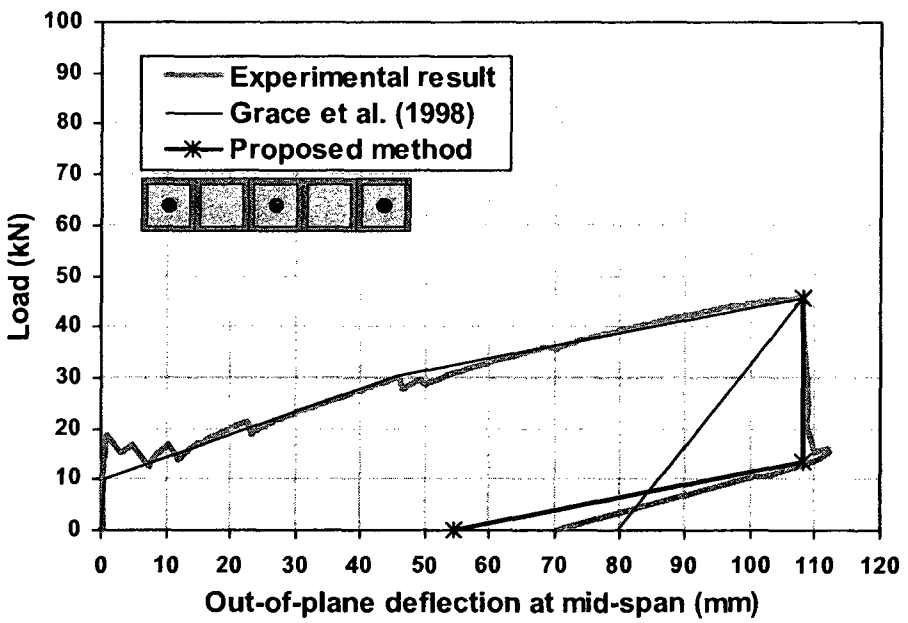

Figure 6.7. Prediction of the unloading curve for wall G-3#13-F

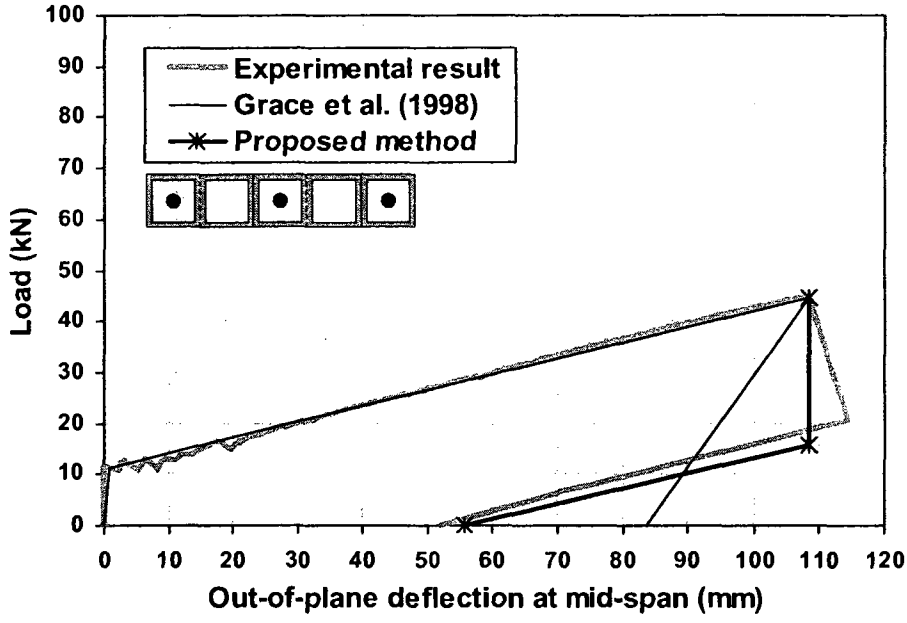

Figure 6.8. Prediction of the unloading curve for wall G-3#13-P

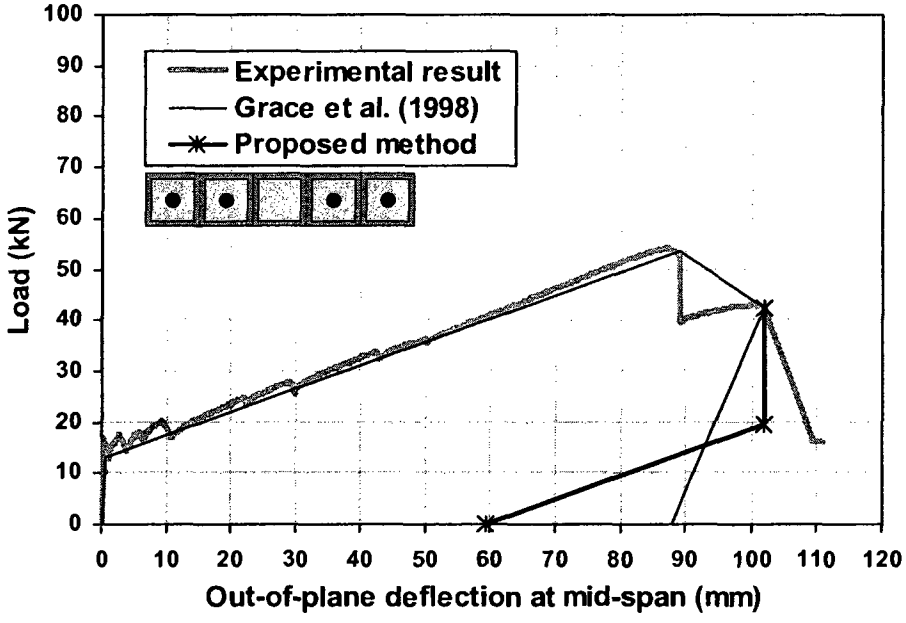

Figure 6.9. Prediction of the unloading curve for wall G-4#13-F

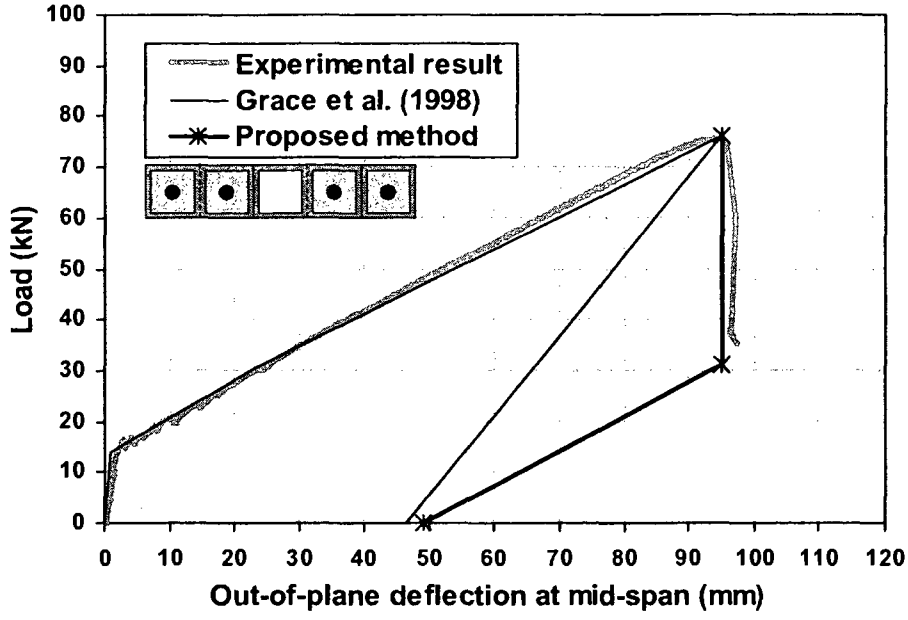

Figure 6.10. Prediction of the unloading curve for wall G-4#13-P

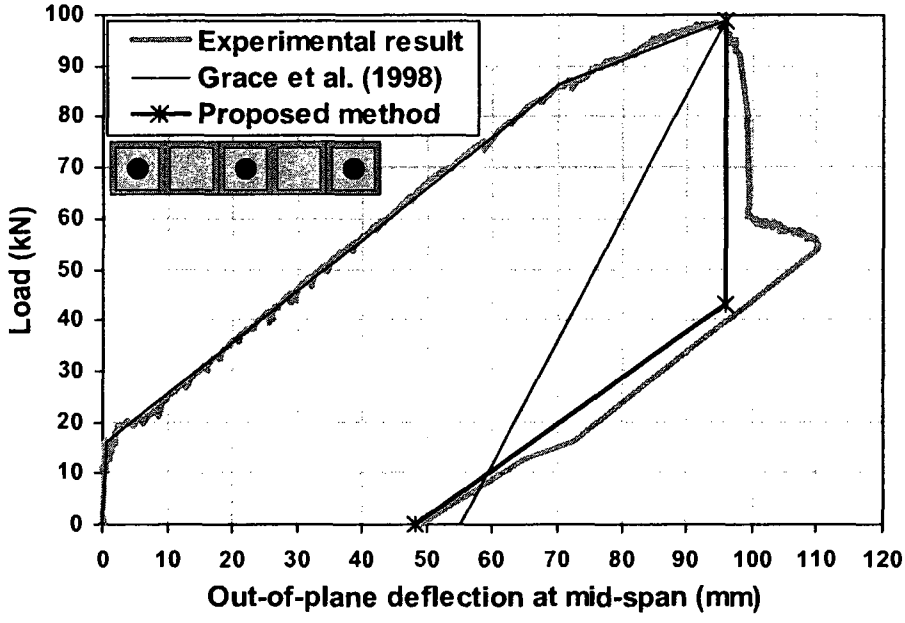

Figure 6.11. Prediction of the unloading curve for wall G-3#19-F

CHAPTER 7

SUMMARY, CONCLUSIONS, AND RECOMMENDATIONS

7.1 Summary

Unreinforced masonry structures are known as one of the oldest types of structures and have been frequently used since ancient times. However, lack of tensile strength of the masonry assembly has been barricading the structural engineers when it comes to design unreinforced masonry structures for lateral loads. This deficiency manifests itself especially in seismic prone areas where adequate lateral load bearing strength is required while the dimensions of the structural components should not be massive. Reinforced masonry walls are known as one of the most common structural masonry elements that are widely used to undertake vertical loads as well as lateral loads. Depending on the loading conditions they can be subjected to out-of-plane lateral loads due to wind, soil pressure, or seismic excitations, in which situations, flexural reinforcement is the critical factor influencing the flexural strength and behaviour of the walls. Steel reinforcing rebars are currently employed as the accustomed internal reinforcement for concrete masonry walls.

The objective of this study was to extract GFRP bars, with better durability characteristics, as the internal flexural reinforcement of the concrete masonry walls, so that the design constraint of having to not exceed the balanced reinforcement ratio (in the case of steel-reinforced walls) is resolved. Thus, higher flexural strength could be attained for the same cross-sectional dimensions; while, the ductility of the GFRP-reinforced walls, as an imperative factor of serviceability, is inspected to ensure that the

pre-failure behaviour of the wall is agreeable, disregarding the presence of GFRP in lieu of steel.

In order to fulfill the goals of this research, eight full-scale masonry walls (unreinforced and reinforced with steel and GFRP rebars) were built and tested under out-of-plane bending condition, in addition to the auxiliary masonry prisms that were meant to attain the properties of the masonry assemblage. One wall was unreinforced; another wall was reinforced with steel rebars and the other six walls were reinforced with different amounts of GFRP reinforcement. Two of the GFRP-reinforced walls were only grout-filled in the cells with the reinforcing bars in order to examine the effect of extent of grouting. The behaviour of the walls was studied by monitoring the cracking patterns and measuring the tensile strains of the reinforcing bars and deflections of different locations up to the ultimate failure.

Besides the experimental program, various methods of analyses and numerical models were examined for predicting different facets of the response of the walls (i.e. flexural capacity and deflection). Moreover, efforts have been made to come up with finer numerical models, the results of which were closer to those of the tests of the walls. Accordingly, a design diagram is proposed based on the relative performance of the GFRP-reinforced walls, having theorized their flexural response. Lastly, the deformability of the GFRP-reinforced walls are inspected through different approaches asserting the fact that even though FRP's are known as not-ductile materials, the tested walls have exhibited a sufficiently ductile behaviour.

7.2 Conclusions

Based on the results of the main and auxiliary tests and analyses performed on different aspects of behaviours of the walls, the following can be concluded:

1. The partially grouted walls cracked at fairly lower levels of applied load when compared to their analogous companions (i.e. fully grouted). However, type of the reinforcement (i.e. steel or GFRP) was noted to have no effect on the onset of cracking, nor did it on the immediate width of the cracks.

2. It was observed that for all the tested walls, the compression failure at the constant moment region occurred in the section of the bed joint that has shear reinforcement. This would imply that shear reinforcement could result in weakening of the bond in the block-mortar interface.

3. It was observed that after the first crack the tensile strain and accordingly the tensile stress of GFRP rods increase linearly with the applied load up to the failure of the walls.

4. The two GFRP-reinforced specimens that were designed to achieve ultimate limit flexural capacities equivalent to the steel-reinforced wall showed sufficient flexural deformability to forewarn the failure.

5. The performance of G-3#19-F compared to that of S-5M10-F shows that we can reach higher capacities with acceptable deformability that could not be achieved by steel-reinforced masonry walls due to the constraint of not exceeding the balanced reinforcement ratio.

6. The ratio of flexural strength to the self-weight of the walls increased for more GFRP reinforcements up to 9.6 (for wall G-3#19-F). This ratio was magnified 62% and

55%, respectively, for G-3#13-P and G-4#13-P compared to their analogous specimens (i.e. fully grouted ones).

7. The stress-strain model proposed by Dhanasekar and shrive (2002) showed good agreement with the experimental results which suggests that it could be used in developing capacity charts for designing masonry walls reinforced with GFRP.

8. Despite the fact that the use of GFRP instead steel diminishes the ductile behaviour of the masonry walls, it was observed that all the GFRP-reinforced walls have exhibited sufficient deformability.

In addition, the succeeding observations were noticed in the course of this research:

1. The compressive auxiliary prisms failed due to splitting the face shells preceded by cone and shear cracks that were caused by the excess of grout expanding inside the cells. The relatively lower strength of the prisms compared to their constituent materials can be attributed to this fact.

2. The GFRP-reinforced masonry walls exhibited a linear behaviour up to and after cracking moment, but the stiffness was decreased significantly after the first crack. It was observed that the stiffness of the GFRP-reinforced walls increased with higher reinforcement ratios.

3. The fact that the steel-reinforced wall encountered less shear cracks highlights the relatively higher contribution of steel reinforcement in shear strength compared to GFRP. On the other hand, the less wide cracks in the GFRP-reinforced walls underline the superior bond characteristics of this type of reinforcement.

4. All the GFRP-reinforced walls encountered flexural failure due to the compressive failure of masonry as opposed to the unreinforced wall that collapsed due to tensile failure in the bed joint.

5. It was concluded that with larger amounts of GFRP reinforcement post-failure resistance and elastic deformation increase significantly. The post-failure strength that the FRP-reinforced walls exhibited was enough to carry the dead load and also considerable amount of live load.

6. Except for G-3#19-F, the depth of the compressive zone was found to be less than the face shell thickness. Hence, grouting the cells with no reinforcement is not necessarily effective since the grout is not contributing to the bending actions of the section. The results of the wall tests acknowledged this matter.

7.3 Recommendations

It should be noted that the abovementioned conclusions are based on the limited experimental work described herein and the author believes that further studies and experiments on FRP-reinforced masonry have to be conducted in order to validate and generalize the findings of this experimental program.

As the results and mode of failure of the compressive masonry prisms highlighted, the importance and effects of the right choice of grout and concrete block on compressive strength of the masonry assemblage should be studied further.

The need to reinforce masonry walls for shear forces, especially for GFRP-reinforced masonry walls, calls for more research in shear strength of these walls and efforts to find more effective techniques to replace the joint reinforcement.

Since the compressive performance of GFRP is not notable, the response of GFRP-reinforced masonry walls when subjected to axial loads should be also inspected. More importantly, it is required to carry out further research on the beam-column behaviour of these walls, as in the actual situations walls are subjected to a combination of axial and lateral loads.

In this study, a few advantages of designing partially-grouted concrete masonry walls were revealed. Further investigation should be focused on different aspects of behaviour of partially-grouted walls in order to ensure that design deficiencies are not accompanying the mentioned benefits.

Lastly, since the walls that were tested in this dissertation were designed to have width of 1.0 m, representing the one-way load-transferring masonry wall systems, it is also necessary to inspect the effect of different width of the walls on their response.

REFERENCES

Abboud, B., Hamid, A., and Harris, H. (1996). "Flexural Behavior of Reinforced Concrete Masonry Walls under Out-of-plane Monotonic Loads." ACI Structural Journal., 93(3), 327- 335.

Abdalla, H. A. (2002). "Evaluation of deflection in concrete members reinforced with fiber reinforced polymer (FRP) bars." Composite Structures, 56(1), 63–71.

Ahmed, E. A., El-Salakawy, E., and Benmokrane, B. (2006). "Behaviour of post-installed GFRP adhesive anchors in concrete." Technical report, Department of Civil Engineering, University of Sherbrooke, Sherbrooke, Québec.

American Association of State Highway and Transportation Officials (AASHTO). (2000) "Standard specifications for design of highway bridges." AASHTO, Washington, DC.

American Concrete Institute (ACI). (2008). "318-08/318R-08: Building Code Requirements for Structural Concrete and Commentary." Detroit, MI.

American Concrete Institute (ACI). (2006). "440.1R-06: Guide for the design and construction of concrete reinforced with FRP bars." Farmington Hills, MI.

American Society of Testing and Materials (ASTM). (2002). "C1314-02: Standard Test Method for Compressive Strength of Masonry Prisms." West Conshohocken, PA.

American Society of Testing and Materials (ASTM). (2002). "C270-02: Standard Specification for Mortar for Unit Masonry." West Conshohocken, PA.

American Society of Testing and Materials (ASTM). (2002). "C476-02: Standard Specification for Grout for Masonry." West Conshohocken, PA.

American Society of Testing and Materials (ASTM). (2002). "C780-02: Standard Test Method for Preconstruction and Construction Evaluation of Mortars for Plain and Reinforced Unit Masonry." West Conshohocken, PA.

American Society of Testing and Materials (ASTM). (2002). "E518-02: Standard Test Method for Flexural Bond Strength of Masonry." West Conshohocken, PA.

Assa, B., and Dhanasekar, M. (2002). "A numerical model for the flexural analysis of short reinforced masonry columns including bond–slip." Computers and Structures, 80, 547–558.

Benmokrane, B., Chaallal, O., and Masmoudi, R. (1996). "Flexural response of concrete beams reinforced with FRP reinforcing bars." ACI Structural Journal, 91(2), 46-55.

Benmokrane, B., El-Salakawy, E., El-Ragaby, A., and Lackey, T. (2006). "Designing and testing of concrete bridge decks reinforced with glass FRP bars." ASCE Journal of Bridge Engineering, 11(2), 217-229.

Bentz, E. C. (2000). "Sectional analysis of reinforced concrete members." Ph.D. thesis, Department of Civil Engineering, University of Toronto, Toronto, Ontario.

Brown, V. L., and Bartholomew, C. L. (1993). "FRP reinforcing bars in reinforced concrete." ACI Materials Journal, 90(1), 34–39.

Brown, V. L., and Bartholomew, C. L. (1996). "Long-term deflections of GFRP-reinforced concrete beams." Proceeding, ICCI, Tuscon, AZ, 389–400.

Canadian Standards Association (CSA). (2004). "A179-04: Mortar and Grout for Unit Masonry." Mississauga, Ontario.

Canadian Standards Association (CSA). (2004). "S304.1-04: Design of Masonry Structures." Mississauga, Ontario.

Canadian Standards Association (CSA). (2006). "S6-06: Canadian Highway Bridge Design Code (CHBDC)." Mississauga, Ontario.

Canadian Standards Association (CSA). (2006). "S806-02: Design and Construction of Building Components with Fibre-Reinforced Polymers." Mississauga, Ontario.

Chen, B. (2002). "Masonry walls with openings under out-of-plane loading." M.A.Sc. Thesis, McMaster University, Hamilton, Ontario.

Desayi, P., and Krishnan, S. (1964). "Equation for the stress-strain curve of concrete." ACI Journal, 61, 345–350.

Dhanasekar, M., and Shrive, N. G. (2002). "Strength and Deformation of Confined and Unconfined Grouted Concrete Masonry." ACI Structural Journal, 99(6), 819-826.

Drysdale, R.G. and Hamid, A.A. (2005). "Masonry structures – Behaviour and design." Canada Masonry Design Centre, Mississauga, Ontario.

Ehsani, M. R., and Saadatmanesh, H. (1996-a). "Design recommendations for bond of GFRP rebars to concrete." ASCE Journal of Structural Engineering, 122(3), 247-254.

Ehsani, M. R., and Saadatmanesh, H. (1996-b). "Seismic Retrofit of URM Walls with Fiber Composite." Journal of The Masonry Society, 14(2), 63-72.

Ehsani, M. R., Saadatmanesh, H., Abdelghany, I. H., and Elkafrawy, W. (1993). "Flexural Behaviour of Masonry Walls Strengthened with Composite Fabrics." Proceedings, ACI International Symposium on FRP-Reinforcement for Concrete Structures, Vancouver, British Columbia, ACI SP, 138, 497-507.

El-Ragaby, A., El-Salakawy, E., and Benmokrane, B. (2006). "Fatigue analysis of concrete bridge deck slabs reinforced with E-glass/vinyl ester FRP reinforcing bars." Composites: Part B, 38, 703-711.

Faza, S. S., and GangaRao, H. V. S. (1992). "Pre- and post-cracking deflection behaviour of concrete beams reinforced with fibre reinforced plastic rebars." Proceedings of the 1st International Conference on Advanced Composite Materials in Bridges and Structures, Sherbrooke, Québec, 151–160.

Galal, K. E., Ghobarah, A., Drysdale, R. G., and Mosallam, A. (2003). "Strengthening unreinforced masonry walls with openings for extreme load." Response of structures to extreme loading conference, Toronto, Ontario, 8 pages.

Galati, N., Tumialan, G., and Nanni, A. (2006). "Strengthening with FRP bars of URM walls subject to out-of-plane loads." Construction and Building Materials, 20(1-2), 101-110.

Gao, D., Benmokrane, B., and Masmoudi, R. (1998). "A calculating method of flexural properties of FRP-reinforced concrete beam." Technical report, Department of Civil Engineering, University of Sherbrooke, Sherbrooke, Québec.

Ghobarah, A., and Galal, K. E. (2004). "Out-of-plane strengthening of URM walls with openings" ASCE Journal of Composites for Construction, 8(4), 298–305.

Gilstrap, J. M., and Dolan, C. W. (1998). "Out-of-plane bending of FRP reinforced masonry walls." Composites Science and Technology, 58, 1277–1284.

Grace, N. F., Soliman, A. K., Abdel-Sayed, G., and Saleh, K. R. (1998). "Behavior and ductility of simple and continuous FRP reinforced beams." ASCE Journal of Composites for Construction, 2(4), 186–94.

Hamid, A., Chia-Calabria, C., and Harris, H. (1992). "Flexural Behavior of Joint Reinforced Block Masonry Walls." ACI Structural Journal., 89(1), 20- 26.

Hamoush, S. A., McGinley, M. W., Mlakar, P., Scott, D., and Murray, K. (2001). "Out-of-plane strengthening of masonry walls with reinforced composites." ASCE Journal of Composites for Construction, 5(3), 139–145.

Hamoush, S. A., McGinley, M. W., Mlakar, P., and Terro, M. J. (2002). "Out-of-plane behaviour of surface-reinforced masonry walls." Construction and Building Materials, 16(6), 341–351.

Horton, R., T., and Tadros, M. K. (1990). "Deflection of reinforced masonry members." ACI Structural Journal, 87(4), 453–463.

The Canadian Network of Centres of Excellence on Intelligent Sensing for Innovative Structures (ISIS Canada). (2001). "Design manual No. 3: Reinforcing concrete structures with fibre reinforced polymers." Winnipeg, Manitoba.

Jaeger, G. L., Tadros, G., and Mufti, A. A. (1995). "Balanced Section, Ductility and Deformability in Concrete with FRP Reinforcement." Research Report No. 2, Industry Center for Computer-Aided Engineering, Technical University of Nova Scotia, Halifax, Nova Scotia.

Jeong, S. M. (1994). "Evaluation of ductility in prestressed concrete beams using fiber reinforced plastic tendons." Ph.D. Thesis, University of Michigan, Ann Arbor, MI.

Kiss, R. M., Kollar, L. P., Jai, J., and Krawinkler, H. (2002). "FRP strengthened masonry beams, part 2: test results and model predictions." Journal of Composite Materials, 36(9), 1049-1063.

Kodur, V. K. R., and Bisby, L. A. (2005). "Evaluation of fire endurance of concrete slabs reinforced with fiber-reinforced polymer bars." ASCE Journal of Structural Engineering, 131(1), 34-43.

Laoubi, K., El-Salakawy, E., and Benmokrane, B. (2006). "Creep and durability of sand-coated glass FRP bars in concrete elements under freeze/thaw cycling and sustained loads." Cement & Concrete Composites, 28, 869-878.

Lee, J. (2001). "Computational evaluation of strengthening the out-of-plane behavior of masonry walls using fiber reinforced polymers." M.Eng. Thesis, University of California, Berkeley, CA.

Liu, Y. (2002). "Beam-column behaviour of masonry structural elements." Ph.D. Thesis, University of New Brunswick, Saint John, New Brunswick.

Loov, R. E. (1991). "A General Stress-Strain Curve for Concrete." Canadian Society of Civil Engineering Conference, Edmonton, Alberta, 302-311.

Masonry Standards Joint Committee (MSJT). (2005). "Building Code Requirements for Masonry Structures." ACI 530/ASCE 5/TMS 402-99, the Masonry Society, Boulder, CO.

Mierzejewski, W., Fam, A., MacDougall, C., and Chidiac, S.E. (2008). "Out-of-Plane Testing of Masonry Walls with Near-Surface Mounted (NSM) Reinforcement." 2nd Canadian Conference on Effective Design of Structures, McMaster University, Hamilton, Ontario.

Mota, C., Alminar, S., and Svecova, D. (2006). "Critical review of deflection formulas for FRP-RC members." ASCE Journal of Composites for Construction, 10(3), 183–194.

Park, R., Priestley, M. J. N., and Gill, W. D. (1982). "Ductility of square confined concrete columns." ASCE Journal of Structural Engineering, 108(4), 929–950.

Priestley, M. J. N., and Elder, D. M. (1983). "Stress-strain curves for unconfined and confined concrete masonry." ACI Journal, 80(3), 192–201.

Pultrall. (2007) "V-ROD^{TM} fibre reinforced polymer (FRP) bars: product guide specifications." Pultrall inc., Thetford mines, Québec.

Rasheed, H. A., Nayal, R., and Melhem, H. (2004). "Response prediction of concrete beams reinforced with FRP bars. "Composite Structures, 65, 193–204.

Saafi, M. (2002). "Effect of fire on FRP reinforced concrete members." Composite Structures, 58, 11–20.

Simard-Beaudry. (2001). "Blocs de béton: résumé des données techniques." St-Eustache, Québec.

Taly, N. (2001). "Design of reinforced masonry structures." McGraw-Hill.

Tan, K. H. F., and Patoary, M. K. H. (2004). "Strengthening of masonry walls against out-of-plane loads using fiber-reinforced polymer reinforcement." ASCE Journal of Composites for Construction, 8(1), 79–87.

Thériault, M., and Benmokrane, B. (1998). "Effects of FRP reinforcement ratio and concrete strength on the flexural behaviour of concrete beams." ASCE Journal of Composites for Construction, 2(1), 7-16.

Turco, V., Secondin, S., Morbin, A., Valluzzi, M. R., and Modena, C. (2006). "Flexural and shear strengthening of un-reinforced masonry with FRP bars. "Composites Science and Technology, 66, 289–296.

APPENDIX A: SECTION ANALYSIS

In this appendix, section analysis based on Whitney stress block for wall G-3#13-F is presented in details to explain the way the flexural capacity of the GFRP-reinforced walls is calculated in Chapter 5. There is no need to have an example for the section analysis based on the stress-strain model for masonry, since the only difference is that the stress block factors are substituted with the real values calculated by equation (5.9).

Dimensions of the wall:

Clear span:	$L = 2400\ mm$
Width:	$b = 990\ mm$
Thickness:	$h = 190\ mm$

Properties of the masonry:

Compressive strength:	$f'_m = 10.9\ MPa$
Flexural bond strength:	$R = 1.11\ MPa$
Ultimate compressive strain:	$\varepsilon_{m,u} = 0.003$

Reinforcement specifications:

Type of the rebars:	GFRP
Number of the rebars:	3
Diameter of the rebars:	13 *mm*
Effective depth:	$d = 100\ mm$
Modulus of elasticity:	$E_{FRP} = 46.3\ GPa$

Ultimate tensile strength: $f_{u,FRP} = 786\ MPa$

Ultimate tensile strain: $\varepsilon_{FRP,u} = 0.0017$

Calculation of the cracking moment:

$$I_g = \frac{bh^3}{12} = 571.6\times10^6\ mm^4$$

$$S_g = \frac{I_g}{h/2} = 6.02\times10^6\ mm^3$$

$$M_{cr} = R\times S_g = 6.44\ kN.m$$

Calculation of the flexural strength:

$$A_{FRP} = 3\times\frac{\pi(13)^2}{4} = 398.2\ mm^2$$

$$\rho_{FRP} = \frac{A_{FRP}}{bd} = 0.004$$

$$\beta_1 = 0.8-0.10\left(\frac{f'_m-20}{10}\right) = 0.8$$

$$\alpha_1 = 0.8$$

$$f_{FRP} = 0.5E_{FRP}\varepsilon_{m,u}\left[\left(1+\frac{4\alpha_1\beta_1 f'_m}{\rho_{FRP}E_{FRP}\varepsilon_{m,u}}\right)^{\frac{1}{2}}-1\right] = 443.8\ MPa$$

$$c = \frac{f_{FRP}A_{FRP}}{\alpha_1\beta_1 f'_m b} = 23.8\ mm$$

$$M_n = f_{FRP}A_{FRP}\left(d-\frac{\beta_1 c}{2}\right) = 15.88\ kN.m$$

APPENDIX B: CALCULATION OF DEFORMABILITY FACTOR

This appendix explains, in detail, the calculation of experimental curvature based on the deformed shape of the wall, at service and ultimate stage, through an example (Wall G-4#13-P). The experimental curvatures were used in calculating the deformability factor in Chapter 6.

In order to calculate the maximum curvature at each stage, the deformed shape of the wall is drawn using the recorded deflection at mid-span, third-spans, and quarter-span. It is assumed that the deflection at the other quarter-span is identical to the recorded one. It is also assumed that the deflection at both ends of the wall is zero. Afterwards, the shape of the wall is fit to a second-degree polynomial equation (i.e. parabola) having seven points of the deformed shape. The absolute value of the second derivative of this polynomial with respect to x (which represents the length of the wall) is the curvature at that stage.

Service stage:

Deflection: $\Delta(x) = y = -6.5x^2 + 15.5x - 0.1$

Rotation: $\theta(x) = y' = -13x + 15.5$

Curvature: $\psi(x) = y'' = -13$

Max. Curvature: $\psi(x = 1.2\ m) = 13\ {}^{10^{-6}}/_{mm}$

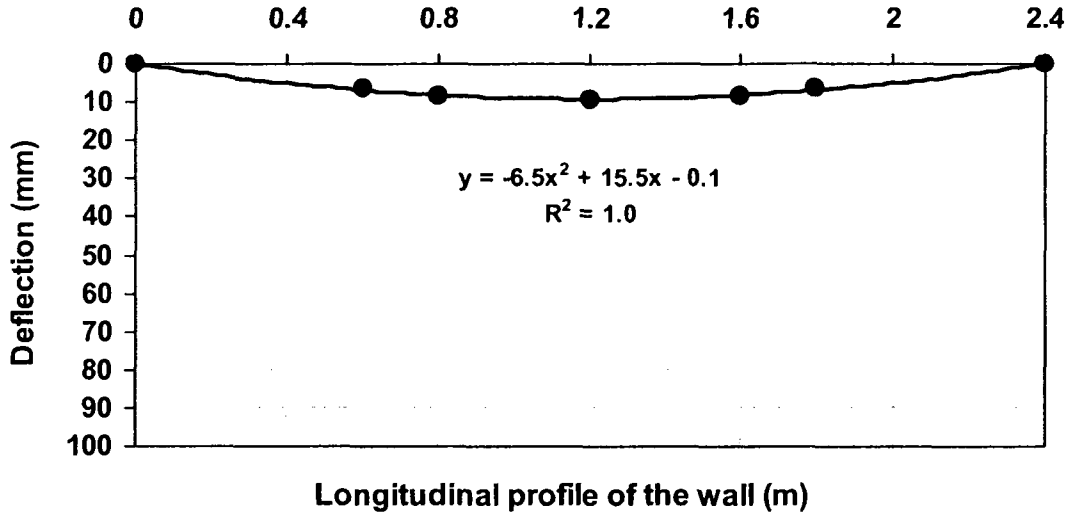

Ultimate stage:

Deflection: $\Delta(x) = y = -65.5x^2 + 157.1x - 0.5$

Rotation: $\theta(x) = y' = -131x + 157.1$

Curvature: $\psi(x) = y'' = -131$

Max. Curvature: $\psi(x = 1.2\ m) = 131\ {}^{10^{-6}}/_{mm}$

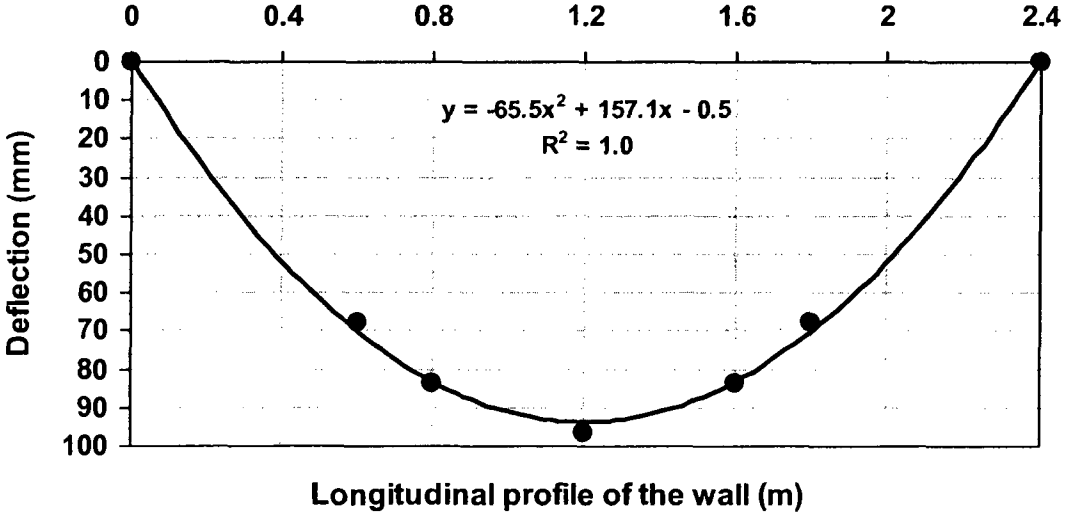

Calculating the deformability factor:

Curvature factor: $\frac{\psi_u}{\psi_s} = \frac{131}{13} = 10.08$

Moment factor: $\frac{M_u}{M_s} = \frac{30.3}{8.1} = 3.76$

Deformability factor = Curvature factor × Moment factor = 10.08 × 3.76 = 37.9

APPENDIX C: DESIGN EXAMPLE

This appendix exemplifies the application of the capacity chart proposed in Chapter 5 (Figure 5.10) for designing masonry walls reinforced with GFRP. For this matter, a hypothetical design problem is defined as such:

It is required to determine the ratio of longitudinal reinforcement using GFRP rods with ultimate tensile strength of 790 MPa, ultimate tensile strain of 0.0018, and tensile modulus of elasticity of 46.4 GPa, for a fully grouted 190 mm hollow concrete masonry wall spanning 3.0 m vertically to carry 5.0 kN/m^2 unfactored wind load. f'_m is reported 10.9 MPa from prism tests.

Dimensions of the wall:

Clear span:	$L = 3000\ mm$
Width:	$b = 1000\ mm$
Thickness:	$h = 190\ mm$

Properties of the masonry:

Compressive strength:	$f'_m = 10.9\ MPa$

Reinforcement specifications:

Type of the rebars:	GFRP
Effective depth:	$d = 95\ mm$
Modulus of elasticity:	$E_{FRP} = 46.4\ GPa$
Ultimate tensile strength:	$f_{u,FRP} = 790\ MPa$

Ultimate tensile strain: $\varepsilon_{FRP,u} = 0.0018$

Factored load and moment:

$$w_f = 1.4 \times 5.0 \, kN/m^2 = 7.0 \, kN/m^2$$

$$M_f = \frac{\left(7.0 \, kN/m^2\right)(3.0m)^2}{8} = 7.9 \, kN.m/m$$

Normalized moment factor:

$$M_n/\Phi_{FRP} = M_f = 7.9 \, kN.m/m$$

$$M_n = M_f \Phi_{FRP} = 15.8 \, kN.m/m$$

$$M_n/bd^2 = \frac{\left(15.8 \, kN.m/m\right)\left(10^6 \, N.mm/kN.m\right)}{(1000 \, mm)(95 \, mm)^2} = 1.8 \, MPa/m$$

Having M_n/bd^2 = 1.8 MPa for 1.0 m of width of the wall, the required reinforcement ratio can be found from Figure 5.10, which is 0.0051.